COMPUTER SIMULATION OF LIQUID FLOW PATTERNS ON DISTILLATION TRAYS

A THESIS SUBMITTED

BY

ANTHONY GORDON WALTON B.Eng.

A candidate for the degree of

Doctor of Philosophy

DEPARTMENT OF CHEMICAL ENGINEERING

AND

APPLIED CHEMISTRY

UNIVERSITY OF ASTON IN BIRMINGHAM

OCTOBER 1995

CONTAINS DISKETTE

UNABLE TO COPY

CONTACT UNIVERSITY

IF YOU WISH TO SEE

THIS MATERIAL

UNIVERSITY OF ASTON IN BIRMINGHAM

COMPUTER SIMULATION OF LIQUID FLOW PATTERNS ON DISTILLATION TRAYS

ANTHONY GORDON WALTON B.Eng.
A candidate for the degree of Doctor of Philosophy - October 1995

Abstract

This thesis describes work carried out to improve the fundamental modelling of liquid flows on distillation trays. A mathematical model is presented based on the principles of computerised fluid dynamics. It models the liquid flow in the horizontal directions allowing for the effects of the vapour through the use of an increased liquid turbulence, modelled by an eddy viscosity, and a resistance to liquid flow caused by the vapour being accelerated horizontally by the liquid. The resultant equations are similar to the Navier-Stokes equations with the addition of a resistance term.

A mass-transfer model is used to calculate liquid concentration profiles and tray efficiencies. A heat and mass transfer analogy is used to compare theoretical concentration profiles to experimental water-cooling data obtained from a 2.44 metre diameter air-water distillation simulation rig. The ratio of air to water flow rates are varied in order to simulate three pressures: vacuum, atmospheric pressure and moderate pressure.

For simulated atmospheric and moderate pressure distillation, the fluid mechanical model constantly over-predicts tray efficiencies with an accuracy of between +1.7% and +11.3%. This compares to -1.8% to -10.9% for the *stagnant regions model* (Porter et al. 1972) and +12.8% to +34.7% for the *plug flow plus back-mixing model* (Gerster et al. 1958). The model fails to predict the flow patterns and tray efficiencies for vacuum simulation due to a change in the mechanism of liquid transport, from a liquid continuous layer to a spray as the liquid flow-rate is reduced. This spray is not taken into account in the development of the fluid mechanical model.

A sensitivity analysis carried out has shown that the fluid mechanical model is relatively insensitive to the prediction of the average height of clear liquid, and a reduction in the resistance term results in a slight loss of tray efficiency, but these effects are not great. The model is quite sensitive to the prediction of the eddy viscosity term. Variations can produce up to a 15% decrease in tray efficiency.

The fluid mechanical model has been incorporated into a column model so that statistical optimisation techniques can be employed to fit a theoretical column concentration profile to experimental data. Through the use of this work mass-transfer data can be obtained.

Keywords: DISTILLATION, FLOW PATTERNS, MASS TRANSFER, TRAY EFFICIENCY, COMPUTERISED FLUID DYNAMICS

Acknowledgements

This work has only been possible through the cooperation and support of a large number of people. In particular, I would like to express my gratitude to the following people:

Professor K.E. Porter and Dr J.P. Fletcher for their guidance and advice throughout my research.

Dr S. Generalis for sharing his extensive knowledge of CFD with me.

B.P. Oil and B.O.C. Cryoplants Ltd for their generous financial support through the Advanced Studies In Distillation (ASID) consortium.

D. Bleby and F.M. Lea for their technical expertise and assistance with the computer systems.

My family and Lily for their encouragement and patience.

Finally I would like to thank all the others, too numerous to name, for helping me to maintain my sanity.

Table of Contents

Table of Figures

Table of Tables

Nomenclature

Roman alphabet:

a,b,c,d	-	constants in Equation 3.13	
A	-	bubbling area of tray	m^2
A_F	-	fractional free area of tray (area occupied by holes / total bubbling area)	
$A_{Region\ 1}$	-	bubbling area in central region of the tray (Region 1 in Figure 2.7)	m^2
b	-	constant in Equation 4.1	
C	-	concentration of most volatile component in the liquid phase	mole fraction
C_B	-	constant in Equation 6.18 (defined in Equation 6.19)	
C_d	-	coefficient of discharge	
C_n	-	average concentration of the most volatile component in liquid exitting tray n	mole fraction
C_p	-	specific heat capacity	$kJ\ kmol^{-1}\ K^{-1}$
C_r	-	reduced concentration (defined by Equation 4.24)	
C_v	-	concentration of most volatile component in the vapour phase	mole fraction
$C_{v\,n}$	-	vapour concentration leaving a point on tray n	mole fraction
$\bar{C}_{v\,n}$	-	average vapour concentration leaving a point on tray n	mole fraction
$C_{v\,n-1}$	-	vapour concentration entering a point on tray n	mole fraction
$\bar{C}_{v\,n-1}$	-	average vapour concentration entering tray n	mole fraction
C_v^*	-	vapour concentration in equilibrium with the liquid at a point	mole fraction
$C_v^*{}_n$	-	vapour concentration in equilibrium with the liquid exiting tray n	mole fraction
CP	-	capacity factor (defined by Equation 2.1)	$m\ s^{-1}$
D	-	tray diameter	m
$D_{i,j}$	-	divergence from continuity (defined by Equation 3.27)	s^{-1}

D_e	-	eddy diffusivity	$m^2\ s^{-1}$
D_e^G	-	eddy diffusivity predicted by the Gerster et al. (1958) correlation	$m^2\ s^{-1}$
D_{es}	-	eddy diffusivity in the spray regime	$m^2\ s^{-1}$
d_h	-	hole diameter	m
E_{MV}	-	vapour phase Murphree plate efficiency (defined by Equation 2.3)	
E_{OG}	-	average vapour phase point efficiency (defined by Equation 2.4)	
F_{lv}	-	dimensionless vapour resistance (defined by Equation 6.4)	
F_s	-	superficial F factor (defined by Equation 6.14)	
$F_{s\ max}$	-	modified superficial F factor (defined by Equation 6.14)	
Fr'	-	modified Froude number (defined by Equation 6.17)	
FP	-	flow parameter (defined by Equation 2.2)	
g	-	acceleration due to gravity	$m\ s^{-2}$
G	-	vapour flow rate	$kmol\ s^{-1}$
G'	-	vapour flow rate per unit bubbling area	$kmol\ m^{-2}\ s^{-1}$
G_x	-	sum of forces acting on a unit of froth in the x-direction	N
h	-	height above tray floor	m
H	-	air enthalpy	$kJ\ kmol^{-1}$
H_1	-	average enthalpy of air entering the tray	$kJ\ kmol^{-1}$
H_2	-	average enthalpy of air leaving the tray	$kJ\ kmol^{-1}$
H_{2i}	-	enthalpy of air leaving a point	$kJ\ kmol^{-1}$
h_f	-	froth height	m
h_l	-	average height of clear liquid	m
h_s	-	normalised concentration of spray	

$$h_s = \frac{h_s'}{h_{s\ inlet}'}$$

h_s'	-	concentration of spray	m^3 / m^2

$H_T^*{}_i$	-	enthalpy of saturated air at the temperature of the liquid at a point	kJ $kmol^{-1}$
$H_T^*{}_{out}$	-	enthalpy of saturated air at the average temperature of the liquid exiting the tray	kJ $kmol^{-1}$
h_w	-	weir height	m
k	-	constant in Equation 6.15	
k_1 - k_6	-	constants (defined in Equation 4.14)	s^{-1}
l	-	flow path width	m
l_m	-	mixing length	m
L	-	liquid flow rate	kmol s^{-1}
m	-	gradient of equilibrium line	
M	-	mass flow of liquid	kg s^{-1}
N_G	-	number of gas phase mass-transfer units	
N_L	-	number of liquid phase mass-transfer units	
N_{OG}	-	overall number of gas phase mass-transfer units	
N_x	-	molar flow of spray in the x-direction	kmol s^{-1}
N_y	-	molar flow of spray in the y-direction	kmol s^{-1}
P	-	dynamic liquid pressure	Pa
Pe	-	Peclet number (defined locally)	
Pe_s	-	Peclet number in the spray regime	
Q_L	-	volumetric liquid flow rate	m^3 s^{-1}
R	-	dimensionless resistance	
Re_B	-	boundary layer Reynolds number (defined by Equation 6.4)	
Re_{ED}	-	eddy Reynolds number (defined by Equation 6.4)	
t	-	time	s
T	-	water temperature at a point on a tray	K
T_{in}	-	inlet water temperature	K
T_{n-1}	-	water temperature in equailibrium with the vapour entering the tray	K
T_r	-	reduced temperature (defined by Equation 4.23)	
u	-	liquid velocity along the flow-path length	m s^{-1}

U	-	dimensionless velocity (defined by Equation 6.4)	
u_b	-	bubble rise velocity	m s^{-1}
u_f	-	fluid velocity based on average flow path width	m s^{-1}
u_h	-	liquid velocity in the boundary layer at height h above the tray floor (defined by Equation 3.13)	m s^{-1}
u_v	-	superficial vapour velocity	m s^{-1}
u_0	-	bulk liquid velocity	m s^{-1}
U_0	-	liquid velocity at the inlet	m s^{-1}
v	-	liquid velocity parallel to the inlet weir	m s^{-1}
V	-	reduced velocity in the y-direction (defined by Equation 6.4)	
W	-	weir length	m
x	-	distance along axis parallel to the flow path	m
x_c	-	characteristic length used to calculate boundary layer thickness	m
X	-	dimensionless distance in the x-direction (defined locally)	
y	-	distance along axis parallel to the inlet weir	m
Y	-	dimensionless distance in the Y-direction (defined locally)	
Z	-	length of liquid flow path	m

Greek alphabet:

α_c	-	concentration similarity ratio	
α_e	-	volumetric liquid hold-up fraction in froth	m^3 liquid / m^3 froth
β	-	relaxation parameter	
δ	-	boundary layer thickness	m
Δ	-	increment length used in finite difference approximations	m

ε	-	volumetric vapour hold-up fraction	m^3 vapour / m^3 froth
η	-	defined by Equation 2.11	
$\eta_{i,j}$	-	constant used in velocity calculations (defined in Appendix 1)	m s^{-1}
θ	-	convergence parameter (defined by Equations 3.28 & 3.29)	kg m^{-1} s^{-1}
λ	-	ratio of the molar flow rates of gas to liquid multiplied by the gradient of the operating line	
μ	-	dynamic viscosity	kg m^{-1} s^{-1}
ν	-	kinematic viscosity	m^2 s^{-1}
ν_e	-	kinematic eddy viscosity	m^2 s^{-1}
$\xi_{i,j}$	-	constant used in velocity calculations (defined in Appendix 1)	m s^{-1}
Π	-	dimensionless pressure (defined by Equation 6.4)	
ρ_L	-	liquid density	kg m^{-3}
ρ_L'	-	molar liquid density	kmol m^{-3}
ρ_v	-	vapour density	kg m^{-3}
σ	-	normal stress	N m^{-2}
σ_s	-	surface tension	N m^{-1}
τ	-	shear stress	N m^{-2}
τ_{vx}	-	resistance due to vapour acting in the x-direction	N m^{-2}
τ_{vy}	-	resistance due to vapour acting in the y-direction	N m^{-2}
$\tau_{\delta x}$	-	resistance due to skin friction acting in the x-direction	N m^{-2}
$\tau_{\delta y}$	-	resistance due to skin friction acting in the y-direction	N m^{-2}

CHAPTER 1

1. INTRODUCTION

Distillation is often described by those working in competing fields as a mature process. This refers to the large amount of research work which has been done since the development of the petrochemical industry first necessitated the better understanding and prediction of performance of distillation columns, mainly for design purposes. This work was driven by a need from industry and created a large number of correlations and rules of thumb, based on empirical or trial and error approaches, which a designer could use in order to avoid failure of the proposed design. The approximate nature of this work required the use of large safety factors to ensure success. This was the cause of additional expense in the capital costs, incurred through the need for additional separation stages, and operating costs, through operating at a high rate of reflux.

The majority of the early work dealt with the operation of tray columns, because problems initially met in the design and operation of large packed distillation columns prohibited their use. These problems were later overcome through the better design of liquid and vapour distribution systems. This means that the use of packings as contacting devices is becoming more widespread in distillation. Since the majority of previous designs involved the use of trays, and due to the fact that for some situations trays are still the preferred vapour-liquid contacting medium, there are still many tray distillation columns in industrial use. Henceforth, only the operation of tray distillation columns will be considered.

The combination of empirical correlations and rules of thumb led to improved predictions for only a limited range of conditions and helped to avoid conditions where standard design methods were known not to apply (Porter and Jenkins, 1979). For the main part, no attempt was made to put the explanation of the phenomena which occur on a fundamental basis.

Porter and Jenkins (1979) explained how a lack of understanding of the fundamental processes involved in distillation could lead to attempts being made to interpret phenomena using inappropriate parameters. They showed how physical properties often change in correlation to each other, and that a given range of such properties are met under similar conditions for different systems. This means that they cannot be varied independently, and so, variations in the relative physical properties in a vapour-liquid system can be expressed in terms of a density ratio.

Rush (1979) investigated the economics of replacing distillation by other, competing technologies. He concluded that although distillation was heavily energy intensive, it remained, in many cases, the best way to achieve a given separation on an industrial scale, though improvements could be made to optimise the processes and run them "leaner and harder". Even small improvements in efficiency were found to be economically viable, since it was conservatively estimated that in 1976 distillation consumed 3% of all energy produced in the USA, and that the pay-back time for retro-fitting an improved control system or higher efficiency trays was only one year (Mix et al. 1980).

In order for a process to be designed and operated to minimise costs, the best option would be extensive process integration. This involves the use of energy removed from one part of a process as useful heat elsewhere. To maximise this energy integration, the modifications to the process could lead to designing and operating columns outside the limited range where experience has already been gained, creating uncertainties in the design process. This could be counteracted by increasing safety factors, but this is undesirable as it increases costs. In reality, it would be economically beneficial if these safety factors could be reduced in order for columns to be operated closer to their minimum specifications. Porter and Jenkins (1982) summed up the situation and advocated:

> "... an increased need for a more detailed understanding of the fundamental mechanisms which determine the performance of full scale separation plant and hence in turn justifies further research on a large

scale on what are regarded as mature separation methods."

With this in mind, a research program was commenced at Aston University in the late 1970's, with the intension of gaining an in depth understanding of the phenomena which effect flows on industrial scale distillation trays. Initial studies on a 1.2 metre diameter air-water distillation simulator (Porter et al. 1987), were added to by the construction of a 2.44 metre diameter single tray air-water simulator (Hine 1990). This apparatus has been used by a succession of workers (Chambers 1993, Fenwick 1995) in order to build up a comprehensive bank of data, including height of clear liquid measurements, tray efficiencies and information about flow patterns, under a range of operating conditions designed to simulate a wide range of distillation conditions.

1.1 Objectives

The aim of the work described in this thesis is to expand the fundamental knowledge of the phenomena which occur on distillation trays by attempting to simulate the liquid flows. In creating a flexible model which is valid over a wide range of operating conditions and tray geometries, a large step has been taken towards the prediction of tray and column efficiencies. Such a tool should be an invaluable aid to the process engineer in the design and trouble-shooting of tray columns.

A mathematical model which describes the flow of liquid across a distillation tray, such as the one presented here, consists of several distinct parts. The main area is the model equations, which describe the flow across the main region of the tray, and the boundary conditions, which describe areas such as the tray inlet, the outlet and the column walls where the flow conditions may differ from those in the central region of the tray. In order to solve these equations a computer program has been written in FORTRAN which uses a mathematical solution algorithm to obtain variables such as liquid velocities and liquid phase concentration profiles. The final area is the data which are required to describe the flow conditions. This consists of properties of the liquid and vapour streams and details which describe the tray geometry. This data

may be used to calculate secondary parameters, such as the eddy diffusivity, from empirical correlations. All these areas are discussed in this thesis.

1.2 Structure of thesis

A brief survey of relevant literature is carried out in Chapter 2 in order to show the major developments in the modelling of distillation trays over the past sixty years. By comparison with experimental data obtained from air-water simulations available in the literature, it will be shown that these models do not reflect the true nature of flow on circular trays, and are at best highly simplified. These models are limited to a restricted range of conditions, usually defined by the assumptions made about the tray geometry and the mechanism of liquid transport.

In Chapters 3 and 4, a model is presented based on the use of Computational Fluid Dynamics (CFD) which describes the liquid flow patterns found in practice on circular trays operating in the mixed-froth and emulsion flow regimes. The model was first proposed by Yu et al. (1991), but was solved incorrectly. A method is demonstrated which allows for the calculation of tray efficiencies. This data is compared with experimental data available in the literature (Chambers 1993). The theory presented, though only applied here to sieve trays, can be used to calculate flows on more complex plate contacting devices.

In Chapter 5 the new liquid flow model is utilised in an overall column model (DISTSIM) in order to move away from the limiting concept of the completely mixed tray, usually assumed when simulating distillation columns. By fitting predicted liquid concentration profiles to those gained experimentally (Sakata and Yanagi 1979), point efficiencies, and hence, mass transfer data is obtained for a *cyclo-hexane - n-heptane* system operating at total reflux in a 1.2 metre diameter column containing ten sieve trays.

Though essentially having a theoretical basis, the model presented in Chapter 2 requires some empirical constants, (eddy diffusivity / viscosity and average height of

clear liquid) which can be easily obtained from a wealth of empirical correlation, and also includes some assumptions regarding the liquid - vapour interactions and frictional losses with the tray floor which have yet to be evaluated experimentally. Through re-arranging the basic flow equations into dimensionless form, the effects of inaccuracies in these data can be determined. This approach can also be used to estimate the model predictions at the extreme conditions represented by an infinitely large tray. This work is carried out in Chapter 6.

The model presented here is the first successful attempt to describe the liquid flow on distillation trays from a fundamental basis and to use the data obtained to predict tray efficiencies.

CHAPTER 2

2. LITERATURE SURVEY

2.1 Introduction

This chapter presents a general overview of the relevant information of the modelling of distillation trays. The areas covered here come under four main subject outlines, which are:

a) a description of the flow regimes which are often encountered and the phenomena which are associated with each regime,
b) the definitions of efficiency used in this work,
c) milestones in the development of tray models,
d) a brief discussion on the modelling of tray distillation columns,
e) a survey of experimental data on trays and observations about tray performance.

A more complete survey of the literature on distillation trays in general is given by Lockett (1986). Relevant references from that work are included here.

2.2 Flow Regimes on Sieve Trays

As with most two-phase systems, the behaviour of the liquid - vapour dispersion on sieve trays can be characterised by looking at the properties and flow rates of the two phases. The limiting cases are when the nature of the dispersion is completely dominated by the effects of one or the other phases. When vapour momentum is dominant the liquid is projected from the surface of the tray as a series of droplets. When the liquid momentum is dominant an emulsion of small vapour bubbles is swept along by the bulk liquid flow. These conditions are referred to as the spray regime and the emulsion flow regime respectively. An additional flow regime (mixed froth), where the dispersion consists of a zone of high liquid content near the tray floor with droplets being projected from its surface, bridges the gap between the two limits. The

proportions of the liquid present in the liquid continuous zone or the vapour continuous zone varies according to the local conditions. Other flow regimes, such as the free bubbling regime and a foaming regime, may occur depending on the system properties and flow conditions, but these are not usually met in industrial columns and so are not considered here. In the case of the foaming regime, it is deliberately avoided to prevent premature flooding of the trays. The transition between the spray and mixed-froth regimes has been widely studied both in order to gain an insight into the mechanism of liquid transport and predict under what conditions this transition occurs. This is a difficult process as the definition of the upper limit of the spray regime is vague. Consideration of the emulsion flow regime is a more recent phenomena (Hofhuis & Zuiderweg 1979, Zuiderweg et al. 1984) and so its study is not as well developed. Figure 2.1 shows the flow regime map as proposed by Hofhuis and Zuiderweg (1979). It ignores the presence of the foaming regime, the existence of which is determined by system properties in addition to relative flow rates.

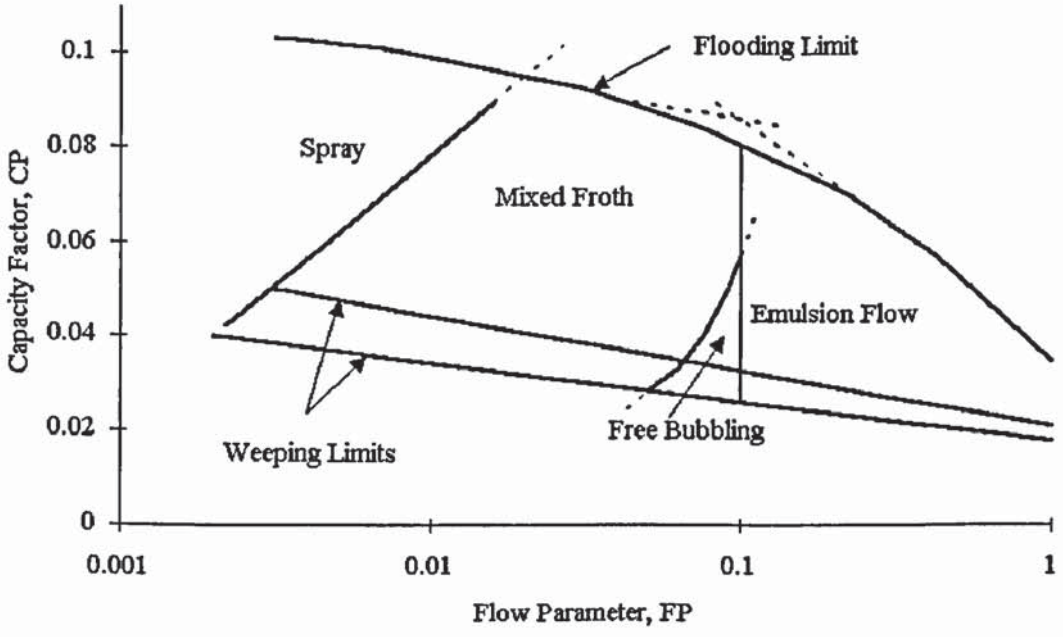

Figure 2.1: The two-phase flow regime map suggested by Hofhuis and Zuiderweg (1979)

The flow conditions are described by Hofhuis and Zuiderweg in terms of the capacity factor, CF, and the flow parameter, FP. The capacity factor (Equation 2.1) is an indication of the effect of the vapour, whereas the flow parameter (Equation 2.2) gives an indication of the liquid / vapour ratio.

$$CF = u_v \left\{ \frac{\rho_v}{\rho_L - \rho_v} \right\}^{0.5} \tag{2.1}$$

$$FP = \frac{L}{G} \left(\frac{\rho_v}{\rho_L} \right)^{0.5} \tag{2.2}$$

A definition of the symbols used throughout this thesis can be found in the nomenclature.

As can be seen from Figure 2.1, the practical operating conditions for a tray are bounded by a flooding limit and a weeping limit. The first of these defines the conditions under which, for various reasons, the liquid cannot exit the tray at a sufficiently high rate, and so, liquid accumulates. This is known as flooding. The second of the limits mentioned here is the weeping limit. This describes the conditions where a relatively low vapour flow-rate cannot support the liquid on the tray. The liquid pressure therefore forces the liquid through the perforations on the tray. The liquid effectively by-passes the tray and as a result does not fully contact the vapour. The mechanisms of both flooding and weeping are not discussed here.

2.2.1 The spray regime

In the spray regime, the liquid is the dispersed phase and the vapour is the continuous phase (see Figure 2.2a). This regime is favoured by low liquid loads and high vapour velocities, such as the conditions often encountered in vacuum distillation. It has been described as being like a fluidised bed of droplets, and attempts have been made to model it as such (Ho et al. 1969, Porter & Wong 1969). This idea was rejected by later workers in this field who suggested that the vertical froth dispersion can be modelled with reasonable accuracy by a free trajectory model (Hofhuis & Zuiderweg

1979, Raper et al. 1979). In this type of model, droplets of liquid are thrown from a droplet formation zone (a thin liquid continuous layer on the tray floor) with a projection velocity between that of the vapour hole velocity and the superficial vapour velocity. Droplets of sufficient size are slowed by gravity and eventually fall back to the tray where they mix and can be re-projected. Those droplets below a given size are entrained by the vapour to the tray above. This type of model has been shown to predict liquid dispersion densities with a good degree of accuracy, but is limited due to the fact that the total amount of liquid in the dispersion must be known a priori. The only attempt at modelling liquid transport across a tray was by Porter et al. (1977) who proposed that liquid was transported by the diffusion of spray across a droplet concentration gradient. This approach is limited due to the low volume of liquid which can be transported by a purely diffusional mechanism. It is discussed further in Section 2.4.4.

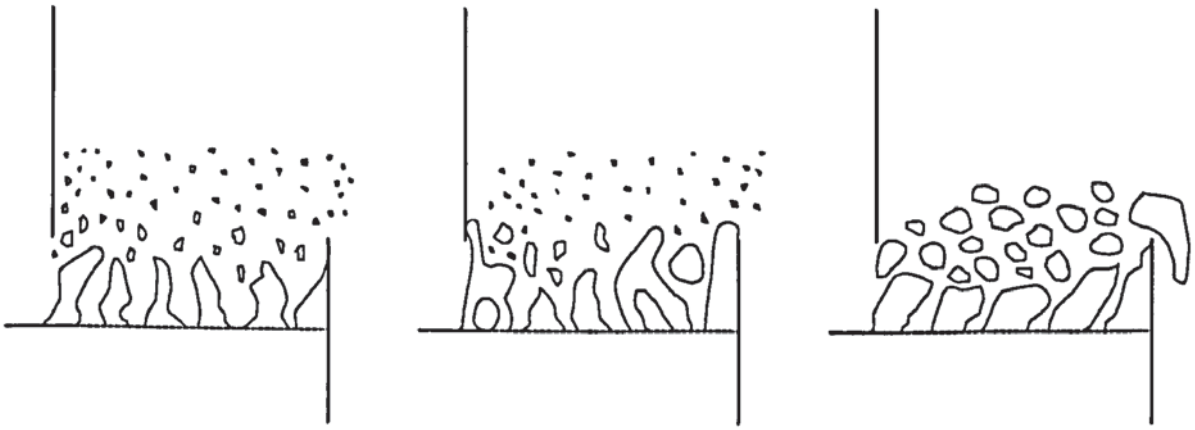

a) spray regime b) mixed-froth regime c) emulsion flow regime

Figure 2.2: Structure of the two-phase dispersions in the different flow regimes

The transition from froth to spray has received quite a lot of attention (Porter & Wong 1969, Muller & Prince 1972, Jeronimo & Sawistowski 1973, Loon et al. 1973, Pinczewski et al. 1973, Payne & Prince 1975, Payne & Prince 1977, Raper et al. 1979, Pinczewski & Fell, 1979, Lockett 1981), but the wide variety of techniques used to identify the transition and the problems with defining the transition point has led to some disagreement. Jeronimo and Sawistowski (1973) suggested that the transition

occurred when 50% of the holes on the tray were jetting, whereas later authors (Pinczewski et al. 1973, Raper et al. 1979) believed that 95%+ was a more realistic figure. One of the main feature of the transition is the change from vapour bubbling to jetting at an orifice (see Figure 2.3). It is this jetting which is responsible for throwing up the liquid in the form of ligands, which break up due to their unstable nature and the vapour momentum. This droplet formation also increases the degree of entrainment of liquid in the vapour phase (Porter & Wong 1969) and has been used to define the spray to froth transition.

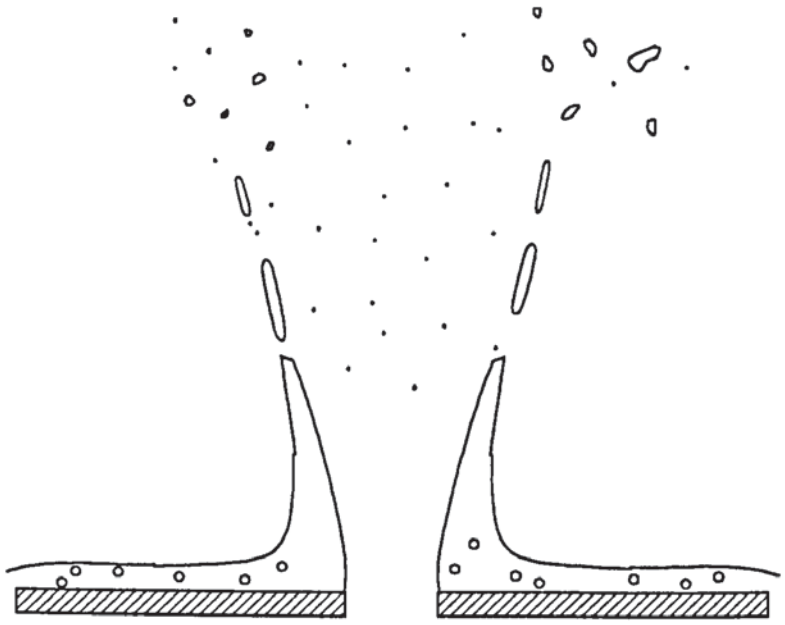

Figure 2.3: Jetting in the spray regime

2.2.2 The mixed-froth regime

This is almost the reverse of the spray regime, with the liquid as the continuous phase and the vapour being transported through it by both jetting and bubbling. Again, the jetting is responsible for throwing up a spray above the main liquid continuous layer (see Figure 2.2b). It is commonly met in atmospheric pressure distillation where neither the liquid nor the vapour momentum is dominant. It could be considered that this is a wide transition region between the emulsified flow regime and the spray regime

2.2.3 The emulsion flow regime

It was Hofhuis and Zuiderweg (1979) who split the froth regime into a mixed- and emulsified flow regime. They noted that when the flow ratio exceeded a value of 0.2 (this coincides with the flow parameter equal to 0.1 on the flow regime diagram), the nature of the liquid transport over the outlet weir changed from being mainly consisting of splashes and slugs of liquid to being a continuous stream. Further study into the emulsion flow regime was later carried out in order to investigate other aspects of tray hydraulics (Zuiderweg et al. 1984).

This type of two-phase flow on trays is found where high liquid momentum dominates the hole vapour momentum, and consists of small vapour bubbles "emulsified" in the liquid phase (see Figure 2.2c).

2.2.4 Flow regimes and modelling

There are implications for modelling which can be concluded from the discussion of flow regimes in the literature. In particular, the work of Hofhuis and Zuiderweg (1979) defines a range of Capacity Factor and Flow Parameter values which define practical operating conditions without flooding or weeping (see Figure 2.1). It is reasonable to assume that trays will be designed to operate within such limits and, therefore, that useful modelling should assume operation away from these limits. It is possible, however, that a model could be used to help define such limits.

2.3 Definitions of Efficiency

Throughout this work, the definitions of tray efficiency and point efficiency referred to are those based on the definitions of Murphree (1925). Though other definitions are available (Hausen 1953, Standart 1965), the Murphree efficiencies are more commonly used by engineers and, hence, are easier for the reader to relate to. The simplicity of the mass-transfer process considered here (a binary system with zero net molar interphase transfer) also does not warrant the extra complications necessary for use of these other definitions of efficiency.

The efficiencies used henceforth are the Murphree vapour phase tray efficiency, E_{MV}, (Equation 2.3) and the local vapour phase efficiency or *point efficiency*, E_{OG} (Equation 2.4).

$$E_{MV} = \frac{\overline{C}_{vn} - \overline{C}_{vn-1}}{C^*_{vn} - \overline{C}_{vn-1}} \qquad (2.3)$$

$$E_{OG} = \frac{C_{vn} - C_{vn-1}}{C^*_{vn} - C_{vn-1}} \qquad (2.4)$$

Definitions of the concentrations used for calculating the Murphree vapour phase tray efficiency and the Murphree point efficiency can be gained from Figures 2.4a and 2.4b respectively.

$C_v{}^*{}_n$ and $C_v{}^*$ are defined as the vapour concentrations in equilibrium with liquid of concentration C_n and C, respectively.

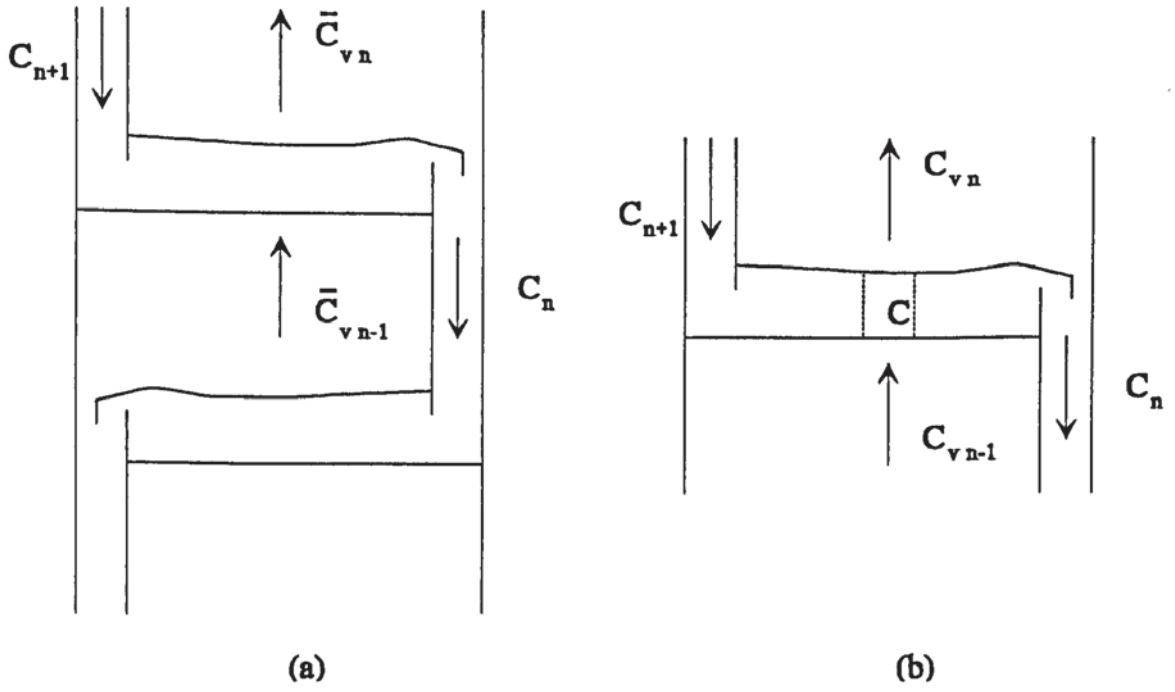

Figure 2.4: Concentrations used for calculating the Murphree vapour phase tray efficiency and the Murphree point efficiency

Throughout this work, the tray performance will be assessed in terms of a tray enhancement factor. This is defined here as the Murphree vapour phase tray efficiency divided by the Murphree point efficiency (E_{MV} / E_{OG}). It represents the enhancement of the tray efficiency over the point efficiency due to the flow pattern. A completely mixed tray has a tray efficiency equal to the point efficiency, and hence a tray enhancement factor of 1.

2.4 Tray Models

Tray models have been developed a great deal over the last sixty years since Kirschbaum (1934) discovered the existence of longitudinal liquid phase concentrations on trays of small diameter, disproving the previous theory that liquid on distillation trays could be considered to be well-mixed.

Models of two general types have been proposed:

a) mixed-pool models which assume that a tray consists of a number of completely mixed pools of liquid with flow between them, analogous to a series of continuous flow stirred tank reactors. The main advantage of this type of model is its computational simplicity, but it has the disadvantage that it does not model the process which actually exists on trays. This limitation was acknowledged by Gautreaux and O'Connell (1955), who stated that

> "....the performance could better be defined by the degree of mixing that occurs."

Problems were also encountered with determining the number of mixed pools to use for a given set of conditions. This problem was later solved (Ashley & Haselden 1970) by relating the number of mixed-pools to the Peclet number,

b) a back-mixing concept was introduced through the use of an eddy diffusivity. This approach produces a better picture of the processes occurring on the trays and can be calculated from experimental data obtained through the use of

tracers injected into the liquid.

These two approaches have been developed in parallel, models developed through the use of one approach often being duplicated by the other, and so the developments in modelling theory can be illustrated through just considering developments in the use of the eddy diffusivity concept. It is the view of the author that the development of high speed computers, reducing the time required for rigorous computational techniques, has made the arguments for the use of mixed-pool models almost redundant. At present, there still exist some advantages for use of this type of model when investigating multi-component mass-transfer.

More recently the field of computational fluid dynamics (CFD) has been recognised as having great potential for use in modelling the flows on trays (Yu et al. 1991, Porter et al. 1992). Care should be taken in the development of these models since CFD has not developed sufficiently to cope with the complex two-phase interactions which occur on trays. It will be shown below (Section 2.4.7) that a lack of understanding of either the phenomena being modelled or the techniques being used can invalidate the model.

The major milestones in the development of tray models are reviewed below.

2.4.1 Lewis model

Lewis (1936) suggested the simplest form of liquid flow model. He proposed that liquid could be assumed to flow across a tray of simplified (rectangular) geometry. He proposed three limiting cases, where the vapour was considered to be either completely mixed, or un-mixed with either co-current or counter-current liquid flow on alternate trays. In the derivation of all of the three cases, Lewis makes the following assumptions:

1) the liquid flows across the tray (plug flow) with no back-mixing,
2) there is no vertical liquid concentration gradient,
3) the equilibrium curve can be considered to be straight over the concentration range,

4) the point efficiency (E_{OG}) is constant across the tray,

5) the liquid and vapour flow-rate are constant.

Case 1: Vapour is completely mixed between trays (see Figure 2.5a). The result for this is independent of the direction of liquid flow on consecutive trays.

$$E_{MV} = \frac{e^{E_{OG}\lambda} - 1}{\lambda} \qquad (2.5)$$

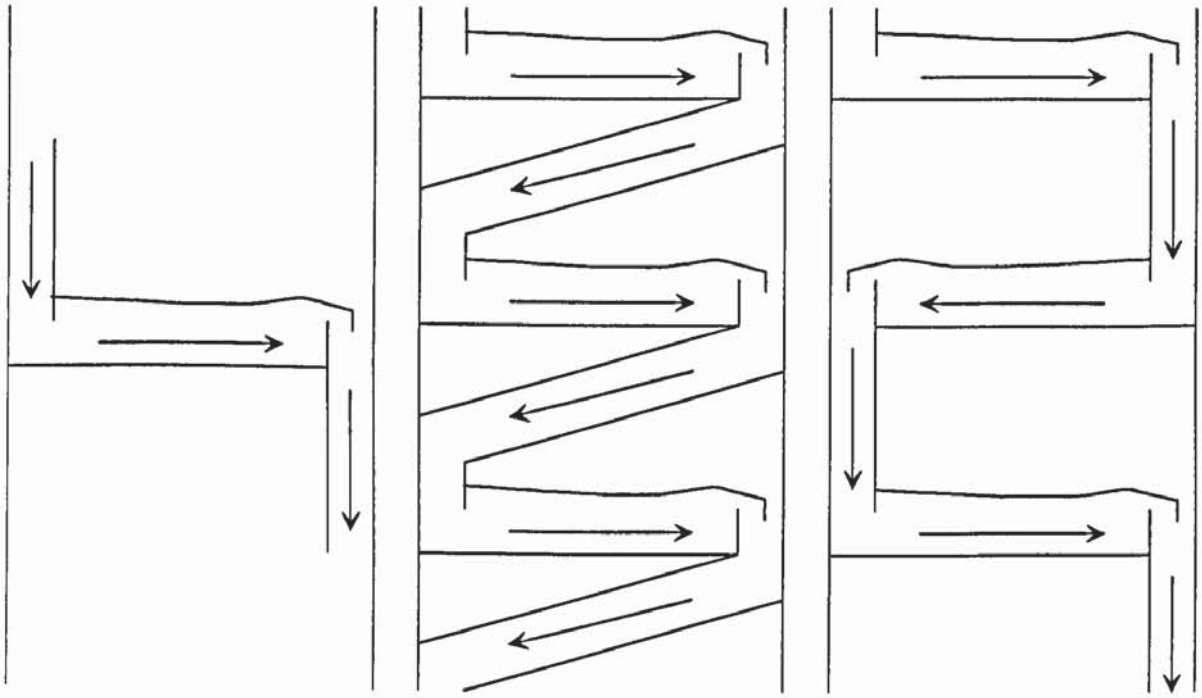

a) Lewis Case 1 b) Lewis Case 2 c) Lewis Case 3

Figure 2.5: Flows on consecutive trays for the Lewis model

For both cases 2 and 3 (defined below) the following relationship is valid. Only the relation used to predict the similarity ratio, α_c, varies. The similarity ratio is the ratio of the vapour concentration leaving a point on a tray n relative to the vapour concentration leaving a point directly below it on tray n-1 (this is assuming that the trays are number consecutively in ascending order from the bottom of the column to the top).

$$E_{MV} = \frac{\alpha_c - 1}{\lambda - 1} \tag{2.6}$$

Case 2: The vapour remains unmixed as it passes between trays and the liquid flow is in the same direction (co-current) on consecutive trays (see Figure 2.5b). It is assumed that the vapour leaving a point on a tray will rise to the corresponding point on the tray above. This results in the relative shape of the concentration profiles for all trays being similar, only they are displaced according to the inlet concentration.

$$\lambda = \left(\frac{1}{E_{OG}} + \frac{1}{\alpha_c - 1}\right) \ln \alpha_c \tag{2.7}$$

Case 3: The vapour rises from the tray without mixing and the liquid flows in the opposite direction (counter-current) on consecutive trays (see Figure 2.5c). The shape of the concentration profiles on consecutive trays are now the mirror image of each other.

$$\lambda = \sqrt{\frac{\alpha_c^2 - (1 - E_{OG})^2}{E_{OG}^2(1 - \alpha_c^2)}} \cos^{-1}\left[1 - \frac{(1 - \alpha_c)(\alpha_c - 1 + E_{OG})}{\alpha_c(2 - E_{OG})}\right] \tag{2.8}$$

when $\alpha_c < 1$, or

$$\lambda = \sqrt{\frac{\alpha_c^2 - (1 - E_{OG})^2}{E_{OG}^2(\alpha_c^2 - 1)}} \cosh^{-1}\left[1 + \frac{(\alpha_c - 1)(\alpha_c - 1 + E_{OG})}{\alpha_c(2 - E_{OG})}\right] \tag{2.9}$$

when $\alpha_c > 1$

Lewis uses these relationships to predict tray and column efficiencies and suggests that they can be used by the designer for calculating the number of actual trays in a column, though he does admit that the actual enhancement of the tray efficiency over the point efficiency will be less than those predicted due to mixing in both the liquid and the vapour phases.

2.4.2 Plug flow plus back-mixing model

Gerster et al. (1958) recommended the use of a model incorporating partial liquid mixing on rectangular trays. They used the concept of eddy diffusivity, D_e, to define the degree of back-mixing. The assumptions made did not differ from those of Lewis (1936) with the exception, of course, of the introduction of liquid back-mixing. The model can be easily derived from the consideration of a section of froth (see Figure 2.6) and a relationship between point efficiency and tray efficiency can be derived by integration with the outlet boundary condition of no diffusion over the outlet weir proposed by Wehner and Wilhelm (1956).

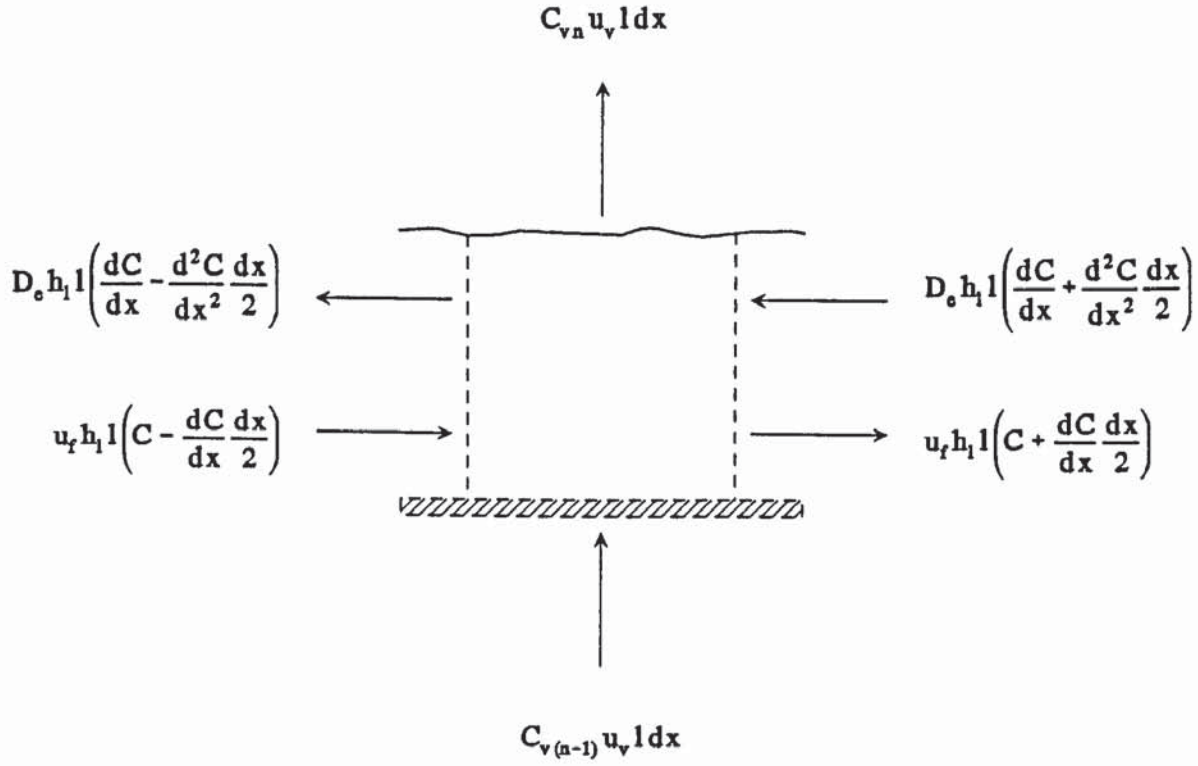

Figure 2.6: Mass balance over a segment of froth for the plug flow plus back-mixing model

$$\frac{E_{MV}}{E_{OG}} = \frac{1 - \exp[-(\eta + Pe)]}{(\eta + Pe)[1 + (\eta + Pe)/\eta]} + \frac{\exp(\eta) - 1}{\eta\,[1 + \eta/(\eta + Pe)]} \qquad (2.10)$$

where,

$$\eta = \frac{Pe}{2}\left[\sqrt{1 + \frac{4\lambda E_{OG}}{Pe}} - 1\right] \qquad (2.11)$$

and

$$Pe = \frac{u_f Z}{D_e} \qquad (2.12)$$

Again, pre-calculated data are available in graphical form which relate the enhancement of the tray efficiency over the point efficiency to the two dimensionless groups, Pe and λE_{OG}. The model presented by Gerster was based on the assumption that the vapour was completely mixed between trays (similar to Lewis Case 1). Diener (1967) went on to develop relationships between overall column efficiency and point efficiency for cases corresponding to Lewis Cases 2 and 3. These relationships are not discussed here.

The models outlined thus far suggest that tray efficiency should increase with tray size. These high efficiencies were never obtained in practice with efficiencies decreasing with size.

2.4.3 Stagnant regions model

Porter et al. (1972) considered, for the first time, the flow of liquid on trays to be two-dimensional. Based on observations on a 7ft diameter water flume and a 4ft diameter air-water distillation simulator, a model was proposed consisting of the plug flow of liquid between the down-comers of a tray (Region 1 in Figure 2.7) and stagnant regions at the sides (Region 2 in Figure 2.7).

The model made the following assumptions:

a) the vapour and the liquid entering the tray are well-mixed,

b) the development of the model was restricted to a binary system where the slope of the equilibrium curve could be considered to be straight over the

concentration range,

c) the point efficiency is constant over the tray,

d) liquid flow is uniform through Region 1,

e) there is no liquid flow in Region 2.

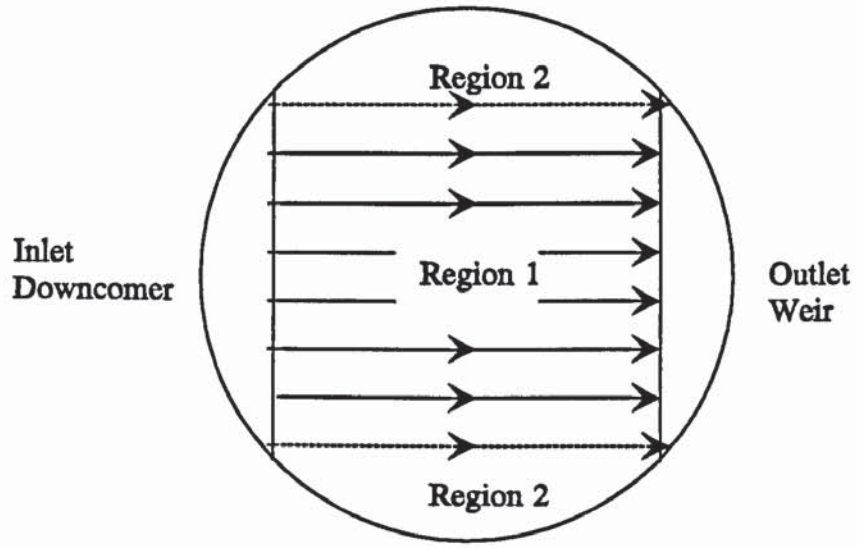

Figure 2.7: Assumed liquid flow pattern for the stagnant regions model

A mass balance on elements in Region 1 and Region 2 yield Equations 2.13 and 2.14 respectively.

$$\frac{1}{Pe}\left\{\frac{\partial^2 C}{\partial X^2}+\frac{\partial^2 C}{\partial Y^2}\right\}-\frac{\partial C}{\partial X}-E_{OG}\lambda\left\{\frac{WD}{A}\right\}\left(C-C^{*}_{en-1}\right)=0 \qquad (2.13)$$

$$\frac{1}{Pe}\left\{\frac{\partial^2 C}{\partial X^2}+\frac{\partial^2 C}{\partial Y^2}\right\}-E_{OG}\lambda\left\{\frac{WD}{A}\right\}\left(C-C^{*}_{en-1}\right)=0 \qquad (2.14)$$

where,

$$Pe=\frac{LD}{Wh_f\rho'_L\alpha D_e} \qquad (2.15)$$

These equations were solved by finite difference techniques with the following

boundary conditions:

a) symmetry about the tray centre-line,

b) partial back-mixing under the inlet down-comer using Danckwerts' boundary condition (Danckwerts 1953),

$$C_{in} = 1 + \frac{1}{Pe}\left\{\frac{\partial C}{\partial X}\right\} \qquad (2.16)$$

c) no diffusion over the outlet weir (Wehner & Wilhelm 1956),

d) no diffusion normal to the column wall.

$$\frac{\partial C}{\partial n} = 0 \qquad (2.17)$$

Equation 2.16 is not entirely correct for this situation. This relationship is only valid for the case of true plug flow. Despite the fact that plug flow is assumed down the centre of the tray, the existence of the stagnant regions at the sides results in a concentration gradient normal to the direction of flow, hence causing a net transfer of one component in this direction by diffusion. This transport is not taken into account. For the majority of cases the concentration gradients normal to the direction of flow at the liquid inlet will be small, so Equation 2.16 can still be used as an approximation.

Porter then goes on to explain the apparent anomalies between existing theory and practice by calculating the width of the zone into which liquid will diffuse from Region 1 into Region 2. It is shown that this *width of a mixing zone* (defined as the distance taken for the liquid concentration to be reduced to 10% of that in Region 1) is approximately 0.3m and is independent of tray size. This phenomena explains some of the deficiencies with the *plug flow plus back-mixing* model discussed previously.

Early theory suggested that tray efficiencies should increase with tray size, but practical experience had shown that the predicted tray efficiencies were not obtained. The concept of the *width of a mixing zone* demonstrated that if the stagnant regions extended beyond 0.3m, then significant vapour by-passing may occur, resulting in a

loss of tray efficiency. This corresponds to a diameter of about 1.5m for a tray with W/D = 0.6.

A limiting condition for large trays was also proposed. In this case, the *width of the mixing zone* could be considered to be negligible in comparison with the tray diameter and the tray could be approximated by a central region where the flow could be represented by the *plug flow plus back-mixing* model and side regions where all the vapour was assumed to pass through the tray without mass-transfer. This limiting solution was given by:

$$\left[\frac{E_{MV}}{E_{OG}}\right]_{Limit} = \frac{A_{Region\,1}}{A}\left[\frac{E_{MV}}{E_{OG}}\right]_{Region\,1} \qquad (2.18)$$

where the enhancement of the tray efficiency over the point efficiency in Region 1 is given by Equation 2.10.

As the Peclet number tends to infinity, this simplifies to

$$\left[\frac{E_{MV}}{E_{OG}}\right]_{Limit} = \frac{\left[\exp\left(\frac{\lambda E_{OG} A_{Region\,1}}{A}\right) - 1\right]}{\lambda E_{OG}} \qquad (2.19)$$

Porter presents concentration profiles calculated using the stagnant regions model and compares them to the residence time distributions measured experimentally by Bell (1972). Both works showed U-shaped profiles with high concentrations (low residence times) in the centre region of the tray with low concentrations (high residence times) at the sides.

In later publications (Lockett et al. 1973, Lockett et al. 1975) the use of this model is extended to a column operating in the absence of vapour mixing, and with partial vapour mixing between stages, to demonstrate that the stagnant regions predicted on single trays have a cumulative effect when multiple trays are considered. This is

caused by vapour effectively travelling the length of the column through the stagnant regions without mass-transfer occurring. Lim et al. (1974) demonstrate that this effect is eliminated if two-pass trays are used instead of single-pass trays.

2.4.4 Spray diffusion model

Most workers attempting to model the spray regime have concentrated their work on the prediction of liquid dispersion densities in the vertical direction and little work has been done on the prediction of liquid transport. One exception is the spray diffusion model (Porter et al. 1977).

Porter suggested that liquid transport in the spray regime was due to the random movement of droplets, with the concentration of droplets being a possible driving force. The magnitude of the random movement was described by a diffusion constant, D_{es}. A differential element of spray is shown in Figure 2.8. The effect of this diffusion is not only to transport the liquid, but results in the concentration profiles being flattened relative to the U-shaped concentration profiles previously reported by Bell (1972) for the froth regime.

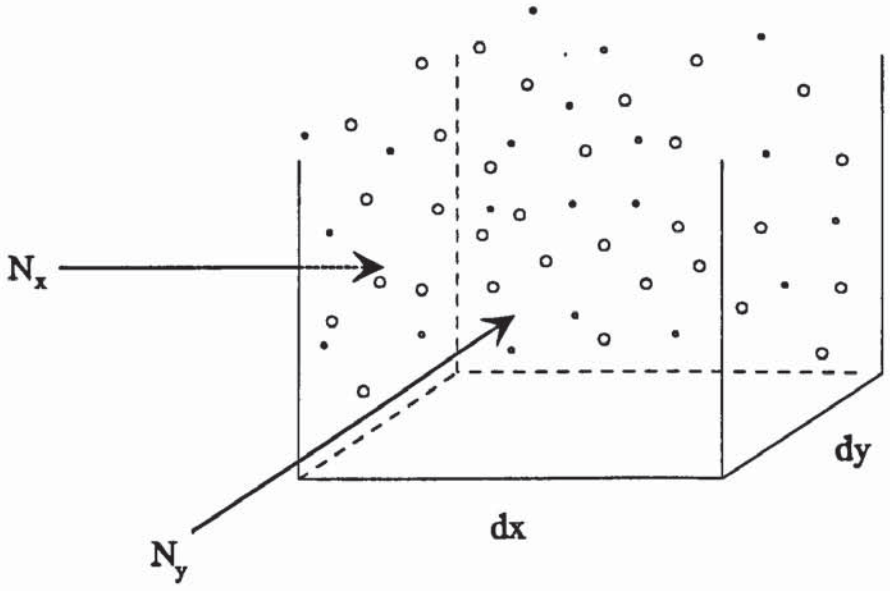

Figure 2.8: Differential element of froth for the spray diffusion model

The net flow of droplets in the x-direction can be calculated from:

$$N_x = -D_{es}\rho'_L dy\frac{\partial h_s'}{\partial x} \qquad (2.20)$$

A similar expression can be derived for the y-direction.
In dimensionless form the continuity equation can be represented by:

$$\frac{\partial^2 h_s}{\partial X^2} + \frac{\partial^2 h_s}{\partial Y^2} = 0 \qquad (2.21)$$

To calculate the droplet concentration profile, Equation 2.21 is solved from $h_s = 1$ at the liquid inlet to an arbitrary (less than 1) value at the outlet. The flow can be considered to be symmetrical about the centre of the tray, with no droplet concentration gradient normal to the tray walls (analogous to Equation 2.17).

In determining the liquid phase concentration profiles, the usual assumptions are made:

a) constant point efficiencies,
b) linear equilibrium relationship,
c) the vapour phase and the liquid phase can be considered to be well-mixed on entering the tray,
d) there are no liquid concentration gradients in the vertical direction.

The boundary conditions are similar to those used in the stagnant regions model.

Porter goes on to derive the following equation for use in calculating concentration profiles:

$$h_s\left[\frac{\partial^2 C}{\partial X^2}+\frac{\partial^2 C}{\partial Y^2}\right]+2\left[\frac{\partial h_s}{\partial X}\frac{\partial C}{\partial X}+\frac{\partial h_s}{\partial Y}\frac{\partial C}{\partial Y}\right]-Pe_s\left(\frac{WZ}{A}\right)\lambda E_{OG}\left(C-C^*_{en-1}\right)=0 \qquad (2.22)$$

where,

$$Pe_s = \frac{ZL}{WD_{es}\rho_L' h_{s\,inlet}'} \qquad (2.23)$$

This model is limited in its application though. Since the only driving force for liquid transport is due to a combination of the droplet concentration gradient and the diffusion coefficient (see Equation 2.20), the maximum liquid flow-rate is determined by these two factors. Porter calculates that the maximum conditions are limited by $Pe_s \leq 1.25$ for a geometry where $W / D = 0.6$.

2.4.5 Other non-fluid mechanical models

A wide variety of other tray efficiency models are available in the literature, but a combination of factors, including the complexity of the model and duplication of work, mean that detailed discussion here is of little value.

Gautreaux and O'Connell (1955) proposed a model where liquid travels along the flow path length through a series of well-mixed pools. This work has been duplicated through the use of eddy diffusivity models. Bruin and Freije (1974), on the other hand, took the *stagnant regions model* of Porter et al. (1972) and reproduced it in the form of a mixed-pool model. The two different approaches to this model yielded similar results.

Many models accept the non-uniformity of the liquid flow on trays and have imposed velocity profiles, but this has lead to the creation of sometimes complex models, with parameters which are difficult to evaluate (Strand 1963, Bell & Solari 1974a, Brambilla 1976, Kafarov et al. 1979, Yu et al. 1983). Other work has tried to expand on areas often ignored for simplicity. The effect of uneven eddy diffusivity was also tested (Lockett & Safekourdi 1976, Solari & Bell 1978, Sohlo & Kouri 1982) and the effect of vapour maldistribution was investigated both in the direction of the flow path (Lockett & Dhulesia 1980) and in the transverse direction (Brambilla 1976). Lockett deduced that tray efficiencies were reduced by vapour maldistribution in the direction

of the flow path (this is irrespective of higher vapour flows either at the inlet or the outlet), while Brambilla (1976) found that if the ratio of the vapour to liquid flow-rates through areas were identical, then efficiencies could be maximised. Deviation from this effectively caused either liquid or vapour by-passing.

Work carried out by Lockett and Safekourdi (1976) investigated the effects of liquid flow pattern on tray efficiency. Through numerically simulating flow patterns on trays of differing dimensions, they concluded that a uniform liquid residence time produced the highest tray efficiency. For small trays (diameter less that 2m) poor flow patterns did produce a loss of tray efficiency, but as long as stagnant regions (Porter et al. 1972) were avoided the loss of efficiency was not great. For trays of larger diameter, it is better to aim for the optimum flow pattern (possibly through the use of flow-straightening devices) to maximise tray efficiency. These conclusions were thought to be due to liquid mixing on smaller trays being able to mask the underlying poor flow pattern, whereas the scale of the mixing was not big enough to be effective on larger trays.

Kouri and Sohlo (1985) investigated the theory that velocity profiles are not the same along the length of the flow path, but are developed as the liquid flows. To do this they modelled the velocity profile as a polynomial expression. These developing flow patterns were found to agree more closely with the patterns observed experimentally than previous models.

2.4.6 The Yu fluid mechanical model

A model based on the principles of fluid dynamics was proposed by Yu et al. (1991) which took a form similar to the Navier-Stokes equations for the two-dimensional flow of an incompressible fluid. This model was essentially a liquid only model, but incorporated the effects of the vapour through the assumptions that there was momentum transfer from the liquid to the vapour, accelerating the vapour from having no horizontal velocity component to having a velocity equal to the local liquid velocity. The second main effect of the vapour was to cause immense turbulence in the liquid. Yu introduced an eddy viscosity term, which he argued was equal to the

liquid eddy diffusivity, to account for this. Yu made several questionable numerical simplifications in order to gain a solution.

This model has been solved in a more complete form in the work reported here using the numerical methods associated with computational fluid dynamics. This will be discussed further in Chapter 3.

2.4.7 Other fluid mechanical models

A collaborative effort between Aston University and Tianjin University in P.R. China resulted in a model proposed by Professor Yu (Tianjin University) being published (Porter et al. 1992) based on the principles of computational fluid dynamics. The model is in the form of the two-dimensional Navier-Stokes equation for turbulent fluid flow. The situation is simplified by assuming that the two-phase dispersion can be modelled as the liquid phase only, with the effects of the vapour passing through the liquid being accounted for through the introduction of a resistance term to model the momentum transfer from the liquid to the vapour.

The adoption of the use of the k-ε model for turbulence must be questioned since it is designed for modelling single phase phenomena only. Though this turbulence model has been used for two phase modelling, it is necessary either to assume that the flow of the bi-phase can be treated as a single homogeneous phase, or to model the flows and interactions of both phases. Neither of these are used in this work. The effect of this is that the turbulence predicted in the model is purely due to the liquid (as though liquid was travelling over a tray in the absence of vapour), whereas the turbulence encountered on distillation trays is dominated by the effects of the vapour.

2.5 Column models

All current commercial distillation column simulation packages assume that trays are completely mixed (ie, the liquid on a tray is of uniform concentration and the vapour rising from a tray is of uniform composition). As we have found, this is a gross over-simplification except in the case of small scale pilot plant columns. A column

simulation package (DISTSIM) has been developed at Aston University which is capable of modelling the distillation of a binary mixture using theoretical tray efficiency models to relate tray efficiency to point efficiency, such as discussed previously.

Previous work (Akebe 1983, Porter et al. 1994) incorporated the tray models of Lewis (1936), Diener (1967) and Lockett et al. (1975) and used these models to interpret column operating data available in the literature (Sakata & Yanagi 1979) to demonstrate how mass transfer information (N_G, N_L, E_{OG}) can be obtained by statistically matching predicted column performances with actual data. This work is discussed further in Chapter 5.

2.6 Experimental data and observations

A review of distillation literature shows a wide variety of data on the flow of the bi-phase across trays and the techniques used to measure it. The majority of this work has been carried out on air-water simulation equipment containing only a small number of trays (sometimes only a single tray) for reasons of safety, ease of access to take measurements and due to the expense of operating an entire column. It has been shown theoretically (Porter et al. 1972) that small scale operation often cannot be scaled up to predict performance on larger trays, and so it is necessary to consider only phenomena which occur when simulating trays of similar sizes to those found industrially. Data and observations are available on full trays of 1.2m diameter (Porter et al. 1972, Porter et al. 1987), 1.8m diameter (Biddulph & Bultitude 1990) and 2.44m diameter (Bell 1972, Hine 1990, Porter et al. 1992, Chambers 1993, Fenwick 1995) and half trays with the equivalent full tray diameters of 2m (Yu et al. 1983) and 7.62m (Weiler et al. 1973), using techniques such as fibre optic techniques to measure residence times (Bell 1972), flow pointers (Hine 1990, Porter et al. 1992, Chambers 1993, Fenwick 1995), dye tracers (Weiler et al. 1973, Porter et al. 1987, Chambers 1993) and strain probes (Biddulph & Bultitude 1990) to indicate flow patterns, and water cooling techniques (Porter et al. 1987, Hine 1990, Porter et al. 1992, Chambers 1993, Fenwick 1995) which produce data analogous to concentration profiles and

allow for the prediction of tray efficiencies.

The data collected by Chambers (Porter et al. 1992, Chambers 1993), which includes flow pointer data and temperature profiles gained from water-cooling experiments, has been chosen for comparison with the work presented in this document due to the fact that it covers a range of both vapour and liquid flow-rates which are of industrial relevance. The data gathered by Hine (1990) were excluded due to problems with vapour distribution which were later corrected by Chambers.

2.7 Conclusions

There is still a need for better, more flexible methods for the prediction of tray efficiencies. Although not the only aspect which needs attention, one of the main areas is the creation of a mathematical model for flow patterns. This can then be used to relate local mass transfer rates (expressed, for example, in the form of a point efficiency) to tray efficiencies. A successful mathematical model should be flexible, valid over as wide a range of operating conditions as possible and easy to use.

A modeller should be aware of the mechanism of liquid transport which is dominant (spray or bulk liquid transport) and the phase interactions which must be taken into account.

Though not the only method for modelling the concept of liquid mixing, the use of an eddy diffusion coefficient is probably the best mathematical technique. Despite other methods (mixed-pool) being superior in terms of mathematical manipulation and solution times, the use of and access to more modern, high-speed computers has made these needs irrelevant and more rigorous techniques which better reflect the mechanisms occurring on trays should now be used.

The development of the methods of computational fluid dynamics has led to the prospect of flexible models being produced. The modeller should be aware, though, of the limitations which are inherent in the use of these techniques, such as the

difficulties still encountered when trying to simulate complex two-phase interactions.

A wide range of experimental data is available in the literature for comparison of results.

CHAPTER 3

3. YU FLUID MECHANICAL MODEL

3.1 Introduction

Yu et al. (1991) proposed a model for liquid flow across a distillation tray based on the principles of computational fluid dynamics. The form of the equations were similar to the two-dimensional Navier-Stokes equations for the laminar flow of an incompressible fluid with an additional term designed to take account of the resistance to flow caused by the vapour rising through the liquid and friction between the liquid and the tray floor.

The model was far superior in form to those developed previously due to its fundamental nature and potential simplicity of use. It not only had the capability to predict liquid flow patterns, but also had the flexibility to be used on any shape of tray and be modified to deal with trays which are not simple sieve trays. Most previous models imposed an assumed flow pattern or involved the use of complex parameters to define the size of areas devoted to reverse flow or stagnant region as discussed in Section 2.4.

The work on this fluid mechanical model was not completed satisfactorily by Yu. It was simplified in order to reduce the number of variables so the equations could be solved by methods which cannot usually be applied to this kind of fluid mechanical problem. This was achieved through evaluating the pressure gradient by assuming it was due to a liquid head gradient calculated from a correlation. This approach is incompatible with the assumptions applied in the derivation of the equations, where it was assumed that there was a constant liquid head over the tray. This effectively eliminated pressure as a variable and allowed Yu to solve a simplified force balance in the x-direction to evaluate u. Once u was known, v was obtained directly from the continuity equation. These steps are sufficiently questionable so as to bring into doubt the results gained.

This model has been re-examined and solved successfully without so much simplification in order to calculate liquid flow patterns on a 2.44 metre diameter sieve tray. The results have been compared with experimental results gained through air-water simulation on a single tray test rig. This comparison shows that this is a very good approach to the modelling of distillation trays. Although applied to only a relatively simple distillation tray geometry, the flow pattern model presented here can be used to predict the performance of more complex tray designs. It is also capable of being extended to a more complex series of equations, so that more complex liquid transport mechanisms can be accounted for.

The rest of this section deals mainly with the equations derived initially by Yu.

3.2 Assumptions and Derivation

The model assumes that the liquid flows in a continuous layer adjacent to the tray floor and so is not valid for flow in the spray regime as described in Section 2.2.1. The rest of the assumptions are listed below.

1) The liquid head is constant. At present, all published models have this basic assumption (although it is not always stated), except where a liquid head profile has been imposed to investigate the effects of vapour maldistribution (Lockett & Dhulesia 1980).
2) The liquid is well-mixed in the vertical direction (i.e. no velocity gradients exist in the vertical direction). This seems to be valid since the liquid is thoroughly mixed due to the rising vapour.
3) The effects of the liquid turbulence created by the vapour passing through can be taken into account by the use of an eddy viscosity term which is assumed to be constant over the tray and is equal in both the axial and transverse directions. This is discussed in more detail later in this chapter.
4) The vapour flow is uniform over the active area of the tray. For most situations this is an accurate reflection of what occurs over the majority of the tray. The known minor deviations from this are neglected.
5) The vapour enters the liquid with no horizontal velocity and is accelerated to

the local liquid horizontal velocity before exiting the liquid. This effectively acts as a force resisting the liquid flow, modelled by terms in the equations.

6) The tray floor exerts a resistance to liquid flow. This skin friction can be modelled in through the use of a boundary layer next to the tray floor.

The model was then developed by Yu et al. (1991) through the use of force balances in the x- and y-directions and a continuity equation to ensure that mass is conserved. This is presented here with some modifications which are indicated.

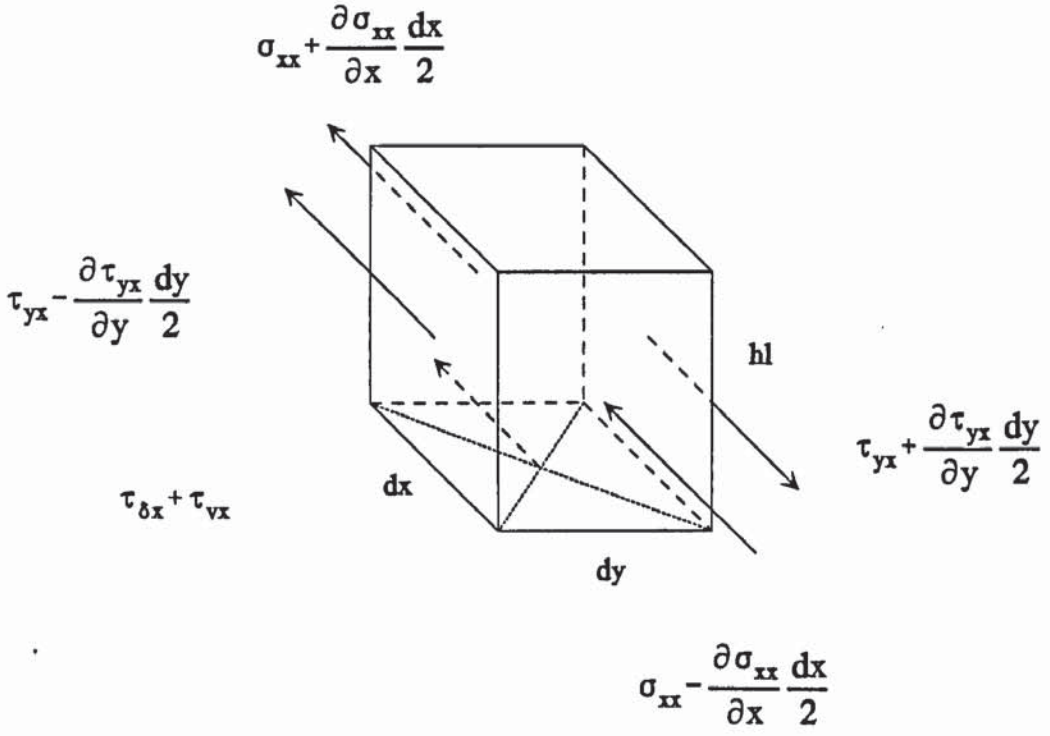

Figure 3.1: A force balance on a segment of froth in the x-direction

Consider a force balance over an element of liquid (x-direction only), see Figure 3.1:

$$\begin{aligned} G_x = &\left(\sigma_{xx} + \frac{\partial\sigma_{xx}}{\partial x}\frac{dx}{2} - \sigma_{xx} + \frac{\partial\sigma_{xx}}{\partial x}\frac{dx}{2}\right) h_l\, dy \\ &+ \left(\tau_{yx} + \frac{\partial\tau_{yx}}{\partial y}\frac{dy}{2} - \tau_{yx} + \frac{\partial\tau_{yx}}{\partial y}\frac{dy}{2}\right) h_l\, dx \\ &- \left(\tau_{\delta x} + \tau_{vx}\right) dx\, dy \end{aligned} \tag{3.1}$$

or,

$$G_x = \left(\frac{\partial \sigma_{xx}}{\partial x} + \frac{\partial \tau_{yx}}{\partial y}\right) dx\, dy\, h_l - \left(\tau_{\delta x} + \tau_{vx}\right) dx\, dy \tag{3.2}$$

According to Newton's second law:

$$G_x = M \frac{Du}{Dt} \tag{3.3}$$

where:

$$M = \rho_L h_l\, dx\, dy \tag{3.4}$$

$$\frac{Du}{Dt} = \frac{\partial u}{\partial t} + u\frac{\partial u}{\partial x} + v\frac{\partial u}{\partial y} \tag{3.5}$$

on substituting Equations 3.3, 3.4, and 3.5 into Equation 3.2, we get:

$$\frac{\partial u}{\partial t} + u\frac{\partial u}{\partial x} + v\frac{\partial u}{\partial y} = \frac{1}{\rho_L}\left(\frac{\partial \sigma_{xx}}{\partial x} + \frac{\partial \tau_{yx}}{\partial y}\right) - \frac{1}{\rho_L h_l}\left(\tau_{\delta x} + \tau_{vx}\right) \tag{3.6}$$

For Newtonian fluids, the shear stress is proportional to the rate of strain caused by the velocity gradient, i.e.

$$\tau_{yx} = \mu\left(\frac{\partial u}{\partial y} + \frac{\partial v}{\partial x}\right) \tag{3.7}$$

$$\sigma_{xx} = -P + 2\mu \frac{\partial u}{\partial x} \tag{3.8}$$

by also considering the continuity equation,

$$\frac{\partial u}{\partial x} + \frac{\partial v}{\partial y} = 0 \tag{3.9}$$

Equation 3.6 becomes:

$$\frac{\partial u}{\partial t} + u\frac{\partial u}{\partial x} + v\frac{\partial u}{\partial y} = -\frac{1}{\rho_L}\frac{\partial P}{\partial x} + \nu\left(\frac{\partial^2 u}{\partial x^2} + \frac{\partial^2 u}{\partial y^2}\right) - \frac{1}{\rho_L h_l}\left(\tau_{\delta x} + \tau_{vx}\right) \tag{3.10}$$

Similarly from a force balance in the y-direction we can obtain:

$$\frac{\partial v}{\partial t} + u\frac{\partial v}{\partial x} + v\frac{\partial v}{\partial y} = -\frac{1}{\rho_L}\frac{\partial P}{\partial y} + \nu\left(\frac{\partial^2 v}{\partial x^2} + \frac{\partial^2 v}{\partial y^2}\right) - \frac{1}{\rho_L h_l}\left(\tau_{\delta y} + \tau_{vy}\right) \tag{3.11}$$

Equations 3.10 and 3.11 are similar to the Navier-Stokes equations for the 2-dimensional flow of an incompressible fluid with the addition of the last term which describes the two resistances to the liquid flow.

The resistance terms were evaluated separately. Firstly, it is assumed that the vapour is accelerated from having no horizontal velocity to having a velocity equal to the local liquid velocity. Therefore,

$$\begin{aligned} \tau_{vx} &= \rho_v u_v u \\ \tau_{vy} &= \rho_v u_v v \end{aligned} \tag{3.12}$$

Since it is assumed that there is a boundary layer on the tray floor, the velocity distribution in this layer in the vertical direction may be represented by:

$$u_h = a + bh + ch^2 + dh^3 \tag{3.13}$$

where a, b, c and d are constants.

Equation 3.13 should also satisfy the following conditions:

$$\begin{aligned} &\text{At} \quad h = 0, \quad u_h = 0 \quad \text{and} \quad \frac{d^2u_h}{dh^2} = 0 \\ &\text{At} \quad h = \delta, \quad u_h = u \quad \text{and} \quad \frac{du_h}{dh} = 0 \end{aligned} \tag{3.14}$$

Substituting the above conditions into Equation 3.13 gives:

$$\frac{u_h}{u} = \frac{3}{2}\frac{h}{\delta} - \frac{1}{2}\left(\frac{h}{\delta}\right)^2 \tag{3.15}$$

Since,

$$\tau_{\delta x} = \mu \left(\frac{du_h}{dh}\right)_{h=0} \tag{3.16}$$

then,

$$\tau_{\delta x} = \mu \frac{3}{2}\frac{u}{\delta} \tag{3.17}$$

In this work, the tray floor boundary thickness, δ, is evaluated from single phase flow boundary layer theory (Bennett & Myers 1982)

$$\delta = 5.0\sqrt{\frac{\nu x_c}{u_o}} \tag{3.18}$$

where:

ν	is the kinematic viscosity ($m^2 s^{-1}$)
x_c	is a characteristic length, related to the hole pitch (m)
u_o	is the bulk liquid velocity ($m s^{-1}$)

Yu et al. (1991) used values gained from experimental observations to evaluate δ.

Work has yet to be carried out in order to quantify the forces suggested in assumptions 5 and 6. It is hoped that work being carried out at this moment (Fenwick 1995, Khan 1995) can illuminate this area.

The eddy viscosity was evaluated by considering the concept of the Prandtl mixing length l_m. The eddy viscosity ν_e in momentum transfer can be represented by:

$$\nu_e = l_m^2 \frac{du}{dy} \tag{3.19}$$

Similarly, the eddy diffusivity D_e in mass transfer is given by:

$$D_e = l_m^2 \frac{du}{dy} \tag{3.20}$$

Thus, if the concept of the mixing length is valid, we obtain,

$$\nu_e = D_e \tag{3.21}$$

After arriving at Equation 3.21, it is now possible to reflect back on assumption 3, which states that the eddy viscosity (effectively the eddy diffusivity) is the same over the tray and is equal in the axial and transverse directions. This has been tested by Yu et al. (1990), who measured axial and transverse eddy diffusivities on at several points on a tray. They found that, although there were slight variations, the values obtained were virtually constant. Hence, assumption 3 is valid.

This set of equations and assumptions are referred to as the Yu fluid mechanical model and are solved using the numerical techniques described below, and not the methods used by Yu et al. (1991).

3.3 Numerical Method

As indicated previously, Equations 3.9, 3.10 and 3.11, which summarise this model,

are essentially the same as the Navier-Stokes equations. Numerical treatment of these equations is quite well developed, many of the methods being based, to some extent, on the *Marker And Cell* (M.A.C.) method (Harlow & Welch 1965). In the decade following the introduction of the M.A.C. method in excess of forty papers were published developing it further, most of the work being carried out by the Los Alamos group in the U.S.A. These are discussed briefly by Browne (1978).

The actual method used was chosen because of its relative simplicity. It is the method developed by Chorin (1968) and Viecelli (1971) as described by Browne (1978). This can be used to solve the unsteady-state Navier-Stokes equations in order to obtain steady-state solutions.

3.3.1 Discretisation

The equations are solved by finite difference approximation based on the M.A.C. finite difference grid as shown in Figure 3.2. This differs from the standard finite difference grid which has all points defined on grid nodes, because only pressure is defined on a grid node. Velocities are defined at the centre of the face perpendicular to the liquid flow. In this way a velocity is sandwiched between the two pressures which form the driving force for the liquid flow. The finite difference technique is forward differencing with respect to time and centre differencing with respect to space (FTCS).

The use of this slightly unusual finite difference grid means that the approximations used must also be defined:

$$\left.\frac{\partial u}{\partial t}\right|^{n}_{i+\frac{1}{2},j} \approx \frac{u^{n+1}_{i+\frac{1}{2},j} - u^{n}_{i+\frac{1}{2},j}}{\delta t} \qquad (3.22)$$

$$\left.\frac{\partial u}{\partial x}\right|^{n}_{i+\frac{1}{2},j} \approx \frac{u^{n}_{i+1,j} - u^{n}_{i,j}}{\delta x} \qquad (3.23)$$

$$\left.\frac{\partial P}{\partial x}\right|^{n}_{i+\frac{1}{2},j} \approx \frac{P^{n}_{i+1,j} - P^{n}_{i,j}}{\delta x} \tag{3.24}$$

$$\left.\frac{\partial^2 u}{\partial x^2}\right|^{n}_{i+\frac{1}{2},j} \approx \frac{u^{n}_{i+\frac{3}{2},j} - 2\,u^{n}_{i+\frac{1}{2},j} + u^{n}_{i-\frac{1}{2},j}}{\delta x^2} \tag{3.25}$$

where,

$$u_{i,j} = \frac{1}{2}\left(u_{i+\frac{1}{2},j} + u_{i-\frac{1}{2},j}\right) \tag{3.26}$$

Other approximations can be derived in a similar fashion.

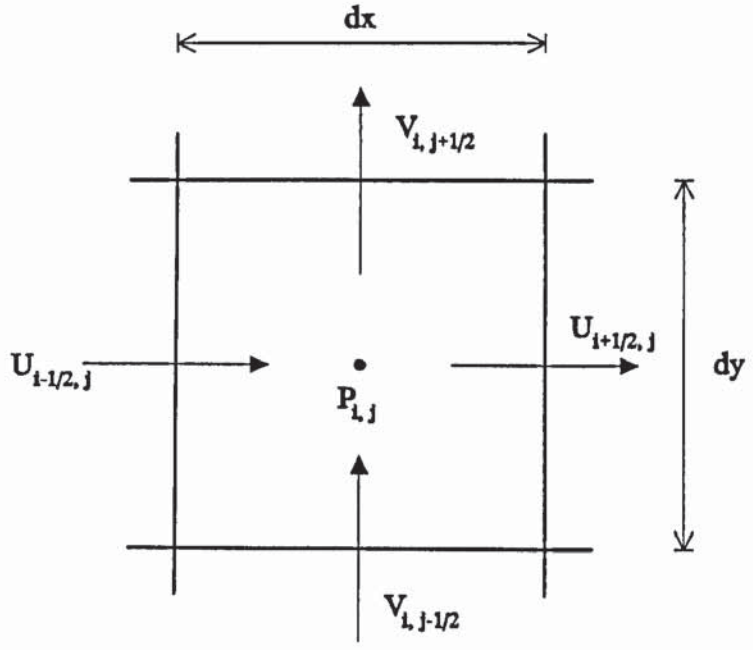

Figure 3.2: The M.A.C. finite difference grid

Boundary conditions are discussed later.

3.3.2 Algorithm

The method outlined by Browne (1978) involves simultaneous iteration on both the velocities and pressure to gain a solution to a time step which obeys continuity. A steady-state solution is obtained by solving the unsteady-state equations and allowing them to develop until the change in the variables with respect to the time iteration becomes negligible (steady-state has been achieved). This requires an initial estimation of the velocity profile. This estimate should not effect the final steady-state velocity profiles provided that a convergence is achieved. It is thought that, for a given set of conditions, only a single solution exists. The solution method for the nth time step is described below. To ensure that continuity is obeyed at all points for time-step n, an inner calculation loop is carried out. This is denoted by the superscript m.

First it is necessary to define a few terms:

a) the divergence from continuity,

$$\left(D_{i,j}^{n+1}\right)^{m+1} = \frac{1}{\delta x}\left\{\left(u_{i+\frac{1}{2},j}^{n+1}\right)^{m} - \left(u_{i-\frac{1}{2},j}^{n+1}\right)^{m}\right\} + \frac{1}{\delta y}\left\{\left(v_{i,j+\frac{1}{2}}^{n+1}\right)^{m} - \left(v_{i,j-\frac{1}{2}}^{n+1}\right)^{m}\right\} \qquad (3.27)$$

b) the dimensional pressure relaxation parameter,

$$\theta \leq \frac{\rho_L}{\delta t\left[\frac{1}{\delta x^2} + \frac{1}{\delta y^2}\right]} \qquad (3.28)$$

In order to minimise the number of iterations Browne suggests,

$$\theta_{optimum} \approx 0.9\,\theta_{maximum} \qquad (3.29)$$

Henceforth, the subscript *optimum* will be omitted for brevity.

c) the pressure is modified using,

$$\left(P_{i,j}^{n+1}\right)^{m+1} = \left(P_{i,j}^{n+1}\right)^{m} - \theta \left(D_{i,j}^{n+1}\right)^{m} \tag{3.30}$$

To obtain a converged solution for a given time-step, the iterative loop is as follows.

1) For the first m-iteration at time-step n+1. Set u^{n+1}, v^{n+1} and P^{n+1} to be the final values of u^n, v^n and P^n from the previous n-iteration for all i and j.

2) Calculate $(D_{i,j}^{n+1})^m$ using Equation 3.27.

3) Calculate $(P_{i,j}^{n+1})^{m+1}$ using Equation 3.30.

4) Recalculate the velocity field using the latest values of the pressure. Assuming that the field is swept with both i & j ascending, this gives:

$$\left(u_{i+\frac{1}{2},j}^{n+1}\right)^{m+1} = \eta_{i+\frac{1}{2},j}^{n} + \frac{\delta t}{\delta x\, \rho_L}\left[\left(P_{i,j}^{n+1}\right)^{m+1} - \left(P_{i+1,j}^{n+1}\right)^{m}\right] \tag{3.31}$$

$$\left(u_{i-\frac{1}{2},j}^{n+1}\right)^{m+1} = \eta_{i-\frac{1}{2},j}^{n} + \frac{\delta t}{\delta x\, \rho_L}\left[\left(P_{i-1,j}^{n+1}\right)^{m+1} - \left(P_{i,j}^{n+1}\right)^{m+1}\right] \tag{3.32}$$

$$\left(v_{i,j+\frac{1}{2}}^{n+1}\right)^{m+1} = \xi_{i,j+\frac{1}{2}}^{n} + \frac{\delta t}{\delta y\, \rho_L}\left[\left(P_{i,j}^{n+1}\right)^{m+1} - \left(P_{i,j+1}^{n+1}\right)^{m}\right] \tag{3.33}$$

$$\left(v_{i,j-\frac{1}{2}}^{n+1}\right)^{m+1} = \xi_{i,j-\frac{1}{2}}^{n} + \frac{\delta t}{\delta y\, \rho_L}\left[\left(P_{i,j-1}^{n+1}\right)^{m+1} - \left(P_{i,j}^{n+1}\right)^{m+1}\right] \tag{3.34}$$

where η & ξ contain velocity values which do not change during the iteration (see Appendix 1 for more details)

5) $(D_{i,j}^{n+1})^{m+1}$ can now be calculated and the procedure repeated to convergence.

Convergence is when $(D_{i,j}^{n+1})_{max}$ is less than some small value. Browne suggests $1*10^{-4}$.

This calculation procedure, as applied to this problem, requires an initial estimate of

the velocity profile which obeys continuity. An assumption that the liquid travels from the inlet directly to the outlet in plug flow has been used for this purpose.

The calculations are said to have achieved a steady state solution when the average of the rate of change in both u and v becomes small (less than 0.01% of the inlet velocity).

The pressures calculated are relative pressures since they only represent a pressure gradient. A datum pressure of zero has been chosen at the centre of the inlet gap.

The velocity calculations are carried out in single precision in the FORTRAN program. The effect of this and other factors on the accuracy of the calculations is discussed in Appendix 3.

3.4 Boundary Conditions

3.4.1 Inlet

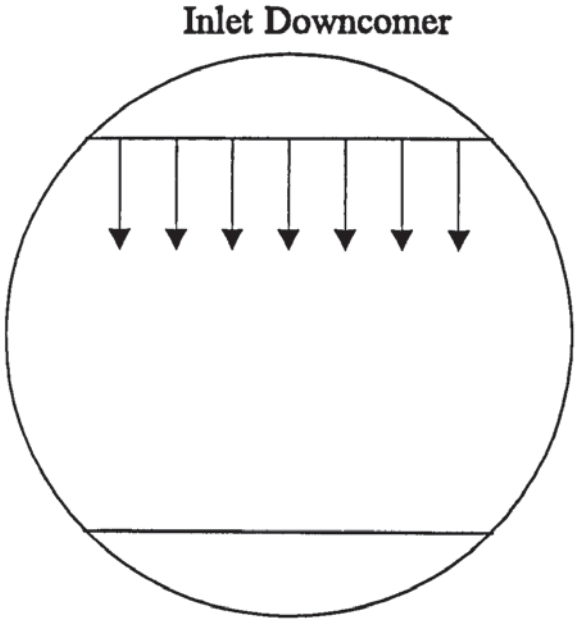

Figure 3.3: The inlet velocity boundary condition for chordal downcomers

At the inlet gap the liquid is assumed to flow normal to the downcomer, i.e. for

chordal downcomers, the liquid velocity will have no component in the y-direction (see Figure 3.3). This may not fully describe the practical situation, but no experimental work is available for this area. Liquid velocity distributions at the inlet may depend on downcomer hydraulics (e.g. liquid back-up) and also the resistance to flow across the tray itself.

In the absence of a more realistic way to model the velocity distribution, the approximation of uniform flow normal to the weir has been used.

3.4.2 Centre-line

The liquid flow pattern is assumed to be symmetrical about the centre-line of the tray. Deviations from this in practice are mainly due to unavoidable imperfections in the installation of trays (e.g. *out-of-levelness*). Chambers (1993) reported liquid swirl on a single tray air-water distillation simulation rig. This effect was due to the gas distribution system and is thought either not to be present in columns (depending on reboiler design) or to be rectified within a few trays of the reboiler as the vapour rises.

At the centre-line, $v_{i,j} = 0$, therefore, utilising a similar relationship to the one presented in Equation 3.25, we get $v_{i,j-1/2} = - v_{i,j+1/2}$. For the x-velocity and the pressure we can use $u_{i,j-1} = u_{i,j+1}$ and $P_{i,j-1} = P_{i,j+1}$, respectively

3.4.3 Wall

Here the assumption is made that there is no slip at the wall (i.e. both the x- and y-velocities are zero). Again, this is probably on over-simplification of the situation, but a lack of data necessitates this assumption. Lockett (Lockett & Safekourdi 1976) quotes Bell (Bell & Solari 1974b) as measuring velocity distributions indicating that there is slip at the wall, but this is not elaborated on.

The possibility exists that a turbulent wall function may be used to describe the liquid flow in this region, but the nature of the turbulence on distillation trays (liquid phase turbulence being dominated by the effects of the vapour phase) would bring into doubt the use of current relationships which are primarily for use with single phase flow.

For the solution of the velocity equations, the tray wall is approximated by a square mesh. This is illustrated for a wall coinciding with the y-edge of a cell in Figure 3.4.

Since there is no slip at the wall, both the x- and y-velocities must be zero. Due to the nature of the numerical method, the calculation procedure must still be carried out for this cell. The result, when continuity is obeyed, must be that the velocities are zero.

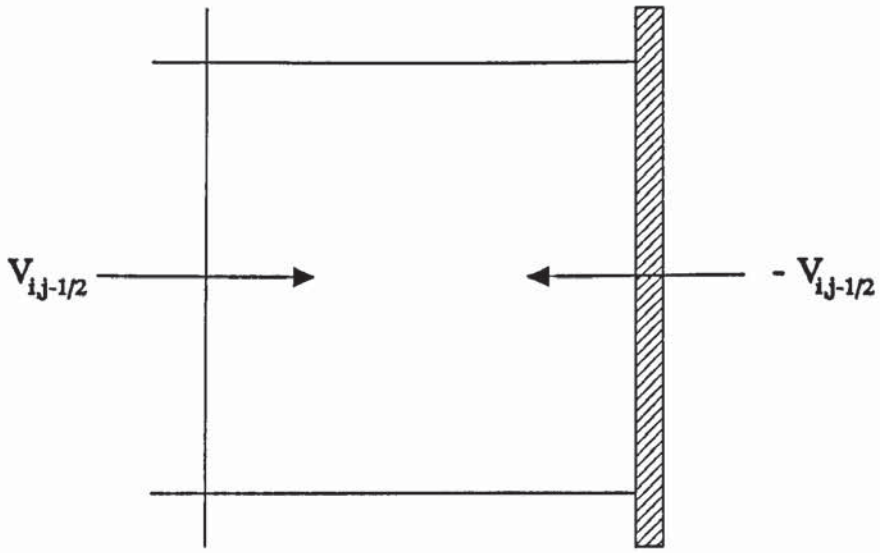

Figure 3.4: The no slip boundary condition for a wall coinciding with the y-edge of a cell

For this cell, the x-velocities are set to zero and the relationship illustrated by Equation 3.25 gives us the y-velocity at the wall. ie. $v_{i,j} = 0$, so $v_{i,j+1/2} = - v_{i,j-1/2}$.

A similar approach is taken with walls coinciding with the x-edge of a cell.

3.4.4 Outlet

The outlet boundary condition is the most difficult to define. Yu et al. (1991) proposed imposing a liquid velocity profile across the outlet but, in addition to this being inflexible, the distribution proposed was found to be almost uniform. This does not agree with flow distributions measured experimentally (Hine 1991) which suggest that the distribution is an inverted parabola with the maxima located just inside the

outer edges of the weir (see Figure 3.5).

In a later publication (Porter et al. 1992), Yu suggests an alternative boundary condition. He assumes that the liquid flow is fully-developed at the outlet. This is not true in practice due to the irregular shape of the tray (a converging channel near the outlet), but this condition can be used as an approximation under certain conditions; those of low viscosity. This means that the velocity profiles at the outlet have a negligible effect flow up-stream. Yu was able to use this condition successfully only because of the inadequate method used to model liquid turbulence (vastly under-predicting it). In practice, the turbulence is still very high at this point (except in cases where an outlet calming zone is used to prevent the liquid being aerated in this region).

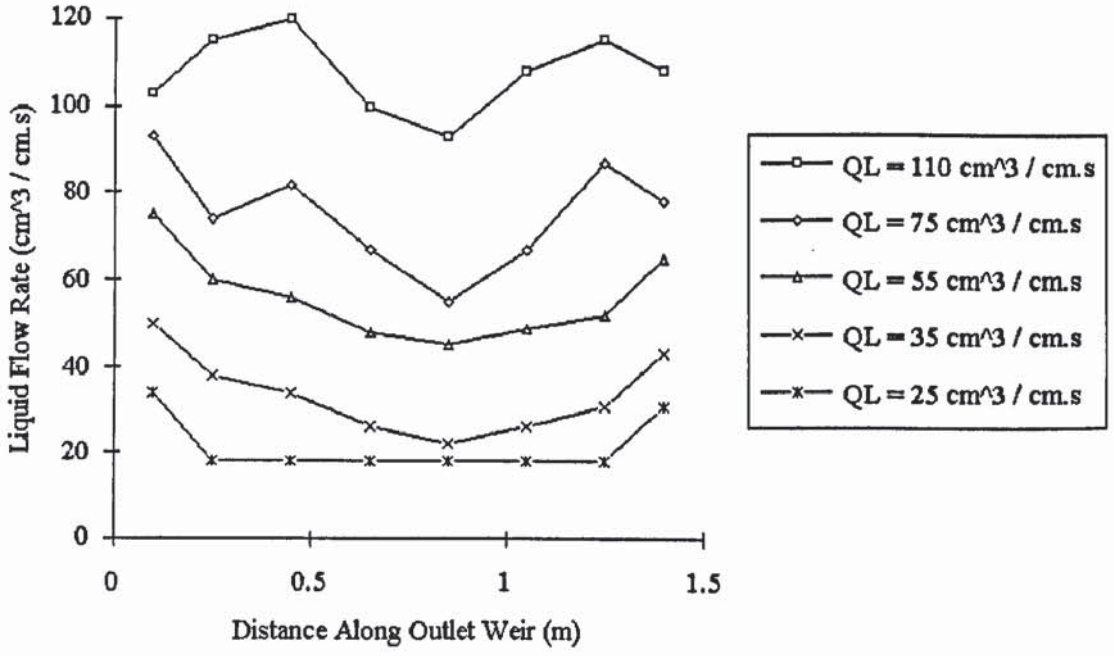

Figure 3.5: A typical flow distribution across the outlet weir of a 2.44 metre diameter sieve tray for a superficial vapour velocity of $0.7ms^{-1}$

A solution indicated in CFD literature (Fluent 1990) for such a situation, is that the calculation domain be extended to a point where the velocity profiles can be approximated be fully developed flow with negligible effect on the velocities in the

area of interest. This effectively would add an additional hypothetical rectangular outlet channel onto the circular tray (see Figure 3.6).

Any effects that the outlet weir itself may have on the velocity profiles are ignored in this work. It can be seen by comparing the velocity experimental velocity distribution (Figure 3.5) with a distribution predicted by this method (Figure 3.7) that the weir must have an effect.

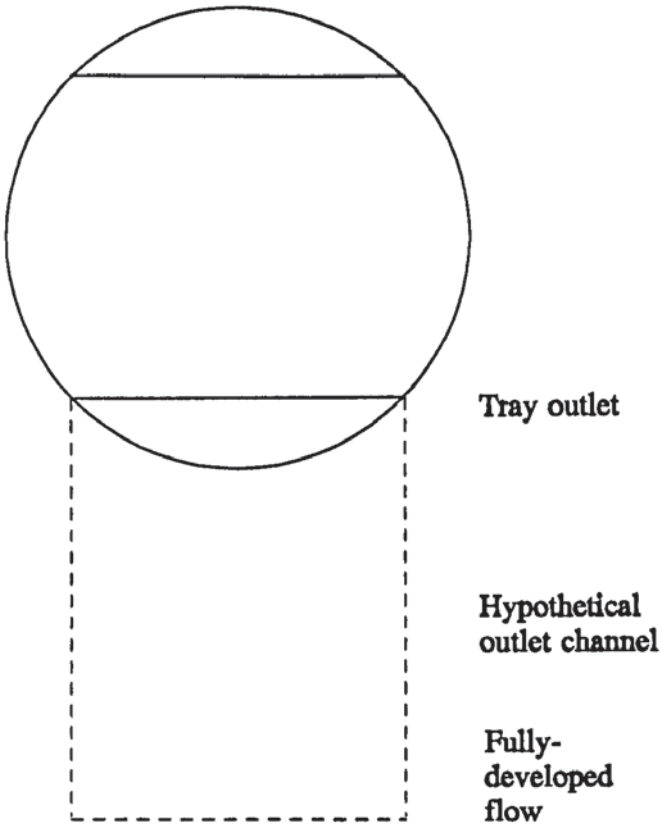

Figure 3.6: The hypothetical outlet channel used to calculate liquid velocity profiles at the tray outlet

Solari et al. (1982) observed that at high liquid rates, liquid impacting against the outlet weir was diverted into the side regions of the tray and induced circulations. This suggests that the outlet weir could be considered as a resistance to flow which could be modelled by modification of the resistance terms in Equation 3.10 at the tray outlet.

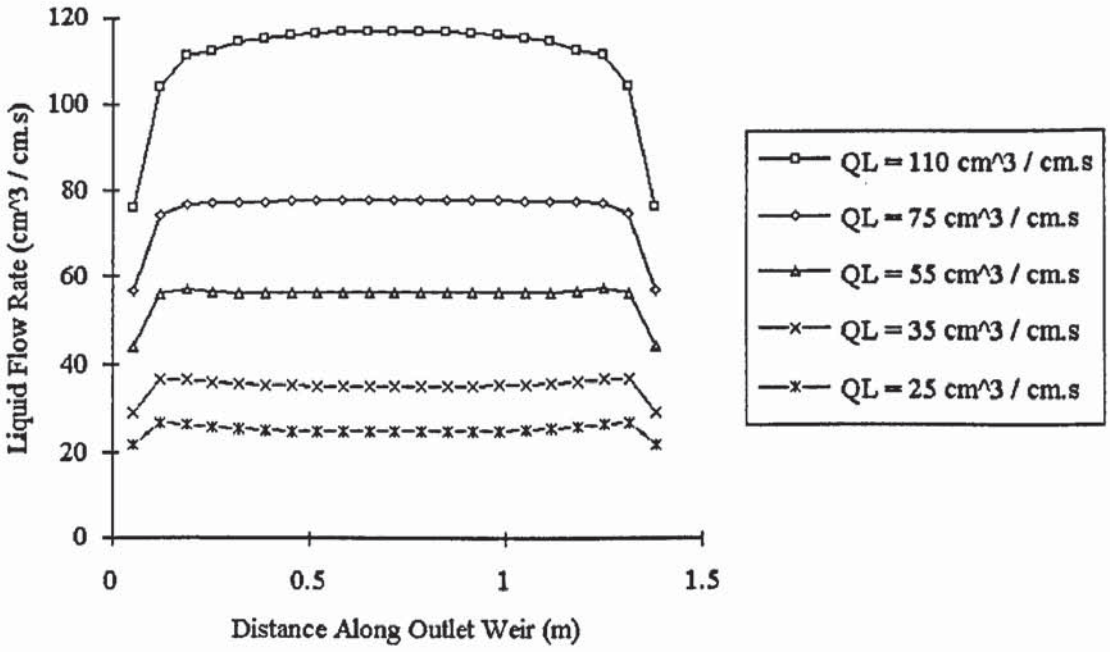

Figure 3.7: Theoretical liquid flow profiles at the tray outlet predicted using the fluid mechanical model for a superficial vapour velocity of 0.7 ms^{-1}

3.5 Comparison of Theoretical Velocity Vector Diagrams With Experimental Flow Pointer Data

Chambers (1993) carried out some studies into liquid flow patterns on a 2.44 metre diameter air-water distillation simulation rig containing a single sieve tray. Some of these experiments have been simulated using this model in order to provide a comparison for the predicted flow patterns over a range of operating conditions. A technique of using 32 flow pointers (a structure similar to a weather vane with an arrow on to indicate the direction of flow) spread over the bubbling area of the tray was used to indicate the direction of flow of the liquid. This technique gives no real idea of the liquid velocities.

Three sets of data were chosen for this comparison corresponding to attempts to simulate the liquid and vapour flow rates present under conditions of vacuum, atmospheric pressure and moderate pressure distillation (see also Table 4.1).

Chambers noted that for vacuum distillation the liquid was in forward flow over the entire tray (see Figure 3.8). The slight deviations from forward flow were accounted for by the initial transverse movement of the liquid into the segmental regions of the tray in the first half of the flow path. The flow pattern predicted by the Yu fluid mechanical model (Figure 3.9) shows similar directions of flow. This will be discussed in more detail in Chapter 4.

The experimental flow patterns for atmospheric and moderate pressure distillation simulation both showed similar trends (see Figures 3.10 and 3.12, respectively). They show the forward flow of liquid down the centre section of the tray with slight circulation present in the segmental areas at the edges of the inlet downcomer. Chambers thought the circulations to be small in nature, occupying between 12% and 15% of the bubbling area of the tray. The flow patterns predicted by the Yu fluid mechanical model show the liquid to be flowing mainly down the centre of the tray with the segmental regions being virtually stagnant (see Figures 3.11 and 3.13). Close inspection of the velocity profile data shows no circulations are predicted for any of the cases simulated here.

Note: the data obtained from experiment is presented in the form of directional arrows with no indication of the actual liquid velocity, whereas the theoretical data obtained from the Yu fluid mechanical model is expressed as normalised velocity vectors, with the length of the arrow being proportional to the velocity of the liquid at a point relative to the liquid velocity at the inlet.

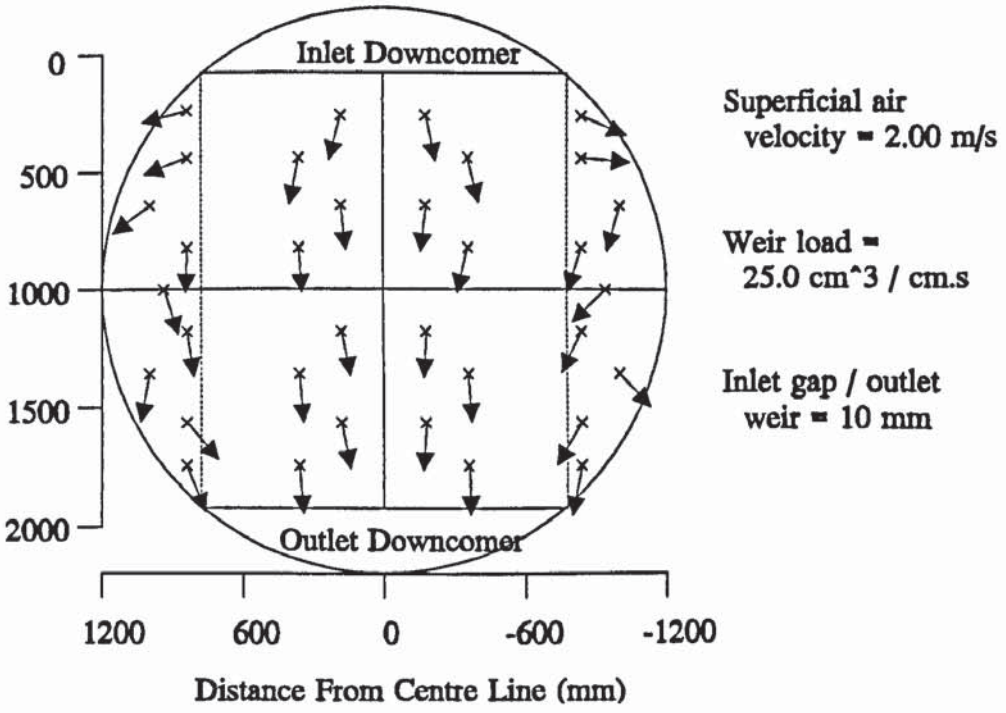

Figure 3.8: Experimental flow pointer data showing forward flow only during the simulation of vacuum distillation

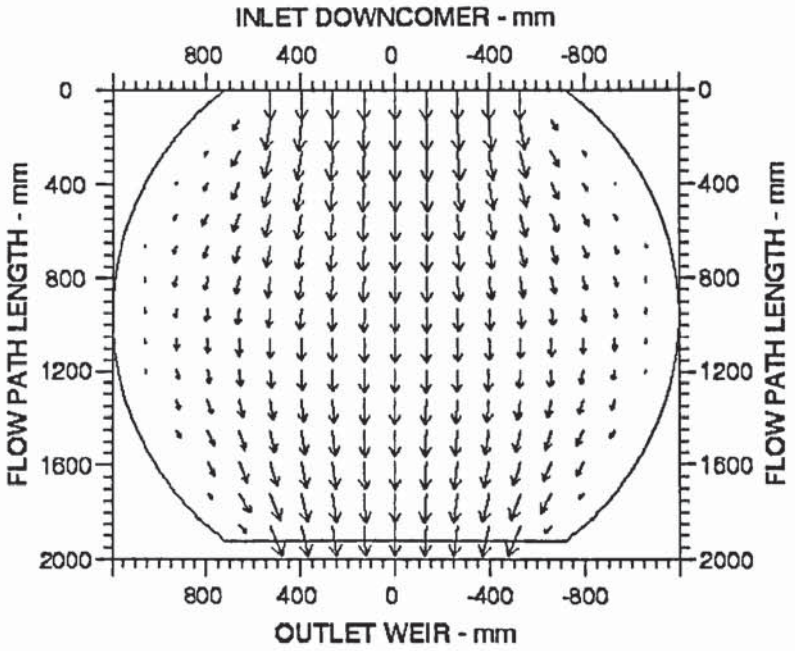

Figure 3.9: Flow patterns for simulated vacuum distillation predicted using the Yu fluid mechanical model (Weir load = 25 $cm^3/cm.s$, superficial air velocity = 2 m/s)

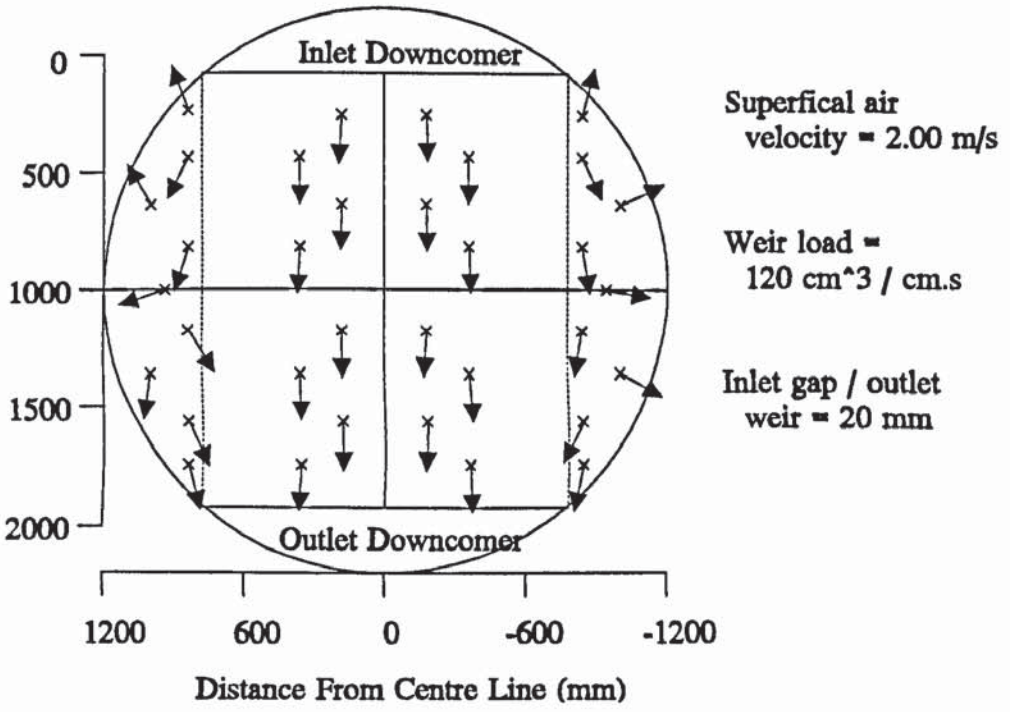

Figure 3.10: Experimental flow pointer data for atmospheric pressure distillation simulation showing small liquid circulations near the inlet downcomer

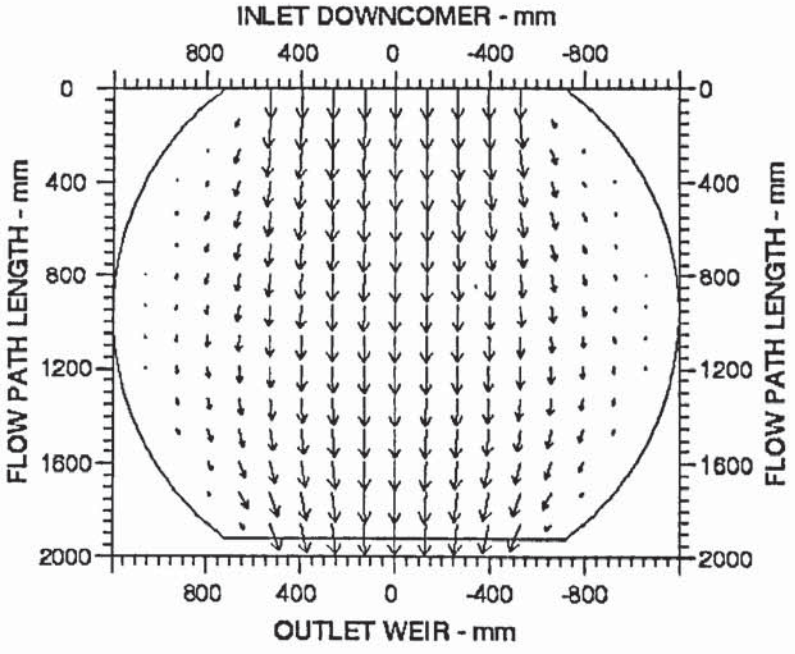

Figure 3.11: Flow patterns for simulated atmospheric pressure distillation predicted using the Yu fluid mechanical model (Weir load = 120 $cm^3/cm.s$, superficial air velocity = 2 m/s)

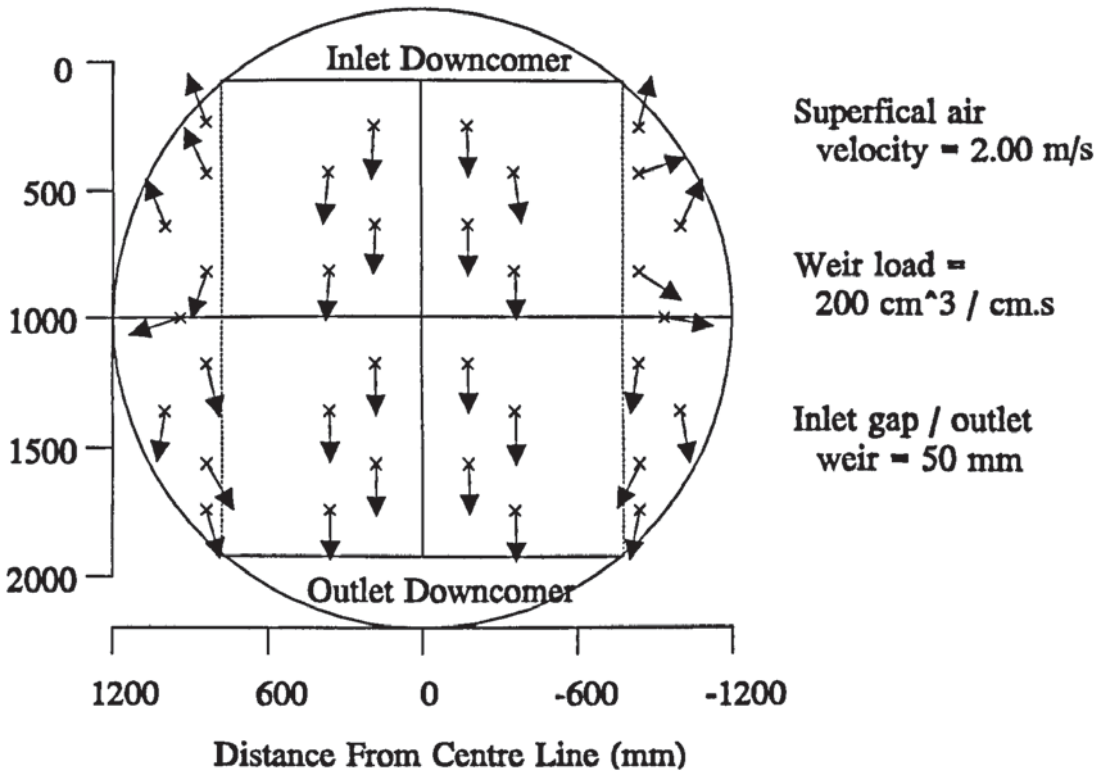

Figure 3.12: Experimental flow pointer data for moderate pressure distillation simulation showing small liquid circulations near the inlet downcomer

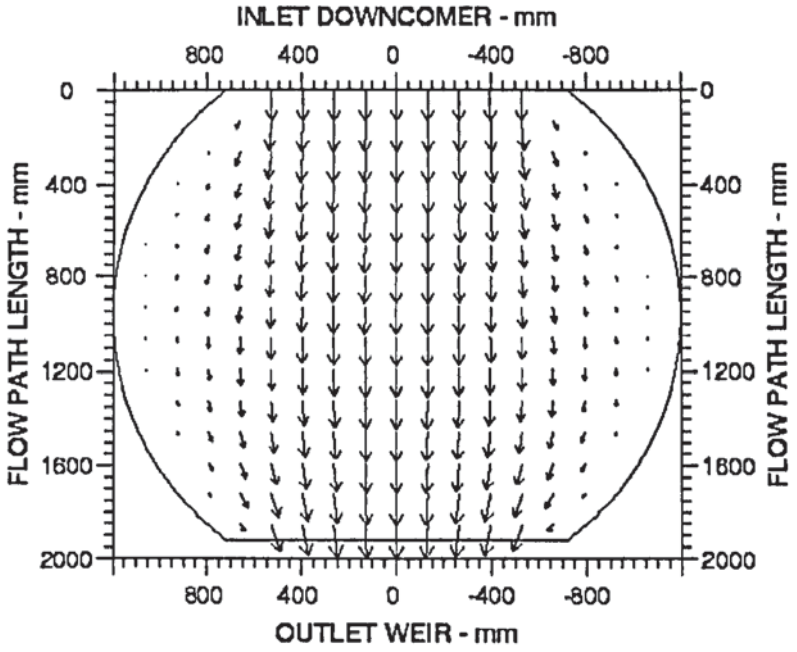

Figure 3.13: Flow patterns for simulated moderate pressure distillation predicted using the Yu fluid mechanical model (Weir load = 200 cm^3/cm.s, superficial air velocity = 2 m/s)

3.6 Conclusions

The Yu fluid mechanical model as presented here seems to be able to predict the general trends in the flow patterns when compared with experimental flow pointer data obtained from the 2.44 metre diameter air-water simulation rig at Aston University.

This method of comparison of experimental flow pointer data against predicted velocity profiles is limited. Due to the nature of the flow pointer, it cannot be relied upon to give any indication of the local liquid velocity, only the direction of flow. For this reason, the accuracy of the predicted velocity profiles cannot be judged purely on this criterion.

For vacuum simulation, both the experimental data and the fluid mechanical model predict forward flow of liquid over the entire tray. Under conditions of atmospheric pressure and moderate pressure simulation, the experimental data seems to indicate the existence of small circulating regions in the segmental regions of the tray near to the edge of the inlet downcomer. The fluid mechanical model fails to predict these; the liquid is predicted to be virtually stagnant in this region, but otherwise seems to model the flow patterns with reasonable accuracy.

CHAPTER 4

4. SIMULATION OF MASS-TRANSFER ON A SINGLE TRAY

4.1 Introduction

In order to test theoretical models against experimental data, it is necessary to have a better range of test criteria than purely the comparison of predicted velocity vectors against flow pointers as described in Chapter 3. In order to achieve this, and to get an idea of the tray efficiencies associated with the flow pattern, it is necessary to calculate concentration profiles which can be compared with experimental temperature profiles.

Another alternative to the calculation of concentration profiles would be to calculate residence time profiles. Despite the fact that residence time profiles are independent of mass-transfer rates, and so can provide data which may be better for the direct comparison of flow patterns, there are some distinct disadvantages when comparing these data to experimental data.

1) It is more difficult to obtain residence time data from experimental measurements than to simply record a series of temperatures from tray-mounted thermometers.
2) Residence time distributions would be highly dependent on the predicted height of clear liquid. It will be shown later that the same is not true for concentration profiles and tray efficiencies (see Section 6.5).

It is for these reasons that this work will be discussed in terms of concentration profiles and not residence time profiles, though it is acknowledged that residence time profiles will be a better measure of the performance of a tray when theoretically comparing alternative tray designs. It must be noted, however, that a change in tray design may also affect the point efficiency and, hence, the flow pattern is not the only factor which must be considered. See, for example, the discussion on how the structure of froth effects point efficiencies presented by Lockett and Plaka (1983).

Previous work (Lockett & Safekourdi 1976) has been carried out into the development of a general mass-transfer program capable of taking velocity profiles and calculating concentration profiles. In its final form, this work took account of flow profiles in the form of a stream function, not as x- and y-velocities, but this approach is easily adapted.

For simplicity, the local rate of mass-transfer is modelled in terms of a point efficiency, which is derived from experimental data (see Section 4.7.2).

4.2 Derivation of Equations

Before the mass-transfer equation is derived, it is necessary to state the assumptions made:

1) the point efficiency is constant over the bubbling area of the tray,
2) the equilibrium relationship can be considered to be linear over the range of concentrations on the tray, and can be represented in the form:

$$C_v = mC + b \qquad (4.1)$$

where:
- C_v is the mole fraction of the most volatile component in the vapour,
- C is the mole fraction of the most volatile component in the liquid,
- m is the slope of the equilibrium curve,
- b is a constant

3) the liquid is perfectly mixed in the vertical direction
4) eddy diffusion can be used to model liquid mixing. It is equal in the axial and transverse directions,
5) the clear liquid height is constant over the tray,
6) vapour flow is uniform across the bubbling area of the tray.

It should be noted that assumptions 3 to 6 are similar to assumptions made in the derivation of the Yu fluid mechanical model (see Section 3.2).

The model is derived from a mass balance about a differential element of froth, shown in Figure 4.1.

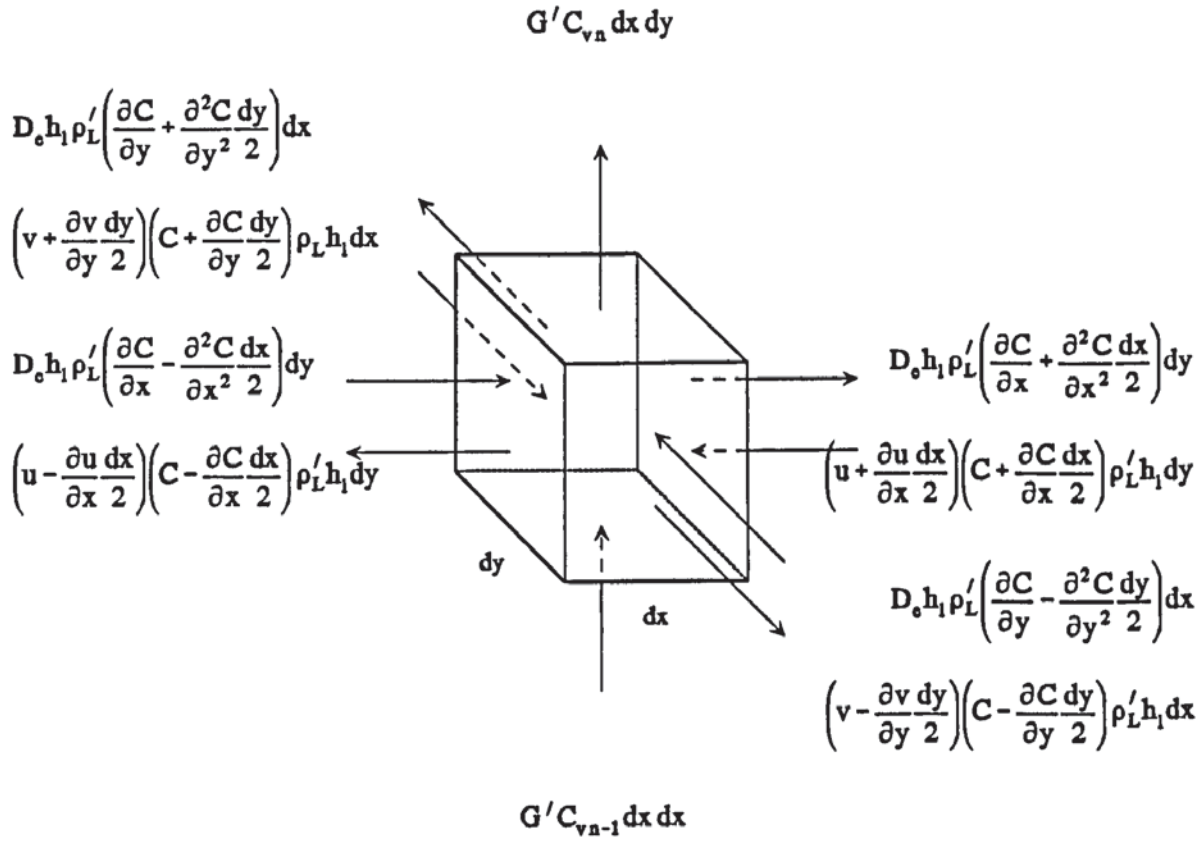

Figure 4.1: Mass balance over a differential element of froth

Here the subscripts n and n-1 refer to the tray from which the vapour is leaving. The vapour leaving the tray in question is denoted by the subscript n, while the vapour leaving the tray below, and hence entering the tray in question, is denoted by the subscript n-1.

At steady-state the mass balance yields:

$$D_e \rho_L' h_l \left\{\frac{\partial^2 C}{\partial x^2} + \frac{\partial^2 C}{\partial y^2}\right\} - \rho_L' h_l \left\{u\frac{\partial C}{\partial x} + v\frac{\partial C}{\partial y} + \frac{\partial u}{\partial x}C + \frac{\partial v}{\partial y}C\right\} + G'(C_{vn-1} - C_{vn}) = 0 \quad (4.2)$$

By using the continuity equation (Equation 3.9), this reduces to:

$$D_e \rho_L' h_l \left\{\frac{\partial^2 C}{\partial x^2} + \frac{\partial^2 C}{\partial y^2}\right\} - \rho_L' h_l \left\{u\frac{\partial C}{\partial x} + v\frac{\partial C}{\partial y}\right\} + G'(C_{vn-1} - C_{vn}) = 0 \quad (4.3)$$

The point efficiency, E_{OG}, is defined as:

$$E_{OG} = \frac{C_{vn} - C_{vn-1}}{C_v^* - C_{vn-1}} \quad (4.4)$$

where $C_{v\,n}$ and $C_{v\,n-1}$ are the composition of the vapour leaving and entering an element of froth respectively. C_v^* is the composition of the vapour in equilibrium with the liquid C_n.

If we define the composition of the liquid in equilibrium with $C_{v\,n-1}$ as $C_{e\,n-1}^*$, then by using Equation 4.1, Equation 4.4 becomes

$$E_{OG} = \frac{C_{vn} - C_{vn-1}}{m\left(C - C_{en-1}^*\right)} \quad (4.5)$$

On re-arranging and substitution into Equation 4.3, we get

$$D_e \rho_L' h_l \left\{\frac{\partial^2 C}{\partial x^2} + \frac{\partial^2 C}{\partial y^2}\right\} - \rho_L' h_l \left\{u\frac{\partial C}{\partial x} + v\frac{\partial C}{\partial y}\right\} - mG' E_{OG}\left(C - C_{en-1}^*\right) = 0 \quad (4.6)$$

We can now use the following substitutions; $G' = G/A$, $L = Q_L\, \rho_L'$ and $\lambda = mG/L$,

$$D_e \left\{\frac{\partial^2 C}{\partial x^2} + \frac{\partial^2 C}{\partial y^2}\right\} - \left\{u\frac{\partial C}{\partial x} + v\frac{\partial C}{\partial y}\right\} - \lambda E_{OG}\left(\frac{Q_L}{Ah_l}\right)\left(C - C_{en-1}^*\right) = 0 \quad (4.7)$$

It is possible to put this equation into dimensionless form

$$\frac{1}{Pe}\left\{\frac{\partial^2 C}{\partial X^2}+\frac{\partial^2 C}{\partial Y^2}\right\}-\left\{U\frac{\partial C}{\partial X}+V\frac{\partial C}{\partial Y}\right\}-\lambda E_{OG}\left(\frac{WD}{A}\right)\left(C-C^{*}_{en-1}\right)=0 \quad (4.8)$$

where,

$$X=\frac{x}{D},\ U=\frac{u}{U_0},\ Pe=\frac{DU_0}{D_e},$$
$$Y=\frac{y}{D},\ V=\frac{v}{U_0},\ U_0=\frac{Q_L}{W h_l} \quad (4.9)$$

4.3 Numerical Method

4.3.1 Discretisation

As with the liquid flow equations, Equation 4.7 is solved by a finite difference technique, but this time using a standard finite difference mesh containing all data defined on grid nodes (see Figure 4.2).

This leads to the finite difference approximations defined below:

$$\frac{\partial C}{\partial x}\approx\frac{C_{i+1,j}-C_{i-1,j}}{2\,\delta x} \quad (4.10)$$

$$\frac{\partial^2 C}{\partial x^2}\approx\frac{C_{i+1,j}-2\,C_{i,j}+C_{i-1,j}}{\delta x^2} \quad (4.11)$$

Terms concerning the y-direction are defined in a similar fashion using the j index.

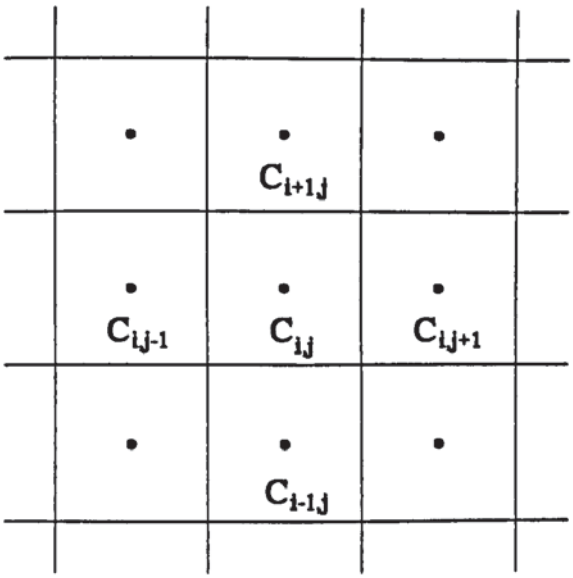

Figure 4.2: Finite difference grid used for solving the concentration equations

On substitution of the finite difference approximations into Equation 4.7, for the case where $\delta x = \delta y = \Delta$, we get

$$\frac{D_e}{\Delta^2}\left(C_{i+1,j}+C_{i-1,j}+C_{i,j+1}+C_{i,j-1}-4\,C_{i,j}\right)-u_{i,j}\frac{C_{i+1,j}-C_{i-1,j}}{2\,\Delta} - v_{i,j}\frac{C_{i,j+1}-C_{i,j-1}}{2\,\Delta}-\lambda\,E_{OG}\left(\frac{Q_L}{A\,h_l}\right)\left(C_{i,j}-C^*_{n-1}\right)=0 \tag{4.12}$$

This is re-arranged to become

$$C_{i,j}=\frac{k_1 C_{i+1,j}+k_2 C_{i-1,j}+k_3 C_{i,j+1}+k_4 C_{i,j-1}+k_5}{k_6} \tag{4.13}$$

where

$$k_1=\frac{D_e}{\Delta^2}-\frac{u_{i,j}}{2\Delta},\quad k_3=\frac{D_e}{\Delta^2}-\frac{v_{i,j}}{2\Delta},\quad k_5=\lambda\,E_{OG}\left(\frac{Q_L}{A\,h_l}\right)C^*_{n-1},$$
$$k_2=\frac{D_e}{\Delta^2}+\frac{u_{i,j}}{2\Delta},\quad k_4=\frac{D_e}{\Delta^2}+\frac{v_{i,j}}{2\Delta},\quad k_6=4\,\frac{D_e}{\Delta^2}+\lambda\,E_{OG}\left(\frac{Q_L}{A\,h_l}\right) \tag{4.14}$$

4.3.2 Algorithm

The mass-transfer profile is solved by a simple iterative relaxation technique. The calculation grid is swept with increasing i and j applying Equation 4.13 at each point using the most recent values of the concentrations calculated for the surrounding points. The new value of $C_{i,j}$ is then computed

$$C_{i,j}^{m+1} = \beta\, C_{i,j}^{m} + (1 - \beta)\, C_{i,j}^{calc} \qquad (4.15)$$

where β is the relaxation parameter ($0 < \beta \leq 1$).

The calculation procedure has converged when the average absolute change in $C_{i,j}$ is small.

Like the velocity calculations, the concentrations are calculated using single precision variables in the FORTRAN program. A discussion of this and other matters dealing with the accuracy of the calculations can be found in Appendix 3.

4.4 Boundary Conditions

4.4.1 Inlet

Previous workers (Porter et al. 1972, Safekourdi 1975) used the Danckwerts boundary condition (Danckwerts 1953) but, as explained in Section 2.3.3, this is not entirely valid since it does not take into account the concentration gradients in the transverse direction caused by the side regions of the tray.

If we consider the liquid inlet (Figure 4.3), then we can see that the high degree of turbulence on the tray caused by the vapour induces liquid back-mixing under the inlet gap. Since, under ideal conditions, no vapour is present in the downcomer to cause the intense turbulence experienced on the tray, any mixing in the downcomer is small compared to the mixing on the tray immediately next to the downcomer and is ignored. When applied to Equation 4.13, this is expressed as $C_{i-1,j} = C_{i,j}$ for all i = 1.

When a simplified case of no transverse concentration gradients is considered, this will be identical to the Danckwerts boundary condition, but it still allows liquid mixing in the transverse direction for more complex flows.

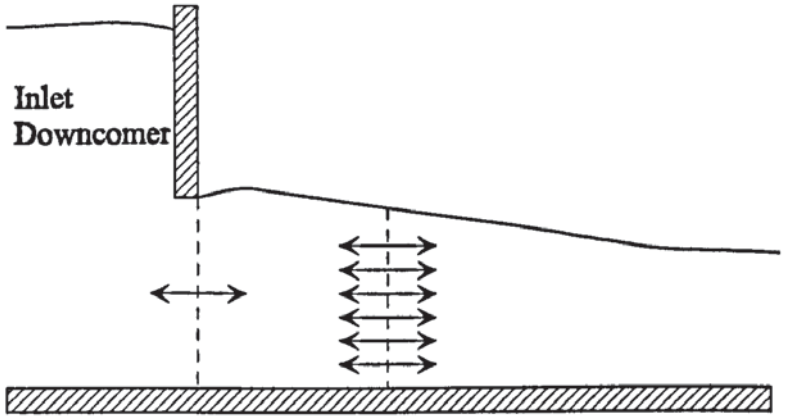

Figure 4.3: Back-mixing at the liquid inlet

4.4.2 Centre-line

As with the fluid mechanical model, symmetry is assumed about the centre-line of the tray.

4.4.3 Wall

Unlike with the fluid mechanical model, here the walls are considered to be curved, though the finite difference grid used to approximate the calculation domain is square. Lim (1973) determined that the curved tray wall could intersect with a grid cell in one of 18 ways. He continued to derive a series of equations for each case based on the assumption that there was no diffusion normal to the tray wall. The procedure for deriving such equations is described by Fox (1962). This is described in more detail in Appendix 2.

4.4.4 Outlet

The outlet condition of no diffusion over the outlet weir (Wehner & Wilhelm 1956) was used.

4.5 Experimental Temperature Profiles

4.5.1 Heat and mass-transfer analogy

The cooling of hot water by rising air on an operating tray provides an analogy between heat and mass transfer. Therefore, a heat balance can be constructed from which point and tray efficiency calculations can be made.

T_{in} represents the temperature of hot water entering the test tray, whereas T_{out} represents the average temperature of the water leaving the tray. Air rises up to the tray with a uniform enthalpy H_1 whilst H_2 represents the average enthalpy of air leaving the froth dispersion. Therefore, on the basis of air enthalpy, the Murphree tray efficiency, E_{MV}, may be defined as:

$$E_{MV} = \frac{H_2 - H_1}{H^*_{Tout} - H_1} \tag{4.16}$$

where H^*_{Tout} is the enthalpy of saturated air in equilibrium with the average temperature of the water leaving the tray. Similarly the Murphree point efficiency in terms of air enthalpy at position i is defined as:

$$E_{OG} = \frac{H_{2i} - H_1}{H^*_{Ti} - H_1} \tag{4.17}$$

where T_i is the local water temperature at position i on the tray and H^*_{Ti} is the saturated air enthalpy at temperature T_i; H_1, H^*_{Tout} and H^*_{Ti} were calculated from psychometric data tables. During water cooling, water temperature data acquisition is carried out at fixed air and water flow-rates which permits the calculation of the overall air enthalpy leaving the froth, H_2, from the heat balance:

$$G(H_2 - H_1) = L C_p(\overline{T}_{in} - \overline{T}_{out}) \tag{4.18}$$

Substituting (H_2 - H_1), from Equation 4.18, into Equation 4.16 will yield the Murphree

tray efficiency. The determination of point efficiency is based on the assumption that it is constant at all points on the tray. The calculation is made easier by noting the arrangement of the resistance thermometers (Figure 4.4) justifies the assumption that each platinum resistance thermometer (PRT) is representative of the same amount of tray area, and thus of the same gas flow rate. It then follows that:

$$H_2 = \frac{1}{n} \sum_{i=1}^{n} H_{2i} \qquad (4.19)$$

where n is the number of working resistance thermometers and H_{2i} is the saturated air enthalpy above the froth at each resistance thermometer i.

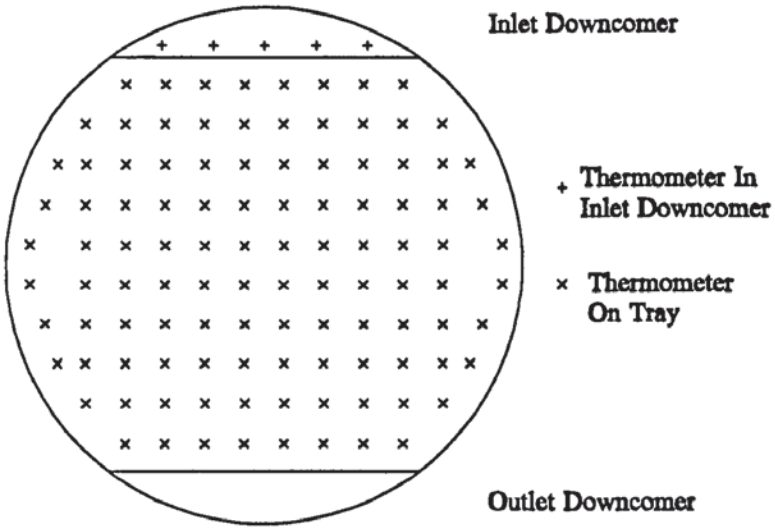

Figure 4.4: The arrangement of the resistance thermometers used in the calculation of the temperature profiles on the 2.44 metre air-water distillation simulation rig at Aston University

Now

$$(H_{2i} - H_1) = E_{OG}\left(H_{Ti}^{*} - H_1\right) \qquad (4.20)$$

and

$$(H_2 - H_1) = \frac{1}{n}\sum_{i=1}^{n}(H_{2i} - H_1) = \frac{E_{OG}}{n}\sum_{i=1}^{n}(H^*_{Ti} - H_1) \qquad (4.21)$$

Thus

$$E_{OG} = \frac{(H_2 - H_1)}{\frac{1}{n}\sum_{i=1}^{n}(H^*_{Ti} - H_1)} = \frac{\frac{L}{G}C_p(\overline{T}_{in} - \overline{T}_{out})}{(\overline{H}^*_{Ti} - H_1)} \qquad (4.22)$$

This is discussed in more detail by Chambers (1993).

4.5.2 The 2.44 metre diameter air - water distillation simulation rig at Aston University

The water-cooling experiments were designed to evaluate the tray efficiency models as described previously. Vapour-liquid contact was simulated by air-water contact and mass transfer was simulated by the combined heat and mass transfer which occurs when hot water is cooled by colder air. As in other water cooling operations, the rate of heat transfer was assumed to be proportional to an air enthalpy driving force. The theoretical justification for the enthalpy driving force is that used in the design of cooling towers (for an example see Porter et al. 1987). The point efficiency, E_{OG}, was also defined in terms of the enthalpy driving force. An important feature of the experimental evaluation is that the point efficiency used in the theoretical models may be determined from the experimental heat balance and the measured liquid temperature field on the tray, i.e. the experimental point efficiency is found independent of the unknown flow pattern.

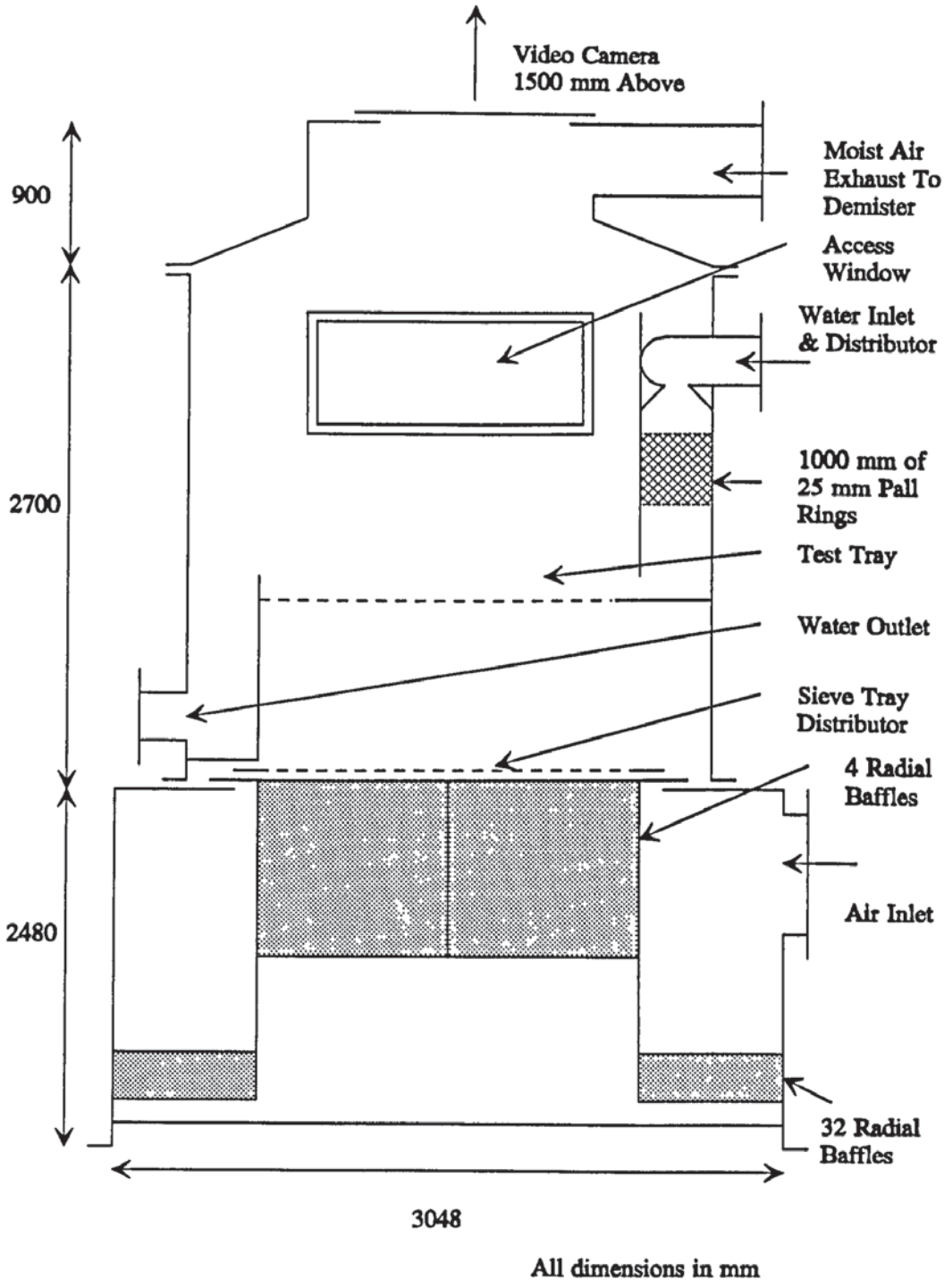

Figure 4.5: The layout of the 2.44 metre diameter test-rig at Aston University

The Aston test rig is 2.44 metres in diameter supplied with air and water flow rates of up to 12.2 m^3/s and 0.09 m^3/s respectively. The water, which is recycled round the ring, is heated by a combination of gas-fired and steam heat exchangers of 1.2 MW capacity. The water temperature is measured at the inlet and outlet and at 108 positions on the tray. Continuous data logging and data processing are used to obtain

temperature profiles (in the form of lines of constant temperature - isotherms), point efficiency and tray efficiency. The air enthalpy is measured by use of a combination of PRTs to measure the air temperature and wet bulb thermometers to measure the moisture content. The air flow rate is measured to within 0.2% and the water flow rate to within 2-3%.

Sieve plates with three sizes of holes have been tested (1 mm, 6 mm and 12 mm) all of 10% free area. A flow sheet of the test tray is given in Figure 4.4 and details of the column layout in Figure 4.5

An important property of the Aston test rig is its size. The previous work of Porter et al. (1972) predicted that the stagnant regions at the sides of the tray (Region 2 in Figure 2.7) become more important as the column diameter increases. This is because of the mixing of the liquid by the gas or vapour which, by moving liquid between Regions 1 and 2 (Figure 2.7), tends to cancel out flow pattern effects in a column of small diameter. A tray of 2.44 metre diameter is large enough to reveal the effects of a non-uniform flow pattern as well as being typical of columns used in industry.

The test rig is also used to support non-circular flow geometries in experiments to investigate the nature of open-channel two phase flow.

As mentioned previously, data from air-water experiments carried out on this rig has been selected for comparison with the predictions from this model. The data obtained simulate a column operating at total reflux under conditions of vacuum distillation, atmospheric pressure distillation and moderate pressure distillation. Since air and water were used as the fluids throughout this work and the simulator has a fixed operating pressure of atmospheric pressure, these variations were achieved through variation of the relative volumetric flow-rates of the air and the water.

The conditions used for comparison with the model predictions are presented in Table 4.1. In addition to the operating conditions, data referring to the height of clear liquid on the tray is also presented as this data was required for the model. Experimental

point efficiencies were also used in the calculation of the theoretical concentration profiles. These data are presented later (see Figures 4.12 to 4.14).

	Vacuum				Atmospheric Pressure				Moderate Pressure			
Inlet Gap / Outlet Weir Height (mm)	10 / 10				20 / 20				50 / 50			
λ	4.96				1.20				0.62			
Liquid Flow Rate ($cm^3/s.$ cm weir)	12.5	18.5	25	31	60	90	120	150	100	150	200	250
Super-ficial Air Velocity (ms^{-1})	1.0	1.5	2.0	2.5	1.0	1.5	2.0	2.5	1.25	1.5	2.0	2.5
Average Liquid Hold-up (mm)	15.3	15.4	13.5	11.0	22.8	23.1	21.1	14.2	36.6	35.5	23.7	22.8
Experi-mental Point Efficincy	0.36	0.41	0.45	0.48	0.77	0.86	0.82	0.81	0.88	0.94	0.87	0.83

Table 4.1: Operating conditions used for the experimental runs chosen for comparison with the theoretical models

4.6 Methods of Comparison Between Experimental and Theoretical Results

Details of the procedure for the calculation of the experimental tray efficiencies from the air-water cooling experiments have been provided previously (see Section 4.5.1) and the calculation of the theoretical concentration profiles has been given in Section 4.2. There are two methods for comparison of the results:

1) comparison of the experimental temperature profiles with the theoretical concentration profiles. To achieve this, both sets of data are scaled in order to ease the comparison. Two new parameters are defined; a reduced temperature and a reduced concentration,

$$T_r = \frac{T - T_{n-1}}{T_{in} - T_{n-1}} \tag{4.23}$$

$$C_r = \frac{C - C_{n-1}}{C_{in} - C_{n-1}} \tag{4.24}$$

When plotted graphically, experimental and theoretical data in this form should be directly comparable.

2) tray efficiencies were calculated for the theoretical concentration profiles for direct comparison with the data derived from the temperature profiles.

4.7 Comparison Between Experimental and Theoretical Profiles

Reduced temperature data obtained from experiment were plotted and contours generated by linear interpolation between the data points in order to obtain reduced isotherms (lines of equal reduced temperature) using the UNIRAS graphics subroutines (Chambers 1993). The reduced concentration data from the fluid mechanical simulation were treated in a similar fashion in order for the data to be directly comparable.

4.7.1 Vacuum simulation

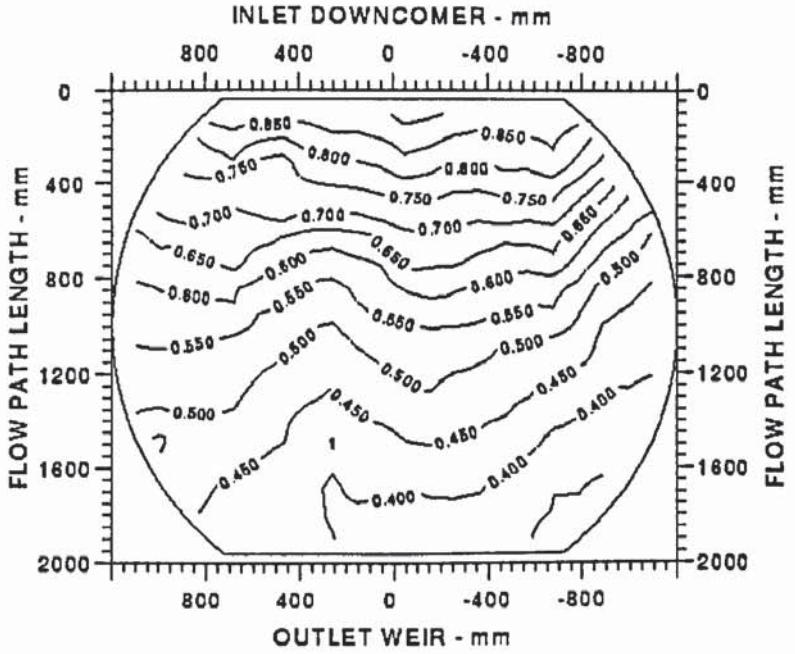

Figure 4.6: Experimental reduced isotherms lying parallel to the inlet down-comer obtained during simulated vacuum distillation (Weir load = 25 cm^3/cm.s, superficial air velocity = 2 m/s)

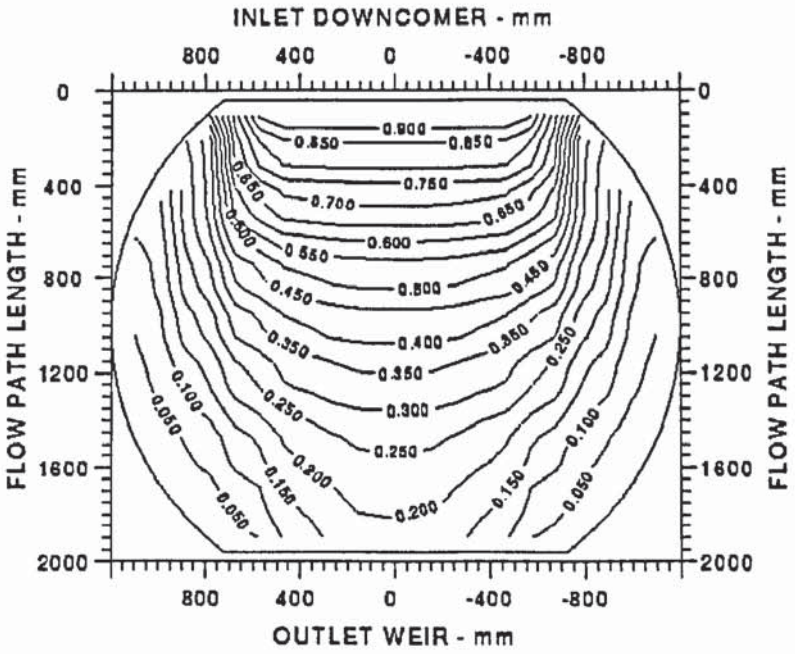

Figure 4.7: Circular reduced concentration contours emanating from the inlet down-comer obtained by simulation of vacuum distillation using the Yu fluid mechanical model (Weir load = 25 cm^3/cm.s, superficial air velocity = 2 m/s)

As can be seen from Figure 4.6, the experimental reduced isotherms seem to lie parallel to the inlet down-comer. This is in contrast to the data predicted from the fluid mechanical model (Figure 4.7) which shows almost circular contours emanating from the inlet. This is despite the similarities in the velocity flow profiles discussed in Chapter 3.

It is thought that the conditions under which the vacuum distillation simulation data were obtained were in the spray regime. This would mean that a significant proportion of the liquid would be transported as spray above a thin liquid continuous layer. This form of liquid transport is not taken into account by the Yu fluid mechanical model, and so, this model is thought not to be valid for these conditions. Concentration profiles of a similar shape to those obtained experimentally can be obtained by use of the *spray diffusion* model (Porter et al. 1977), though it is not capable of being used for liquid flow rates as high as this.

4.7.2 Atmospheric pressure simulation

The experimental reduced isotherms obtained under conditions of simulated atmospheric pressure distillation (see Figure 4.8) show the U-shape more generally associated with distillation outside the spray regime (Bell 1972). The areas of slow liquid circulation near the edges of the inlet down-comer do not seem evident from the contour diagram, possibly indicating that the circulations are very slow or virtually stagnant, as indicated by the fluid mechanical model (see Section 3.5).

The reduced concentration profiles predicted by the fluid mechanical model show the same general U-shape (Figure 4.9), but again, they seem more rounded in nature. This is probably due to the liquid being pushed into the segmental regions of the tray.

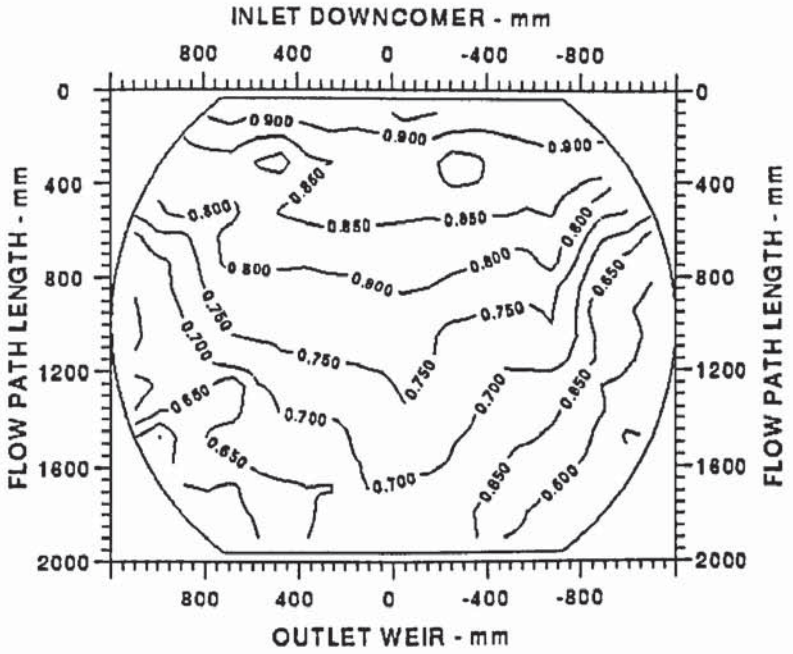

Figure 4.8: Experimental U-shaped reduced isotherms obtained during simulated atmospheric pressure distillation (Weir load = 120 $cm^3/cm.s$, superficial air velocity = 2 m/s)

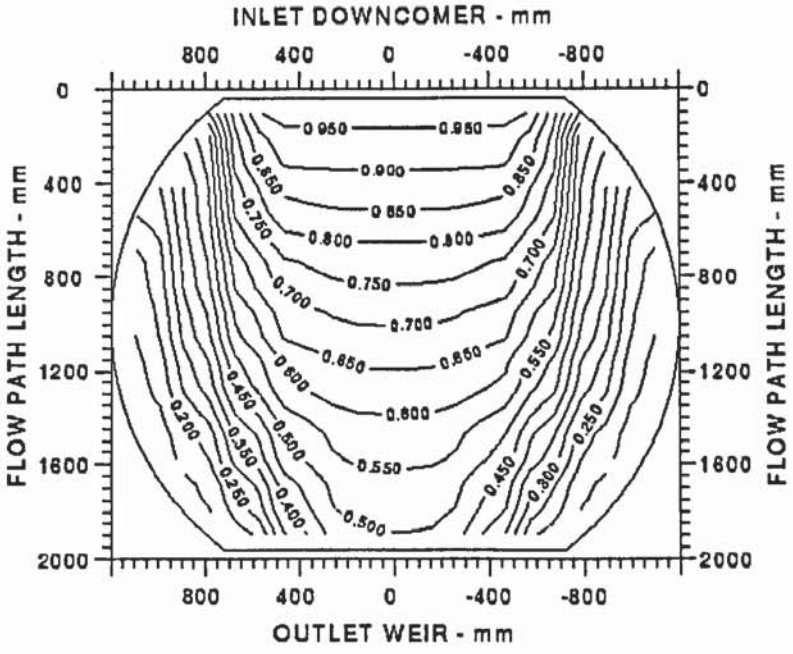

Figure 4.9: U-shaped reduced concentration profiles obtained for simulated atmospheric pressure distillation predicted using the Yu fluid mechanical model (Weir load = 120 $cm^3/cm.s$, superficial air velocity = 2 m/s)

4.7.3 Moderate pressure simulation

The experimental reduced isotherms (Figure 4.10) are U-shaped, though these seem to be sharper than those obtained for atmospheric pressure distillation simulation. Again, the contour diagram seem not to indicate the presence of the regions of liquid circulation near the edges of the inlet down-comer.

The reduced concentration profiles predicted by the fluid mechanical model (Figure 4.11) show also show sharper U-shaped profiles. Of the three simulated pressures, these seem to show the closest similarities between the experimental and predicted data. This is what is expected since the conditions which exist on the tray probably closest approximate to those assumed in the derivation of the model.

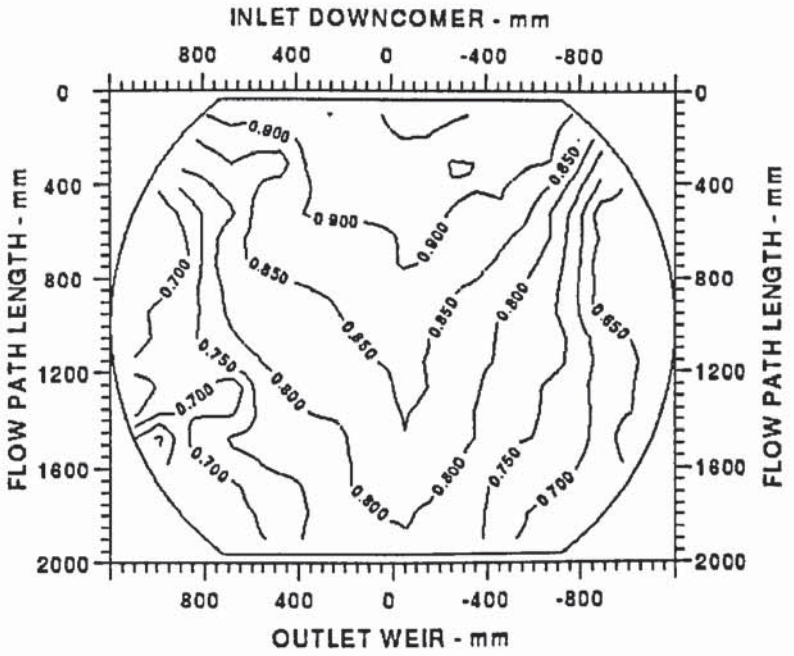

Figure 4.10: Experimental reduced isotherms showing sharp U-shaped profiles obtained for the simulation of moderate pressure distillation (Weir load = 200 $cm^3/cm.s$, superficial air velocity = 2 m/s)

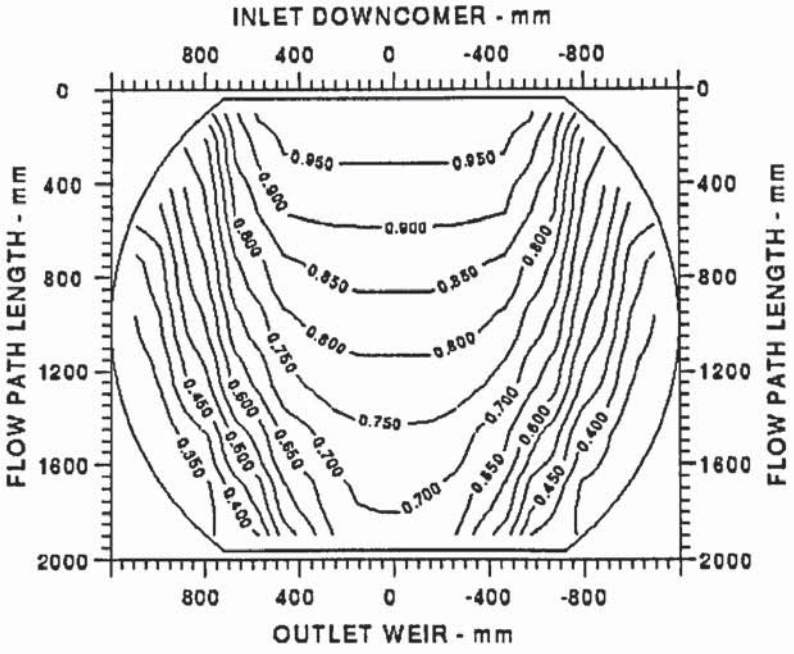

Figure 4.11: Sharp U-shaped reduced temperature profiles obtained for the simulation of moderate pressure distillation using the Yu fluid mechanical model (Weir load = 200 $cm^3/cm.s$, superficial air velocity = 2 m/s)

4.8 Comparison Between Experimental and Theoretical Efficiencies

Tray efficiencies were calculated in order to give a *quick and easy* method of comparing different models. A number of models were selected from those reviewed in Chapter 2; the *plug-flow plus back-mixing* model (Gerster et al. 1958) is both well-known to workers in this field and still widely used, though its deficiencies are acknowledged and the *stagnant regions* model (Porter et al. 1972) represents an intermediate step forward in the evolution of models as it is simple to use, but does not simplify the tray geometry.

4.8.1 Vacuum simulation

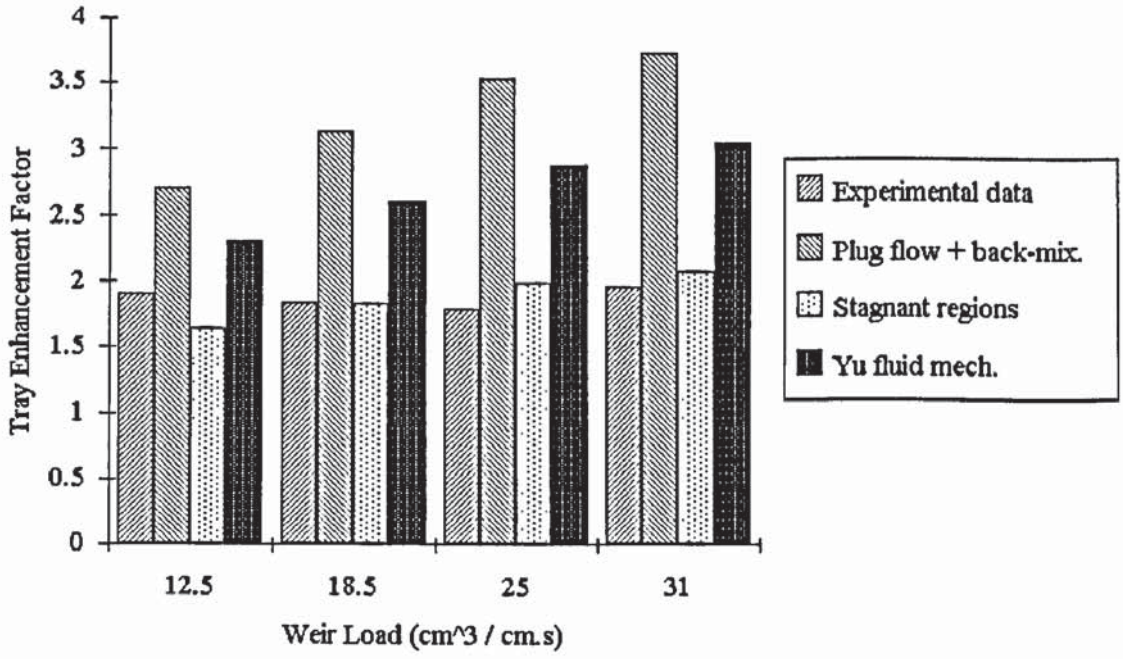

Figure 4.12: Comparison of experimentally determined tray efficiencies with those predicted by different models for simulated vacuum distillation (the numerical data used can be found in Appendix 4, Table A4.1)

As can be seen from Figure 4.12, the models used for comparison here do not predict tray efficiencies at low weir loads with any great degree of accuracy. The main exception to this is the stagnant regions model which seems capable of predicting the tray efficiency to within 14% of the experimental results. This is more by luck than

the accurate modelling of liquid flow and mass-transfer, since the liquid flow across a tray operating in the spray regime is more complex than the simplified flow pattern assumed by Porter et al. (1972). This is evident by a comparison between Figure 4.6 which shows concentration profiles in the spray regime and Figure 4.10 which shows flow patterns typical of liquid channelling between the inlet and outlet down-comers. Both the plug-flow plus back-mixing model and the fluid mechanical model continuously over-predict the experimental tray efficiencies.

At low weir loads the mechanism for liquid transport on distillation trays changes from a liquid continuous mechanism (the mixed-froth or emulsion flow regimes as discussed in Chapter 2) to a vapour continuous mechanism (the spray regime, also discussed in Chapter 2). It is thought that for the experimental simulation of vacuum distillation carried out, the tray was operating in the spray regime. The effect of this change in mechanism for liquid transport is to alter the shape of the concentration profiles. Liquid flow in the mixed-froth or emulsion flow regimes give rise to the U-shaped concentration profiles predicted by the stagnant regions model and the fluid mechanical model, but concentration profiles measured on trays operating in the spray regime give rise to flatter profiles which lie parallel to the inlet downcomer.

The only tray efficiency model to attempt to predict the flow of liquid in the spray regime is the spray diffusion model (Porter et al. 1977), but this is extremely limited in its application and cannot be used for these cases (as discussed in Section 2.4.4).

4.8.2 Atmospheric pressure simulation

For these data the models considered more closely predict the tray efficiencies measured experimentally. The *plug-flow plus back-mixing model* still over-predicts the experimental data by a significant amount (up to 35%) due to the fact that it fails to take into account the circular shape of the tray. The *stagnant region model* and the Yu fluid mechanical model lie either side of the experimental data. The fluid mechanical model over-predicts the experimental data by up to 12% whereas the stagnant region model under-predicts the data by up to 11%. This may demonstrate that the true flow pattern lies somewhere between that predicted by the fluid

mechanical model and that imposed by the stagnant regions model, i.e. some liquid flows into the side regions of the tray, but not as much as currently predicted by the fluid mechanical model.

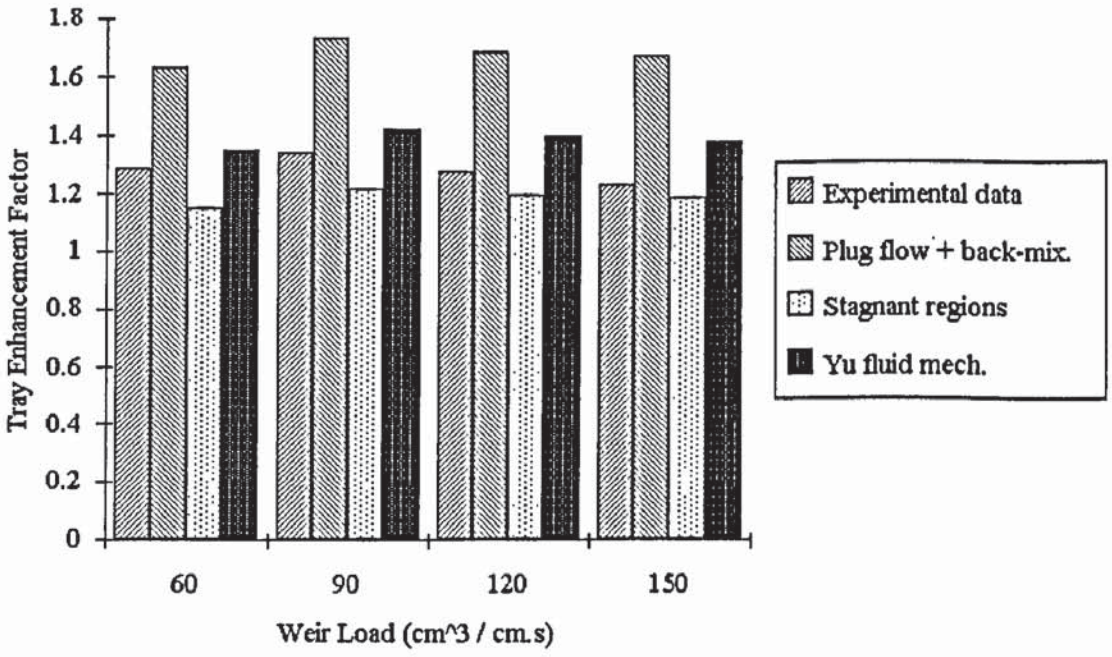

Figure 4.13: Comparison of experimentally determined tray efficiencies with those predicted by different models for simulated atmospheric pressure distillation (the numerical data used can be found in Appendix 4, Table A4.2)

The conditions under which these data were obtained are thought to lie mainly in the mixed-froth regime. This would mean that, while most of the liquid would be transported in a liquid continuous layer near the tray floor, this would be topped by a layer of spray (see Section 2.2.2). The proportion of liquid transported as spray must be small for the models to still be valid.

4.8.3 Moderate pressure simulation

The trends observed for the simulated atmospheric pressure distillation are continued here. Again, they show the experimental data lying between the stagnant regions model and the fluid mechanical model, but with a reduced margin between the two predictions. Now the fluid mechanical model over-predicts the experimental data by

up to 8% while the stagnant regions model under-predicts the data by up to 8%. This show that the models become more valid as the experimental conditions move away from the spray regime and into the emulsion flow regime. It may also indicate that at, an upper limit, the predictions of the fluid mechanical model may match those of the stagnant regions model.

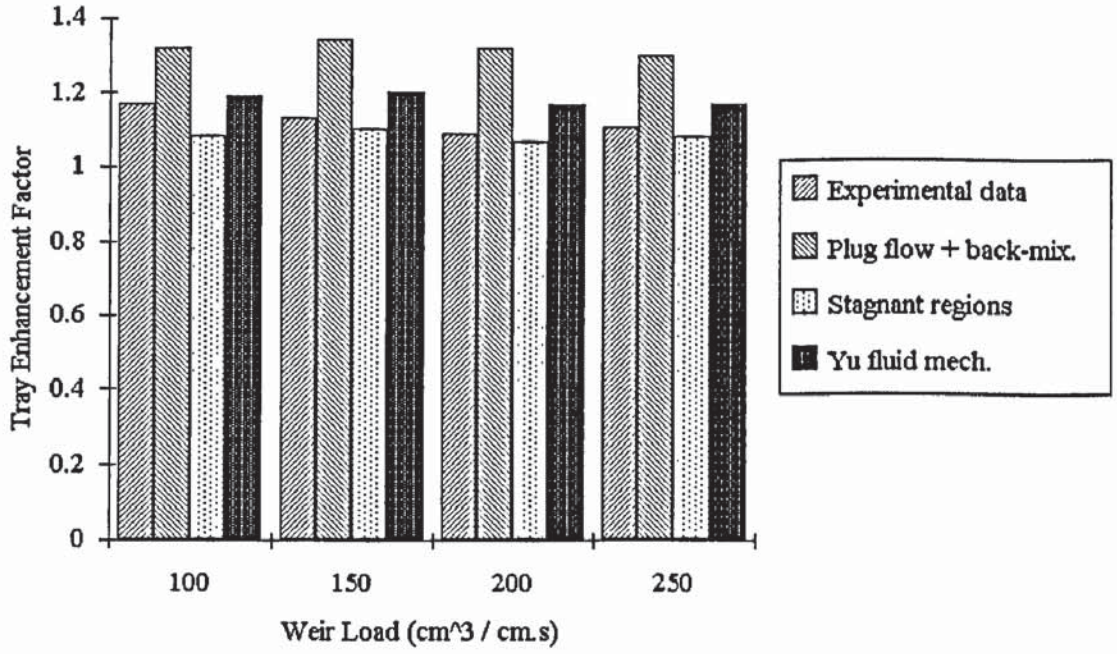

Figure 4.14: Comparison of experimentally determined tray efficiencies with those predicted by different models for simulated moderate pressure distillation (the numerical data used can be found in Appendix 4, Table A4.3)

It should be noted that the relationship between the tray enhancement factor and the liquid flow rate is not simple. Trends in both experimental and theoretical enhancement factors show that, as the liquid flow rate increases, the enhancement factor can either increase or decrease. This is thought to be due to the complex nature of the two-phase interactions which are occurring on the tray.

Factors which have to be taken into account when considering this matter include the two-phase flow regime (discussed in Chapter 2), the vapour hold-up fraction in the froth, the froth height on the tray, the liquid vapour contact area and the degree of

turbulence caused by the vapour (represented here by the eddy diffusivity). The ways in which these parameters change and their interactions with each other are not completely understood and are difficult to predict or extrapolate accurately from experimental data. The interactions of these parameters affects the rate of mass transfer (represented by the point efficiency) and the average height of clear liquid on the tray.

It is these complex interactions which help make the accurate design of distillation equipment so difficult.

4.9 Conclusions

From the comparison between experimental and theoretical data, it is possible to come to the following conclusions:

Vacuum distillation - the fluid mechanical model is not valid for the prediction of liquid flow patterns for these conditions.

The liquid flow patterns presented in Chapter 3 showed that both the experimental and theoretical data indicated the forward flow of liquid over all the tray, but this is as far as any similarities go. The deviations between experimental and theoretical results for both predicted tray efficiencies and simulation of mass-transfer indicate that the fluid mechanical model does not take into account some fundamental mechanism which is crucial to the prediction of liquid behaviour. It is thought that this phenomenum is the transport of liquid as a spray.

Atmospheric pressure distillation - though not an accurate prediction of tray efficiency and flow patterns, the fluid mechanical model is a very good approximation which can be used with a reasonable degree of confidence.

The data presented in Chapter 3 indicated a small area of liquid circulation on the tray. By examination of the experimental reduced isotherms, this has proved to be

negligible in its effect, and hence, it can be assumed to be stagnant as predicted by the fluid mechanical model. Though there are deviations between the experimental reduced isotherms and tray efficiencies and those predicted by theory, there are also strong similarities. The data seems to be in reasonable agreement, so this model can be used as a good approximation.

Moderate pressure distillation - the experimental and theoretical data seem to be in very good agreement. This would indicate that the fluid mechanical model is very good under these conditions.

Moderate pressure distillation, with its high flow-rate of liquid relative to the vapour should be the condition under which the assumptions of this model most closely approximate reality. This is emphasised by the very good agreement between experimental and theoretical tray efficiencies and the similarities between the reduced isotherms obtained experimentally and the predicted reduced concentration contours.

CHAPTER 5

5. DISTSIM

5.1 Introduction

Most commercial process simulation packages are limited in their modelling of distillation columns. Since they are designed as general process engineering tools, the mathematical models used to simulate distillation columns are compromised so that they can produce solutions for complex multi-component separations while the trays are modelled in the most basic manner (i.e. the completely mixed tray). Deviations from non-ideality are allowed for by assigning tray efficiencies to groups of trays.

This chapter outlines the work carried out by the author to incorporate the Yu fluid mechanical model into DISTSIM, a distillation column simulation program developed at Aston University.

5.2 Outline of Previous Work

The development of the DISTSIM program has been made in several stages. The original program, incorporating a model for column operation at finite reflux (Napthali & Sandholm 1971) and a modified Napthali - Sandholm method for column operation at total reflux (Hirose et al. 1980) was assembled. A version of this program modified for use with the Standart (1965) definition of tray efficiency is described by Fletcher (1987). This work used the concept of a completely mixed tray to model tray efficiencies. This formed the basis of the column model later developed by Akebe (1983).

This suite of programs could model a column of up to 28 trays (excluding reboiler and condenser) containing a binary mixture. Equilibrium data was modelled in terms of K-values which were calculated using the UNIFAC (Fredenslund 1977) or Wilson (Wilson 1964) techniques.

Akebe (1983) expanded the work by the addition of tray models. This included the models proposed by Lewis (1936) and Diener (1967) and a modified program written by Bassoon (Lockett et al. 1975) in order to incorporate the *stagnant regions model.*

The program was developed to run as what is essentially two separate models. One of these models is the column model. It requires tray efficiencies in order to calculate liquid and vapour flow rates throughout the column and concentration profiles. The other model is the tray model. This requires liquid and vapour flow rates, and possibly other data depending on the tray model being used, in order to calculate tray efficiencies. It is only when the column concentration profiles from these two models are in agreement that the overall model has converged.

Further work by Akebe allowed for the modelling and interpretation of plant data by statistically fitting a theoretical column concentration profile to an experimental profile using a least squares algorithm. Use was made of the tray efficiency models to relate point efficiencies to tray efficiencies (see Chapter 2) and predict mass transfer coefficients using Equations 5.1 and 5.2.

$$\frac{1}{N_{OG}} = \frac{1}{N_G} + \frac{\lambda}{N_L} \qquad (5.1)$$

$$E_{OG} = 1 - e^{-N_{OG}} \qquad (5.2)$$

Akebe used this combination of tray and column models to try to interpret the experimental data published by FRI (Sakata & Yanagi 1979) for a 1.2 metre diameter column containing a cyclo-hexane - n-heptane mixture operating under total reflux at a pressure of 165 kPa. Mass transfer coefficients obtained were then used to try to predict the performance of a 2.4 metre diameter column operating under similar conditions.

5.3 Incorporation of a Fluid Mechanical Model into a Column Model

In order to incorporate the Yu fluid mechanical model into the DISTSIM model, it was necessary to construct a calculation routine which was capable of predicting the liquid flow pattern on each tray individually to take into account the changes in liquid and vapour flow rates down the column. To save computational time, the flow pattern for each tray was stored and when recalculation was necessary, the profile which corresponded to the flow-rate nearest to the one on the tray in question was recalled to act as a first approximation of the flow-pattern. Using this method, little time is wasted recalculating flow-patterns without resorting to the inflexibility of calculating the flow pattern for a *typical* tray and imposing it on all trays. The mass-transfer routine (as described in Chapter 4) was also incorporated.

The modifications made to the DISTSIM program in order to include the fluid mechanical model are presented briefly in Appendix 9.

5.4 Explanation of Results

The data presented by Sakata and Yanagi (1970) was again used to compare the predictions of the various models. The experimental data used was run 105 which Sakata and Yanagi used to investigate tray pressure drops while operating the column at total reflux. Other data presented was deemed to be unsuitable as it was used to investigate flooding, entrainment or weeping which are effects which are not taken into account in the DISTSIM column model.

Only the extreme cases of no vapour mixing and completely mixed vapour have been used for this comparison. Most commercial scale columns are of sufficient diameter for the scale of the mixing to be considered to be negligible. This would mean that the vapour can be assumed to rise unmixed between trays. The other extreme case, that of complete vapour mixing, is included merely as a comparison. The *stagnant regions model* does allow for the partial mixing of vapour between trays, but this option has not been used because it is not possible to compare it to other models and

for reasons associated with predicting the degree of mixing, discussed below.

The data gained from the Diener (1957) model has not been included. This model is merely an extension of the AIChE *plug-flow plus back-mixing* model which allows for the vapour to be considered to be unmixed between trays. Since the case of complete vapour mixing between trays cannot be considered (ie the AIChE tray model has not yet been incorporated into this column model), this data has been excluded.

There is no method yet published for predicting the degree of mixing in the vapour phase. Lockett et al. (1975) have approached this problem from two different perspectives; the first based on the spreading of jets in pipes and the second based on a semi-intuitive method. These approaches have not been adopted here. A possible approach to this in future could be to model the vapour flow between trays using a commercial CFD package, where complex three-dimensional geometries, such as those found between trays can easily be described. Daly et al. (1995) used this approach to investigate possible vapour maldistribution below a sieve tray in a 2.44 metre diameter test-rig. Even if the vapour was assumed to be either totally mixed or totally unmixed in a mathematical model, these approaches may be used to estimate the scale of mixing and help determine which of the two limiting cases most closely models reality.

Since the DISTSIM program is trying to match the column profiles obtained from the experimental data, the tray efficiencies predicted by the different models for corresponding trays should be virtually identical and so, have not been presented. The data which is of interest is the tray enhancement factors. If a model predicts a flow pattern which is far from the optimal (a low tray enhancement factor), then a high point efficiency is used to compensate for this and achieve the required degree of mass-transfer. With this in mind, we can say that a high predicted tray enhancement factor represents a good liquid flow pattern and a low point efficiency.

The theoretical tray enhancement factors are presented in Figures 5.1 and 5.2. The trays are numbered from the top to the bottom of the column, with the condenser as

tray number 1. These data is tabulated in Appendix 5.

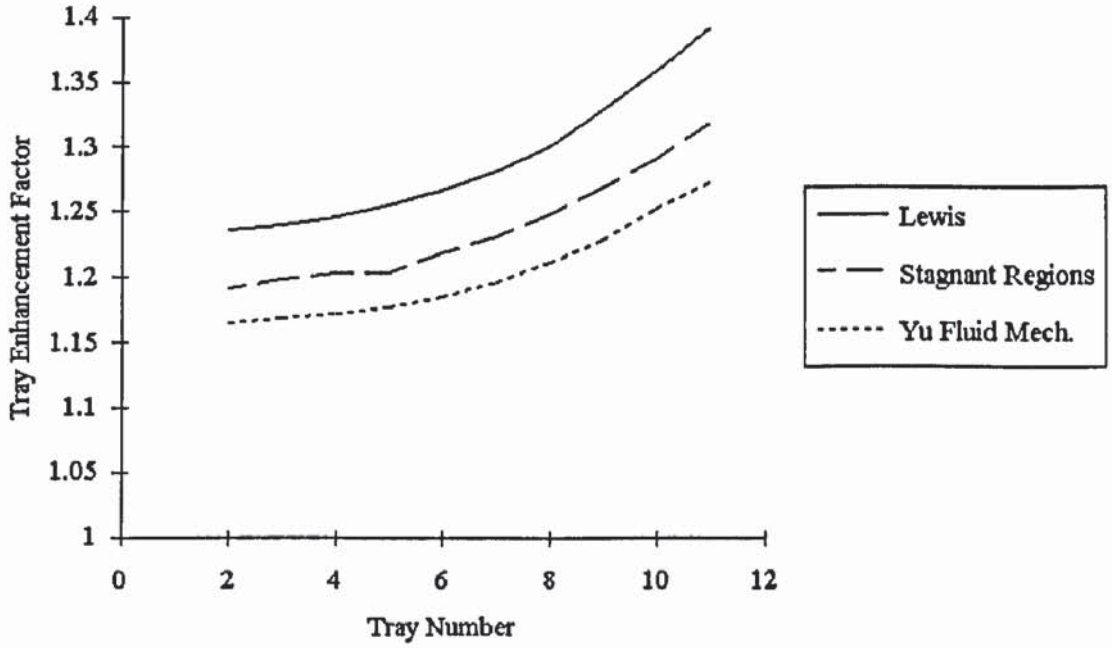

Figure 5.1: Tray enhancement factors calculated using the DISTSIM distillation column simulation program assuming total vapour mixing between trays

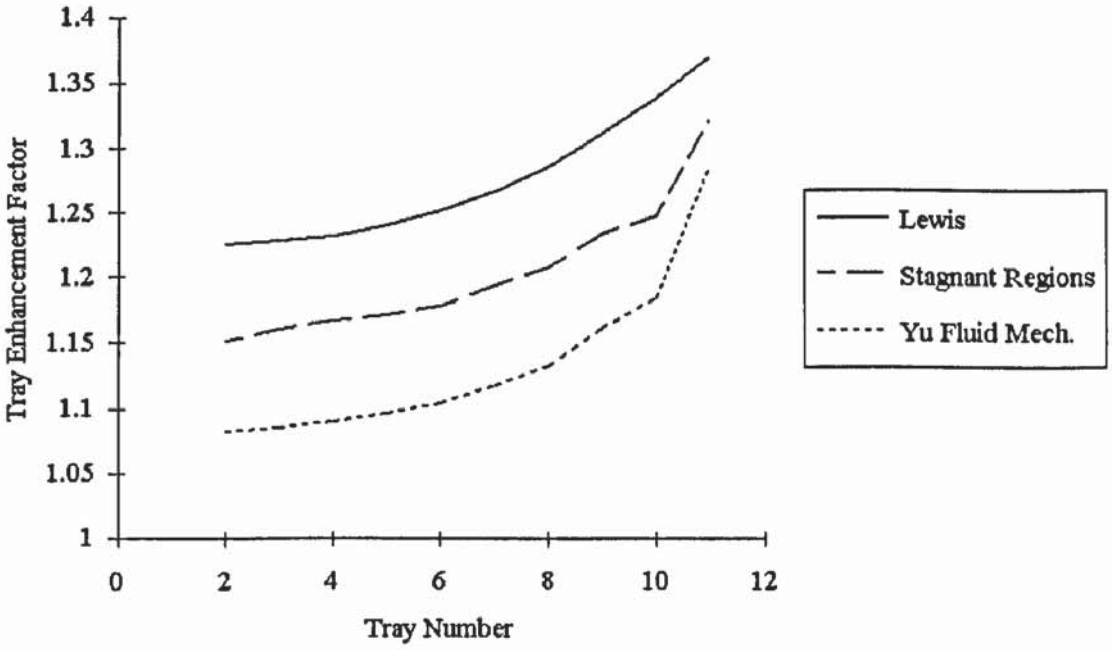

Figure 5.2: Tray enhancement factors calculated using the DISTSIM distillation column simulation program assuming no vapour mixing between trays

We can see that the Lewis model predicts the highest tray enhancement factors. This means that this produces the best flow pattern as expected. We now note that the tray enhancement factors predicted by the *stagnant region model* are higher than those predicted by the Yu fluid mechanical model. This is the opposite to the results obtained from the 2.44 metre diameter column (see Chapter 4). The reasons for these trends for the models have already been discussed for the case of the 2.44 metre diameter tray; we shall now look into the reasons for the trends on the FRI column.

If we consider the layout of a single tray in the FRI column (Figure 5.3) we can see that, due to the smaller diameter and the high weir length (80% of the diameter), the segmental regions of the tray are only small, 12cm at each side. This is well below the *width of a mixing zone*, defined by Porter et al. (1972), which limits the distance which we can expect a component to be transported into these segmental regions by diffusion.

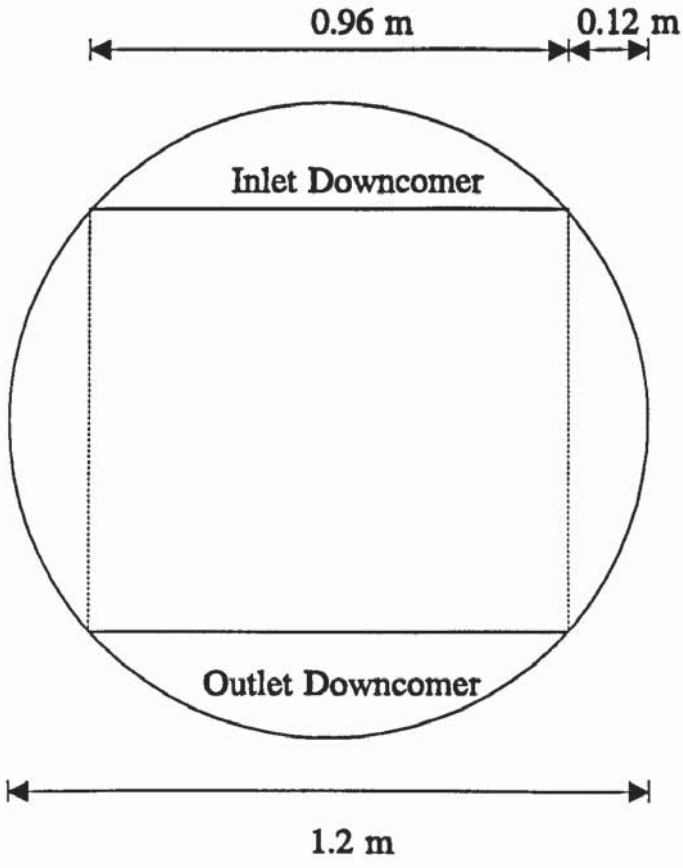

Figure 5.3: The FRI sieve tray used by Sakata and Yanagi (1979)

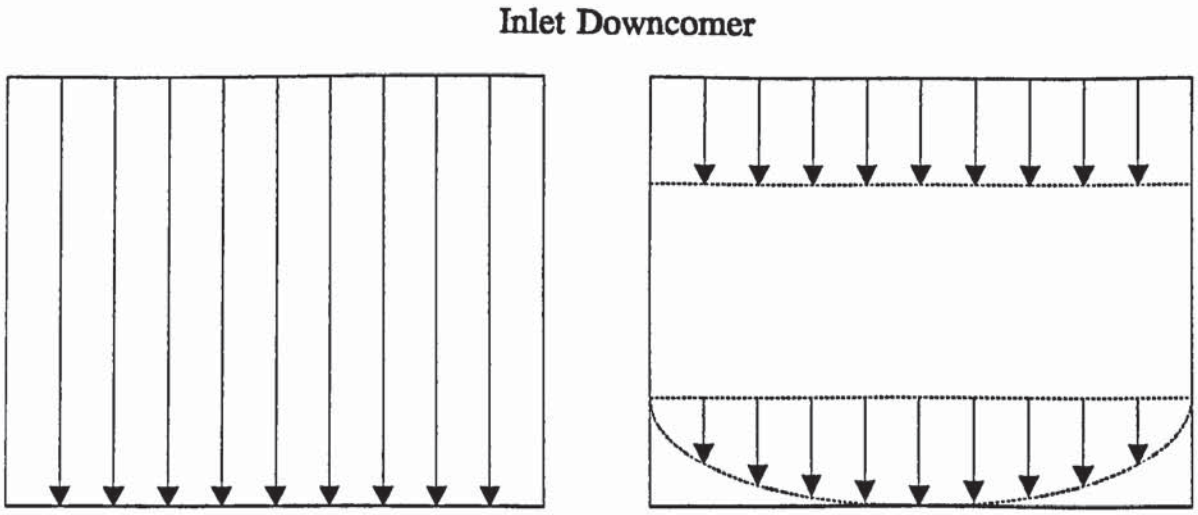

Figure 5.4: Flow patterns predicted by a) the stagnant regions model (Porter et al. 1972) and b) the Yu fluid mechanical model, based on a rectangular tray

Figure 5.4a and 5.4b show the flow patterns generated for the stagnant regions model and the Yu fluid mechanical model respectively, for a rectangular tray.

Lockett and Safekourdi (1976) investigated the effects of liquid flow pattern on tray efficiency. They concluded that the most efficient flow patterns (ie the one which resulted in the highest tray efficiency) was one where the liquid had a constant residence time. They also concluded that the effects of liquid mixing (which they modelled in terms of an eddy diffusivity) could help mask non-uniformities in flow patterns on smaller trays.

If we apply these factors in the interpretation of the flow patterns predicted by the two models for the FRI tray, we can gain a better understanding of the trends observed.

The *stagnant regions model* imposes a uniform liquid flow pattern down the centre of the tray while the side regions remain stagnant. As can be seen from Figure 5.3, these stagnant regions are only small, and so their effect on liquid residence time

distributions are easily masked by liquid mixing and can be ignored (Figure 5.4a shows the flow pattern based on this simplified tray geometry). This produces a reasonable narrow liquid residence time distribution (almost uniform residence time) which are the conditions associated with a high tray efficiency.

If we now consider the flow pattern predicted by the fluid mechanical model (Figure 5.4b based on a simplified tray geometry) we can that the flow down the centre of the tray is less uniform. Since the liquid in the side regions of the tray is easily replenished by diffusion due to the small distances involved, flow in these regions has little effect in raising the tray efficiency. The overall effect of this is to widen the distribution of liquid residence times compared to those predicted by the *stagnant regions model.* The detrimental effects of the non-uniform liquid flow pattern are partially masked by the liquid mixing, but they are still sufficient to produce a reduction in tray performance.

For the larger tray modelled in Chapters 3 and 4, the width of the side regions was such that mixing alone could not replenish the stagnant liquid, causing serious detrimental effects.

The *cross-over point,* below which the *stagnant regions model* will predict a higher efficiency that the fluid mechanical model will be when the size of the side regions of the tray becomes significant. It is thought that this will lie between a diameter of 2.4m and 3.0m for a tray where the weir length is 80% of the diameter, such as the FRI tray (between 1.2m and 1.5m for a tray where the weir length is 60% of the diameter). This is based on the calculations made by Porter et al. (1972) which determined than the tray diameter above which the presence of stagnant regions had a detrimental effect was approximately 1.5m.

The mass transfer data for this system gained from these simulations is presented in Figures 5.5 and 5.6. Since these data cannot be compared to any independent means of estimating mass transfer coefficienct, they will not be discussed here. These data are tabulated in Appendix 5.

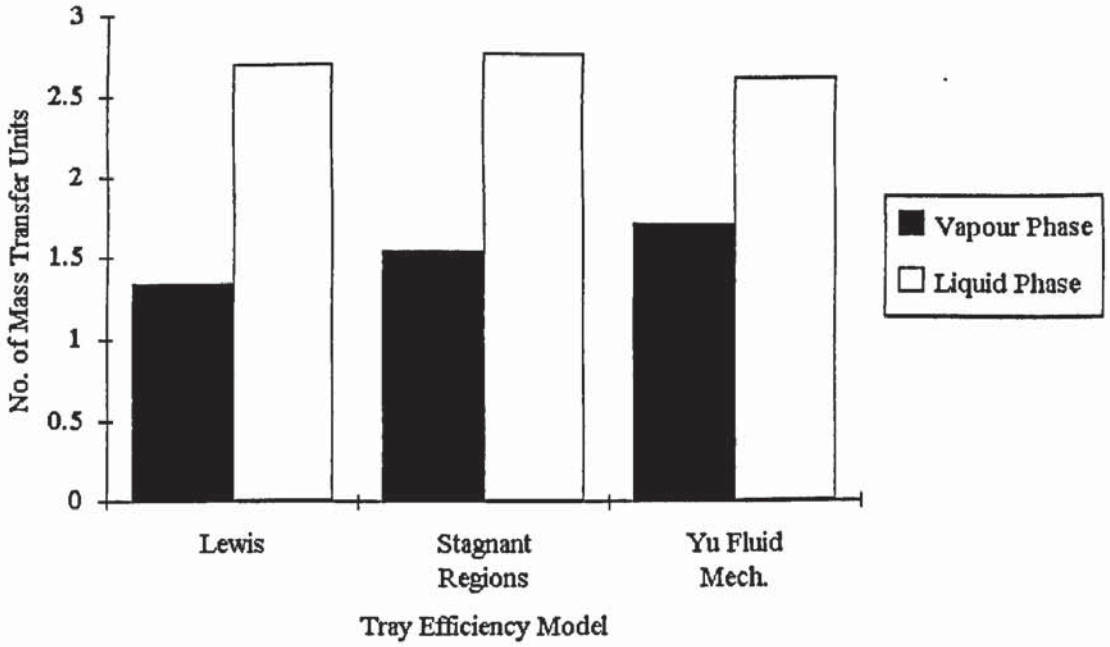

Figure 5.5: Mass transfer data predicted using the DISTSIM program for the case of total vapour mixing

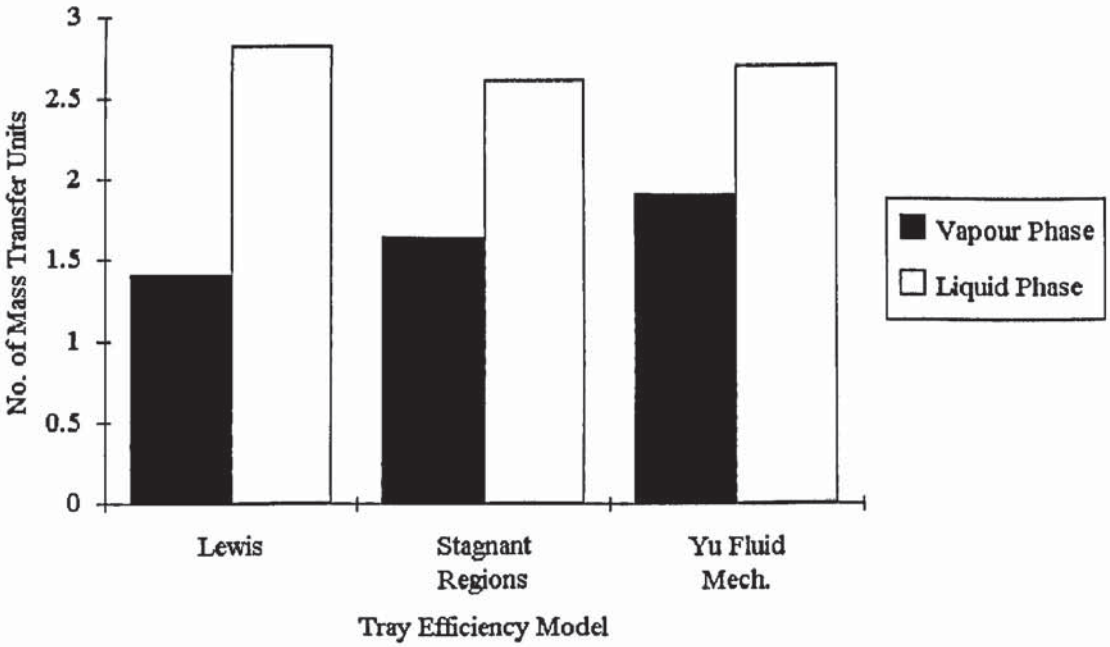

Figure 5.6: Mass transfer data predicted using the DISTSIM program for the case of no vapour mixing

5.5 Conclusions

It has been shown that this method is a feasible way of interpreting plant data and it may be useful to further investigate this approach in order to gain better mass-transfer data for use in the design of new columns or the re-vamp of existing columns.

From the comparison of the results from different models, it can be seen that the Yu fluid mechanical model can predict lower tray efficiencies than the *stagnant regions model* (Porter et al. 1972). This shows that the trends in the results observed in Chapter 4 are not universal, but a feature of the particular geometry of the test tray.

Since there has been no other method of determination of the mass-transfer coefficients, or tray efficiencies for these conditions other than those carried out by Akebe (1983) and in the course of this work, no comment can be made on the predicted data.

CHAPTER 6

6. SENSITIVITY ANALYSIS AND SCALE-UP

6.1 Introduction

This chapter describes the development of a sensitivity analysis to examine the possible errors from uncertain knowledge of some of the parameters used in the Yu fluid mechanical model. In the derivation of the equations (Equations 3.9, 3.10 and 3.11) it was necessary to utilise assumptions which had not been experimentally verified. As a result, there is uncertainty in the magnitude of the resistance terms. In producing results it is necessary to use data gathered either from experiment or from empirical correlations for the average height of clear liquid and the eddy diffusivity. The effect of errors in the assumed or calculated values of these parameters on the predicted tray efficiency is studied in the form of a sensitivity analysis The method used involves deriving dimensionless flow equations based on the flow equations presented in Chapter 3. These dimensionless groups can be used to examine the limiting case associated with flows on large trays. This provides a method to predict flow pattern changes on scale up to larger plant sizes.

In carrying out the sensitivity analysis, theoretical maxima and minima for each of the parameters were calculated and values between these were substituted into the equations. The effect on the entire system of equations, including the concentration equation, is considered simultaneously, i.e. a change in the eddy viscosity, used in the calculation of the velocity profiles, also changes the eddy diffusivity used in the calculation of the concentration profiles, since they are effectively the same thing. Thus, the effect of errors in the prediction of model parameters is viewed as if incorrect data had been input when using the model for design purposes.

The second use of the dimensionless equations derived below is to study the predicted flow patterns as certain terms in the equations either dominate the effects, or become negligible. In this way we can predict changes in the flow patterns as so called

limiting cases are approached. A brief qualitative discussion of the effects on the flow pattern of increasing the tray diameter is presented utilising the results of the sensitivity analysis.

6.2 Dimensionless Equations

By making substitutions for terms in Equation 3.9, 3.10 and 3.11 we can obtain Equations 6.1, 6.2 and 6.3 respectively.

$$\frac{\partial U}{\partial X} + \frac{\partial V}{\partial Y} = 0 \tag{6.1}$$

$$U\frac{\partial U}{\partial X} + V\frac{\partial U}{\partial Y} = -\frac{\partial \Pi}{\partial X} + \frac{1}{Re_{ED}}\left(\frac{\partial^2 U}{\partial X^2} + \frac{\partial^2 U}{\partial Y^2}\right) - U\left(\frac{1}{Re_B} + \frac{1}{F_{lv}}\right) \tag{6.2}$$

$$U\frac{\partial V}{\partial X} + V\frac{\partial V}{\partial Y} = -\frac{\partial \Pi}{\partial Y} + \frac{1}{Re_{ED}}\left(\frac{\partial^2 V}{\partial X^2} + \frac{\partial^2 V}{\partial Y^2}\right) - V\left(\frac{1}{Re_B} + \frac{1}{F_{lv}}\right) \tag{6.3}$$

where:

$$X = \frac{x}{D};\ U = \frac{uWh_l}{Q_L};\quad \Pi = \frac{PW^2h_l^2}{\rho_L Q_L^2};\quad Re_B = \frac{2\delta\rho_L Q_L}{3\mu WD};$$
$$Y = \frac{y}{D};\ V = \frac{vWh_l}{Q_L};\ F_{lv} = \frac{\rho_L Q_L}{\rho_v u_v WD};\quad Re_{ED} = \frac{DQ_L}{Wh_l \nu_e} \tag{6.4}$$

From Equation 6.4, we can see that in addition to requiring dimensionless distances and velocities, we have a dimensionless pressure, Π, an eddy Reynolds number, Re_{ED}, which is used in the determination of the viscous drag forces, and two resistance terms, F_{lv} and Re_B, which represent the momentum transfer from the liquid to the

vapour and the boundary layer skin friction term respectively.

6.3 Sensitivity to Eddy Diffusion / Viscosity

6.3.1 Prediction of eddy diffusivity

A survey of relevant literature was carried out in order to find suitable correlations for the prediction of eddy diffusivity. The correlation used in the calculation of the *base cases*, i.e. those presented previously, was presented by Gerster et al. (1958). Lockett (1986) recommended the use of correlations developed by Harada et al. (1964), Shore and Haselden (1969), Kafarov et al. (1972) and Zuiderweg (1982) for general use, and so these were chosen for comparison. The eddy diffusivity correlations are described by Equations 6.5 to 6.9 respectively.

Gerster at al. (1958) correlation:

$$D_e^{0.5} = 0.00378 + 0.017\,u_v + 3.68\frac{Q_L}{W} + 0.18\,h_w \qquad (6.5)$$

Harada et al. (1964) correlation:

$$D_e = 0.0036\,h_f\,u_v\,(u_h\,d_h)^{-0.37}\varepsilon^{-1} \qquad (6.6)$$

Shore & Haselden (1969) correlation:

$$D_e = 0.31\,h_f\left[u_v\left(\frac{\rho_L}{\rho_v}\right)^{0.5}\right]^{0.63} \qquad (6.7)$$

Kafarov et al. (1972) correlation:

$$D_e = 3.17*10^{-3}\left(\frac{Q_L}{W\,h_l}\right)^{0.17} h_l\,(1-\varepsilon)^{2.83} \qquad (6.8)$$

Zuiderweg (1982) correlation:

$$D_e = \frac{8.3\,\rho_v u_v^2 h_l^2}{\rho_L (Q_L / W)} \qquad (6.9)$$

The above correlations were used to evaluate the eddy diffusivity for each of the twelve cases (four for each of the vacuum, atmospheric pressure and moderate pressure distillation simulation) reviewed in Chapter 4 (see page 85).

The use of some of these correlations requires the knowledge of parameters other than the tray geometry and the liquid and vapour flow rates. There are two such unknown parameters. The first to be dealt with here is the average height of clear liquid on the tray. For the cases studied here, this parameter has been measured experimentally and, therefore, we can use these data. The second parameter is the average fractional vapour hold-up, ε. since there is no method used to measure this during the experimentation, this is estimated using the Colwell (1979) correlation. The final unknown parameter is the average froth height, h_f. This is estimated as a function of the average height of clear liquid and the average fractional vapour hold-up using Equation 6.10.

$$h_f = \frac{h_l}{1 - \varepsilon} \qquad (6.10)$$

The data calculated using these correlations are shown in Figures 6.1 and 6.2 and are tabulated in Appendix 6. It can be seen that a wide range of possible eddy diffusivity values can be predicted by literature correlations. It should be noted that the data predicted by the correlation proposed by Gerster et al. (1958), which are the data used in evaluating the original estimates of the tray efficiency in this work, lie towards the upper end of the range.

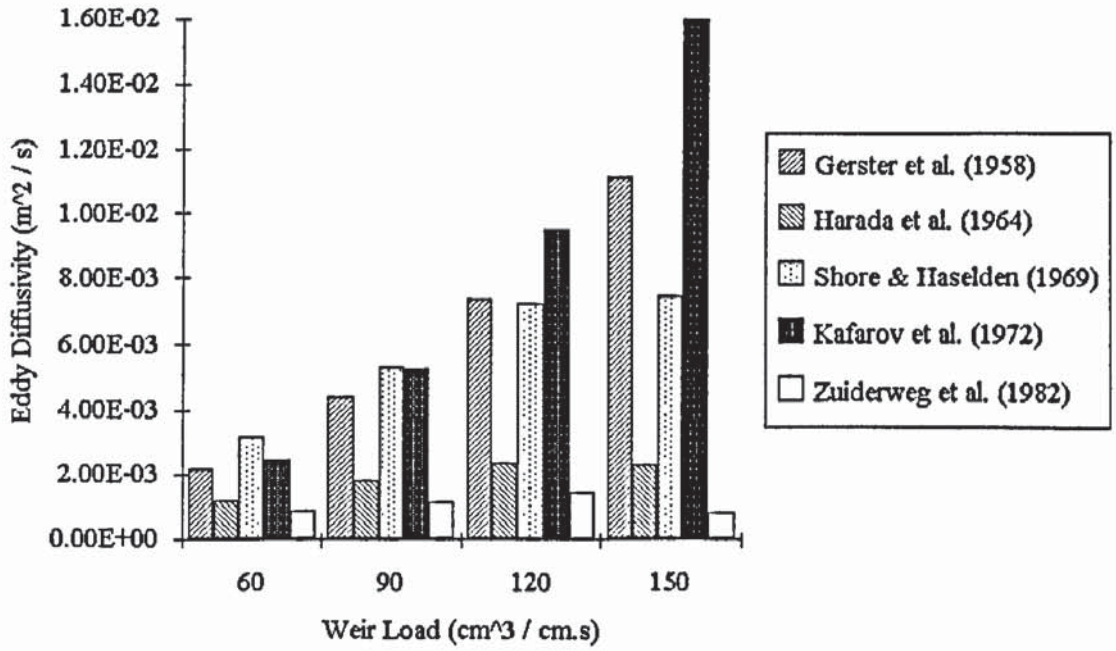

Figure 6.1: Eddy diffusivities predicted by various correlations for simulated atmospheric pressure distillation

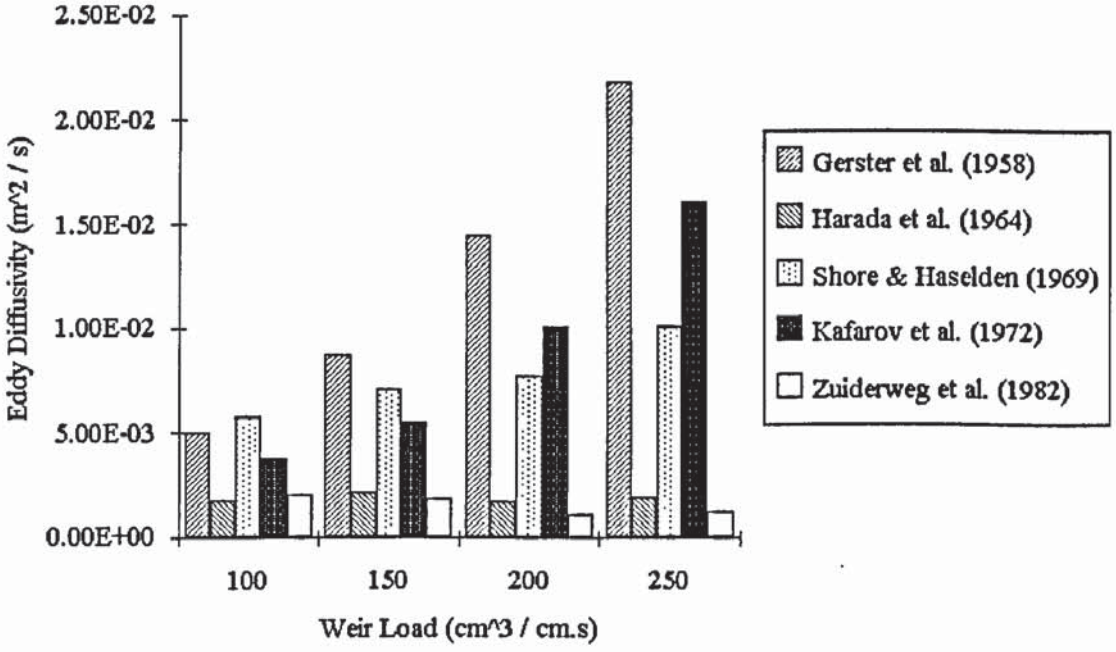

Figure 6.2: Eddy diffusivities predicted by various correlations for simulated moderate pressure distillation

6.3.2 Sensitivity analysis

Based on the data presented in Figures 6.1 and 6.2, it was decided to investigate the effect of the change in eddy diffusivity on the predicted tray efficiencies between the following margins:

Atmospheric pressure simulation	$D_e^G /8$	to	$D_e^G * 2$
Moderate pressure simulation	$D_e^G /10$	to	D_e^G

where D_e^G represents the eddy diffusivity predicted by the Gerster et al. (1958) correlation

Changing the predicted eddy diffusivity only changes the eddy Reynolds number, and so, the effect on the predicted tray enhancement factor of the variations in the predicted eddy diffusivity for atmospheric and moderate pressure simulation, shown in Figure 6.3 and 6.4 respectively, are presented as plots of the eddy Reynolds number against the predicted tray enhancement factor. It should be noted that the eddy Reynolds number, Re_{ED} (defined by Equation 6.4), is inversely proportional to the eddy diffusivity. Hence a high eddy diffusivity corresponds to a low eddy Reynolds number, and vice versa.

The base data on these graphs represents the data obtained when using the Gerster et al. (1958) correlation to predict the tray efficiency. Experimental data are plotted on the basis that the tray enhancement factor and the liquid flow rate are known in order to provide an indication of the value of the eddy Reynolds number.

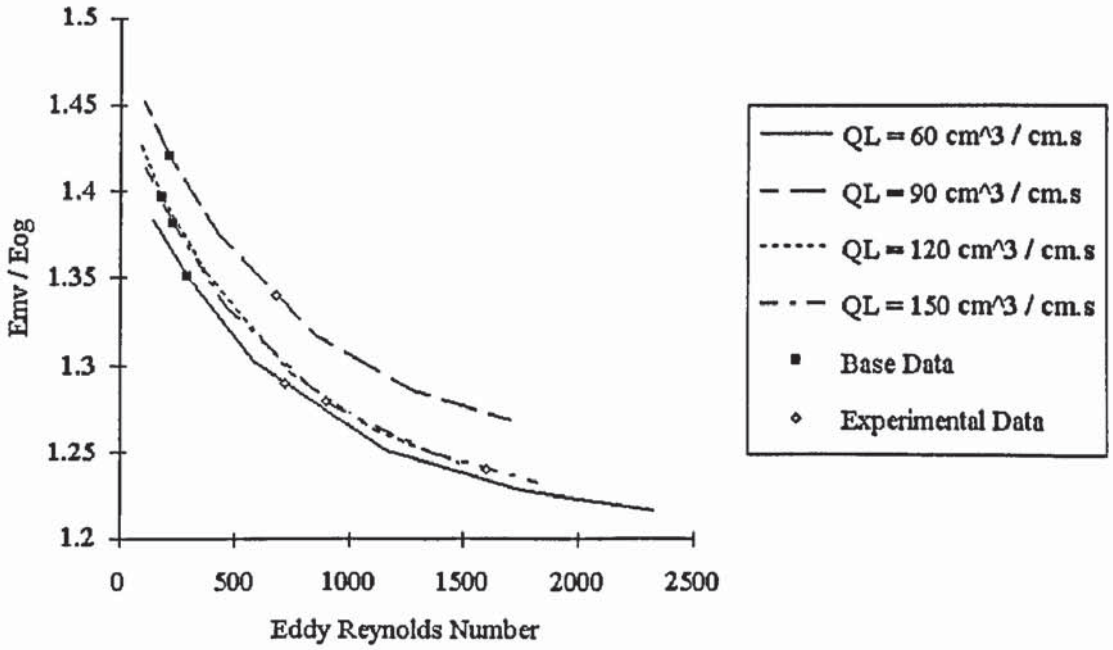

Figure 6.3: Variation in predicted tray enhancement factor with variation in eddy diffusivity for atmospheric pressure simulation

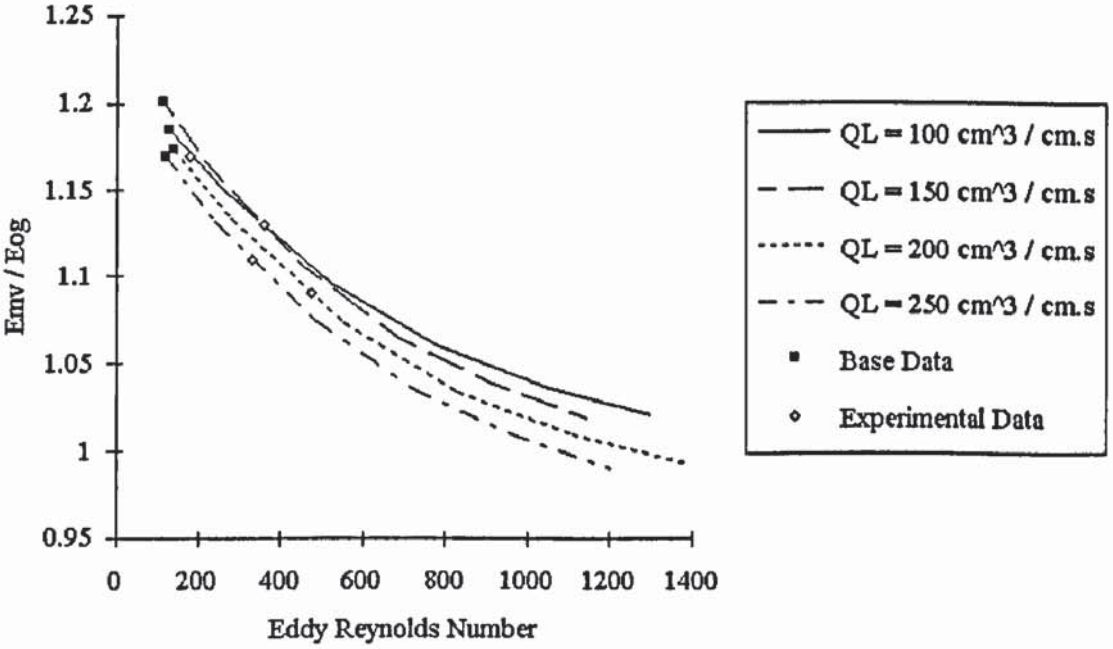

Figure 6.4: Variation in predicted tray enhancement factor with variation in eddy diffusivity for moderate pressure simulation

6.3.3 Comments

As can be seen from Figures 6.3 and 6.4 the predicted eddy Reynolds numbers for the experimental data lie within the range of data predicted by the sensitivity analysis and that the base data lies towards the upper end of the tray efficiency range and the lower end of the range of eddy Reynolds numbers. This may indicate that the Gerster et al. (1958) correlation over-predicts the eddy diffusivity for the conditions which were chosen and that the model may better fit the experimental data if a different correlation for eddy diffusivity were chosen.

The general trend in both graphs is for the predicted tray enhancement factor to decrease with decreasing eddy diffusivity. This shows that the high turbulence on the tray is causing liquid flow into the side-regions by the viscous transfer of momentum. This helps prevent the formation of stagnant regions. The second effect of turbulence is through the eddy diffusivity rather than the viscosity. The high degree of local mixing also transfers liquid into those regions where one of the components may have become depleted through mass-transfer with the vapour phase.

On plates with a more uniform flow pattern, this second phenomenon can produce a deleterious effect on the predicted tray enhancement factor. Though the model is not really valid for the prediction of flow patterns for vacuum simulation (trays operating in the spray regime) results obtained can be used to illustrate this point.

From Figure 6.5, it can be seen that the low liquid momentum and relatively high viscosity of the bi-phase have produced more uniform liquid flow patterns for the simulation of vacuum distillation. This would mean that the negative effects of stagnant regions at the sides of the tray have been largely avoided. If we now consider the effects of varying the eddy viscosity / diffusivity (Figure 6.6) we can see that the effects are the opposite to those observed for atmospheric pressure and moderate pressure simulation (i.e. predicted plate efficiency falls as eddy diffusivity increases). Since the flow pattern can only improve as the eddy viscosity increases, the transfer of momentum from the centre of the tray to the sides increases producing a more uniform flow pattern, this effect can only be caused by the high degree of

liquid back-mixing. This effect is illustrated more clearly if the simplified case of plug flow of liquid across a rectangular tray is considered. If the case of no liquid back-mixing (Lewis 1936) is considered, a higher predicted tray efficiency than for the case of plug flow plus back-mixing (Gerster et al. 1958) is obtained.

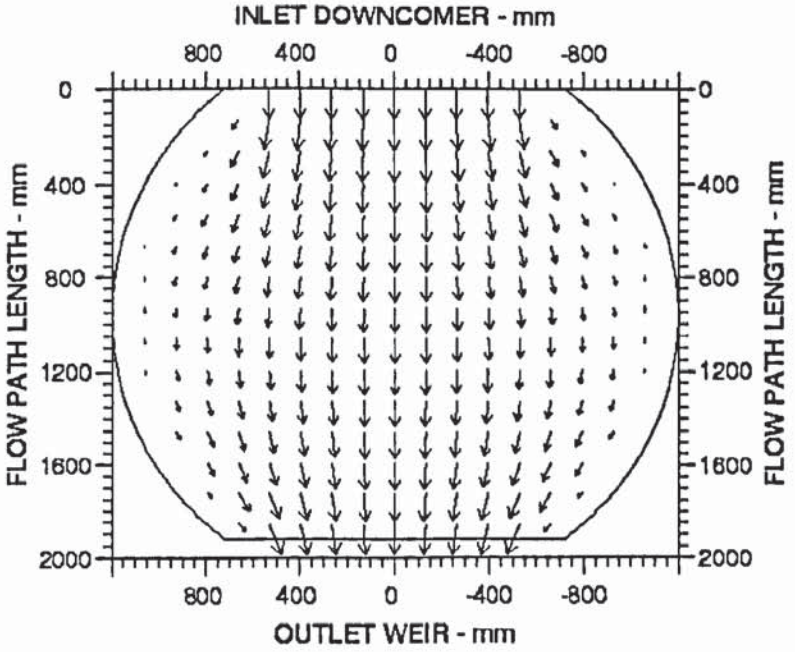

Figure 6.5: Predicted liquid flow patterns for the simulation of vacuum distillation

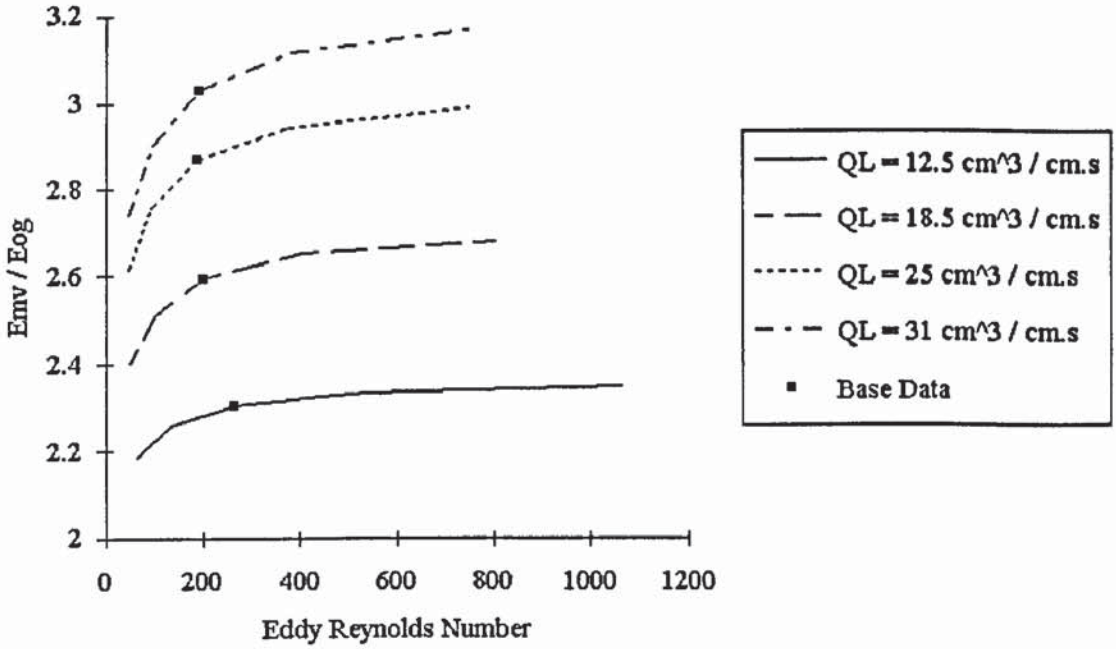

Figure 6.6: Variation in predicted tray enhancement factor with variation in eddy diffusivity for vacuum simulation

N.B. for vacuum simulation the experimental data do not lie within the range of the sensitivity analysis due to the fact that the model is not valid for the conditions under which the tray was operating.

6.4 Sensitivity to the Resistance Terms

6.4.1 Prediction of the resistance terms

At present the resistance terms are predicted on a purely theoretical basis. Several questions must be asked about the assumptions made in the derivation of these terms:

1) Is the liquid / vapour drag force sufficient to accelerate the vapour to the local liquid velocity?
2) Is the concept of a boundary layer next to the tray floor valid for this situation and, if so, is the method for calculating its thickness correct?

Though there may be more questions to be asked about this, just these two points bring into doubt the calculated magnitude of both of these terms.

In order to address this matter, we must first decide the possible magnitude and the direction of the changes in these individual terms.

The resistance due to the rising vapour is easier to deal with. The theoretical value for this term is the maximum possible value (assuming that the vapour does not have a horizontal component to its velocity on entering the liquid). An arbitrary minimum value for this term was chosen to be a quarter of the maximum value.

The tray floor resistance term is a little more complex to study. To do this it must be assumed that the concept of the tray floor boundary layer is valid, and the method of calculating its thickness presented in Chapter 3 (Equation 3.18) can be used. The components of Equation 3.18 now have to be analysed. The main unknown quantity is the *characteristic length*, x_c. This was estimated based on the maximum uninterrupted flow length between holes (the maximum distance liquid can travel without being disrupted by a vapour stream). In order to carry out the sensitivity

analysis, it was decided to see the effects of changes in this constant of between half and double the original value. This would lead to a change in the tray floor resistance term of between 71% and 141% of the value used previously in the calculations.

6.4.2 Sensitivity analysis

The effect of the tray floor resistance term and the vapour resistance term cannot be distinguished in the results of the calculations, and so it was decided to combine the analysis of both terms and vary the total resistance between a maximum and a minimum value.

$$R_{min} = R_{floor} * 0.71 + R_{vapour} * 0.25$$

$$R_{max} = R_{floor} * 1.41 + R_{vapour}$$

The flow patterns and efficiency were also evaluated with no resistance terms.

The results of the sensitivity analysis are illustrated in Figures 6.7 and 6.8.

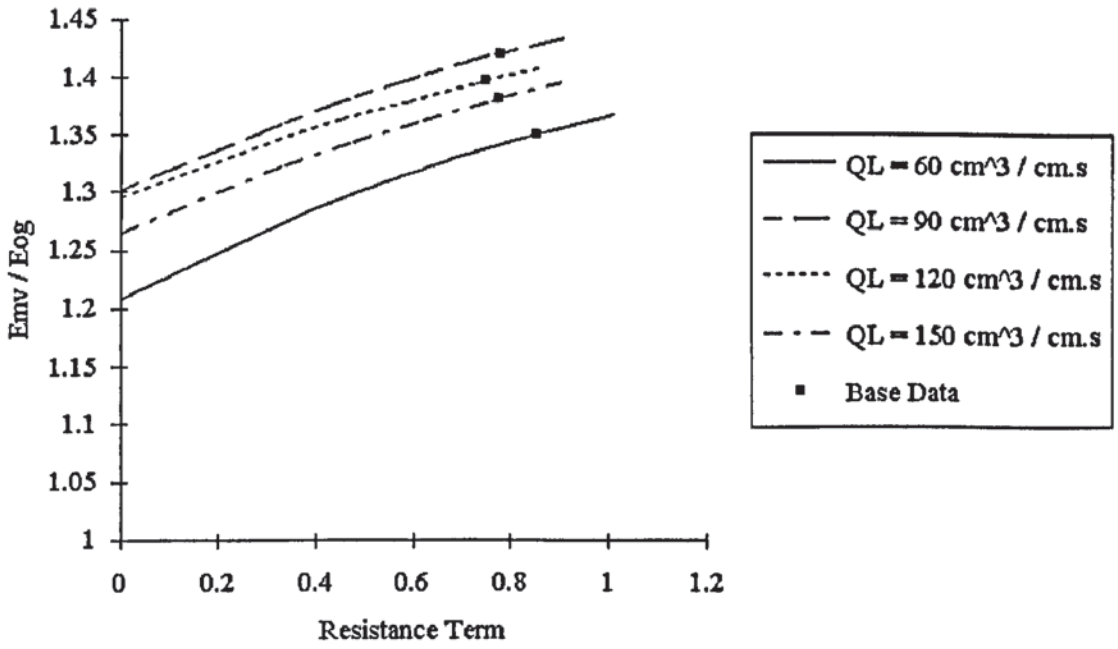

Figure 6.7: The sensitivity of the predicted tray enhancement factor to variations in the resistance term for atmospheric pressure simulation

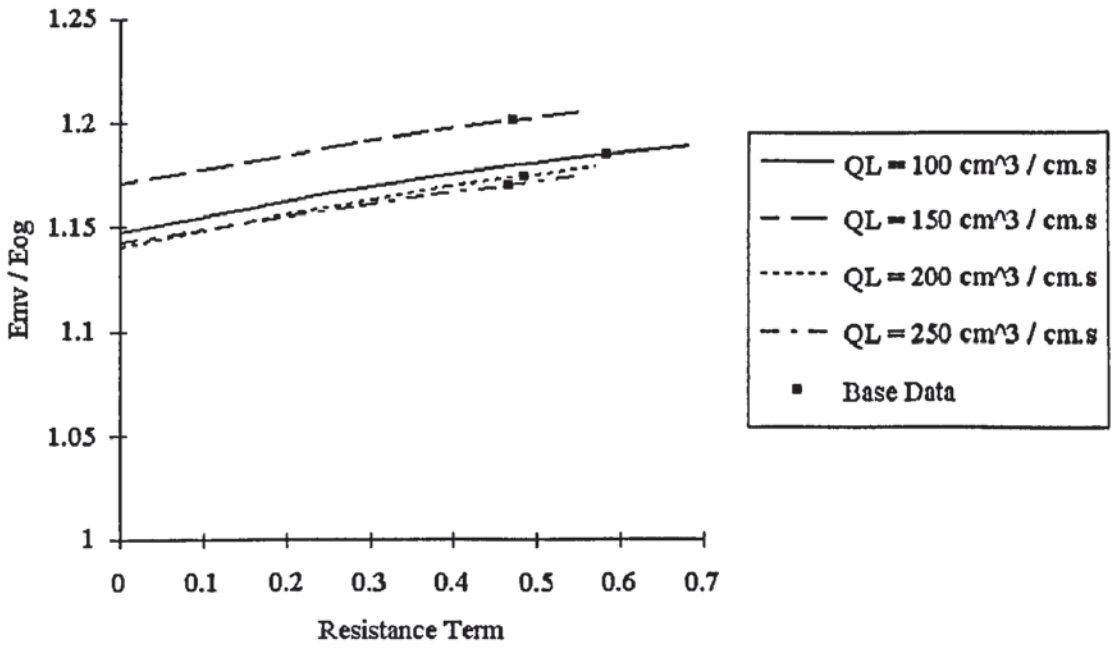

Figure 6.8: The sensitivity of the predicted tray enhancement factor to variations in the resistance term for moderate pressure simulation

The base data refers to the calculation of the resistance term by the method outlined in Chapter 3.

6.4.3 Comments

The data presented in Figures 6.7 and 6.8 shows that the tray efficiency increases with an increase in the resistance term. This is caused by a high resistance to liquid flow in the central region of the tray pushing liquid to the side-regions. This would help to prevent the formation of stagnant zones which decrease tray efficiency.

6.5 Sensitivity to the Average Height of Clear Liquid

6.5.1 Experimental measurement of the height of clear liquid

For the data used in these calculations, the height of clear liquid was measured using manometers fitted to the floor of the operating tray (see Figure 6.9). Datum readings were taken for each manometer with no liquid on the tray and air flowing at the superficial velocities equal to those to be used with liquid present. These datum

values are designed to take into account variations in the data recorded experimentally due to the momentum of the air, the *out-of-levelness* of the tray and capillary rise in the manometers. Once data has been recorded with liquid present on the tray, the datum values are subtracted to give a height of clear liquid.

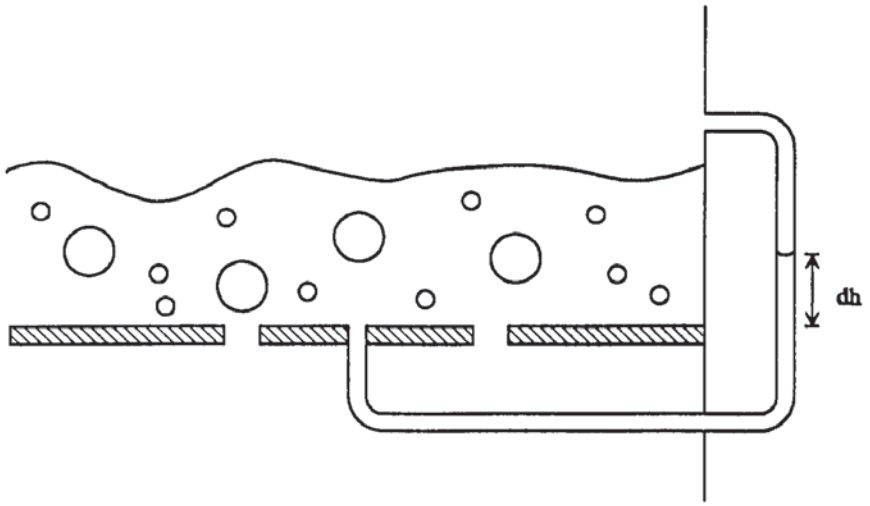

Figure 6.9: A manometer fitted to the tray floor for use in calculating the height of clear liquid

Though this method of taking datum values does not require the use of empirical relationships and so is better than alternative methods, it does have disadvantages due to the differences in the nature of the vapour flow between when liquid is present and in its absence.

When liquid is present maldistribution of the liquid can cause vapour maldistribution. This can lead to areas of liquid which are not aerated, or areas in which vapour flows preferentially. Since the datum values are recorded when air is flowing evenly through all points on the tray, they may not represent what occurs during operation. Care should therefore be taken in interpreting data which show any significant deviation in the average height of clear liquid across a tray.

Other minor effects may be due to varying air flow-rates at individual orifices caused by bubbling. This may effect the correction due to the gas momentum.

Other disadvantages with this method of calculating the height of clear liquid become apparent when we consider tray operation in the spray regime. Here a high degree of liquid is present as droplets suspended in the gas stream as noted by Porter and Wong (1969). Since they are not in contact with the tray floor, they do not exert a pressure on the manometer tapping and, hence, their presence is not accounted for.

6.5.2 Correlations for the average height of clear liquid

As with the work on eddy diffusivities, relevant literature was surveyed for correlations to predict the height of clear liquid on a tray. Lockett (1986) recommends several correlations which are based on the Francis weir flow equation (Francis 1883). The correlations chosen were those formulated by Stichlmair (1978), Colwell (1979) and Bennett et al. (1983). These correlations require the estimation of the liquid hold-up fraction. Correlations published by the same authors were used. The Bennett height of clear liquid correlation is recommended for use only with the Bennett liquid hold-up fraction correlation, but the height of clear liquid correlations of Stichlmair and Colwell were used with both the remaining liquid hold-up fraction correlations. This gives a total of five methods of calculating the height of clear liquid as shown in Table 6.1. Data calculated using the individual correlations are given in Appendix 7.

Height of Clear Liquid Correlation	**Liquid Hold-Up Fraction Correlation**		
	Bennett	**Colwell**	**Stichlmair**
Bennett	Case 1		
Stichlmair		Case 2	Case 3
Colwell		Case 4	Case 5

Table 6.1: Combinations of height of clear liquid correlations and liquid hold-up correlation used to predict the hight of clear liquid

Stichlmair correlations:

$$h_l = (1 - \varepsilon)\left[h_w + \frac{0.49}{C_d^{0.67}}\left(\frac{Q_L}{(1-\varepsilon)W}\right)^{0.67} + \frac{125\,(u_v - u_b)^2 \rho_v}{g\,(\rho_L - \rho_v)\,\varepsilon^2}\right] \qquad (6.11)$$

where

$$u_b = 1.55\left(\frac{\sigma_s\,(\rho_L - \rho_v)\,g}{\rho_L^2}\right)^{0.25}\left(\frac{\rho_v}{\rho_L}\right)^{\frac{1}{24}} \qquad (6.12)$$

and

$$\varepsilon = \left(\frac{F_s}{F_{s\,max}}\right)^{0.28} \qquad (6.13)$$

where

$$F_s = u_v\,\rho_v^{0.5}$$
$$F_{s\,max} = 2.5\,(A_F^2\,\sigma_s\,(\rho_L - \rho_v)\,g)^{0.25} \qquad (6.14)$$

Colwell correlations:

$$h_l = (1 - \varepsilon)\left[h_w + \frac{0.49\,k}{C_d^{0.67}}\left(\frac{Q_L}{(1-\varepsilon)\,W}\right)^{0.67}\right] \qquad (6.15)$$

and

$$\frac{\varepsilon}{1 - \varepsilon} = 12.6\,(Fr')^{0.4}\,A_F^{-0.25} \qquad (6.16)$$

where

$$Fr' = \left(\frac{u_v^2}{g\,h_l}\right)\left(\frac{\rho_v}{\rho_L - \rho_v}\right) \qquad (6.17)$$

Bennett correlations:

$$h_l = \alpha_e\left[h_w + C_B\left(\frac{Q_L}{W\,\alpha_e}\right)^{0.67}\right] \qquad (6.18)$$

where

$$C_B = 0.50 + 0.438\exp\left(-137.8\,h_w\right) \qquad (6.19)$$

and

$$\alpha_e = \exp\left[-12.55\left(u_s\left(\frac{\rho_v}{\rho_l - \rho_v}\right)^{0.5}\right)^{0.91}\right] \qquad (6.20)$$

6.5.3 Sensitivity analysis

The data predicted by the correlations described in Section 6.5.2 are shown in Figures 6.10 and 6.11. It was decided to calculate the flow patterns using the maximum and minimum heights of clear liquid for a particular case (see Tables 6.2 and 6.3) and at several points in between.

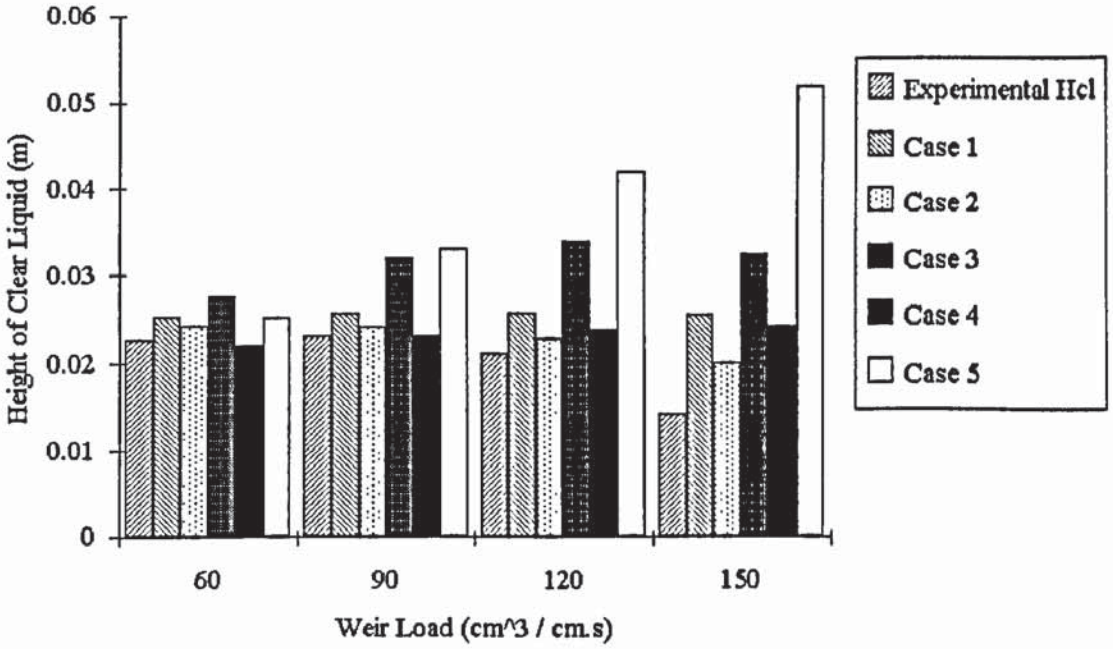

Figure 6.10: A comparison of predicted heights of clear liquid to experimental data for atmospheric pressure simulation

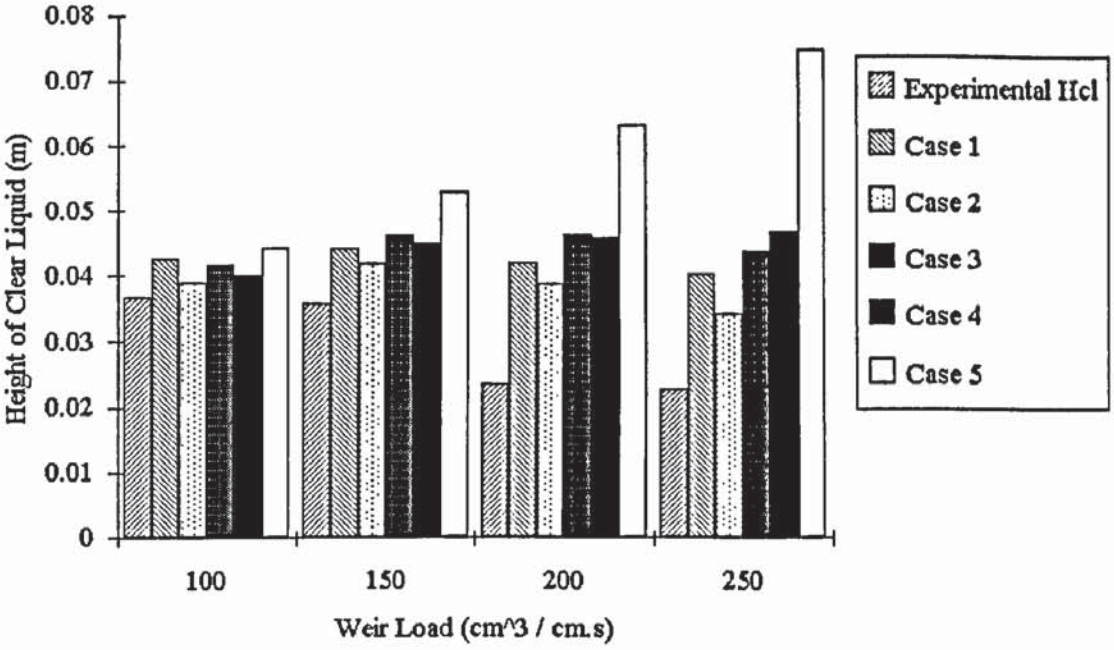

Figure 6.11: A comparison of predicted heights of clear liquid to experimental data for moderate pressure simulation

	Height Of Clear Liquid (mm)		
	Experimental	Minimum Predicted	Maximum Predicted
Atmospheric Pressure Case 1	22.8	22.1	27.6
Atmospheric Pressure Case 2	23.1	23.1	32.9
Atmospheric Pressure Case 3	21.1	22.7	41.9
Atmospheric Pressure Case 4	14.2	20.1	52.0

Table 6.2: Comparison of experimentally measured height of clear liquid values to those predicted by correlation for simulated atmospheric pressure distillation

	Height Of Clear Liquid (mm)		
	Experimental	Minimum Predicted	Maximum Predicted
Moderate Pressure Case 1	36.6	38.9	44.1
Moderate Pressure Case 2	35.5	41.8	53.0
Moderate Pressure Case 3	23.7	38.9	63.2
Moderate Pressure Case 4	22.8	34.1	74.8

Table 6.3: Comparison of experimentally measured height of clear liquid values to those predicted by correlation for simulated moderate pressure distillation

The variation in predicted tray efficiency with height of clear liquid is presented graphically in Figures 6.12 and 6.13.

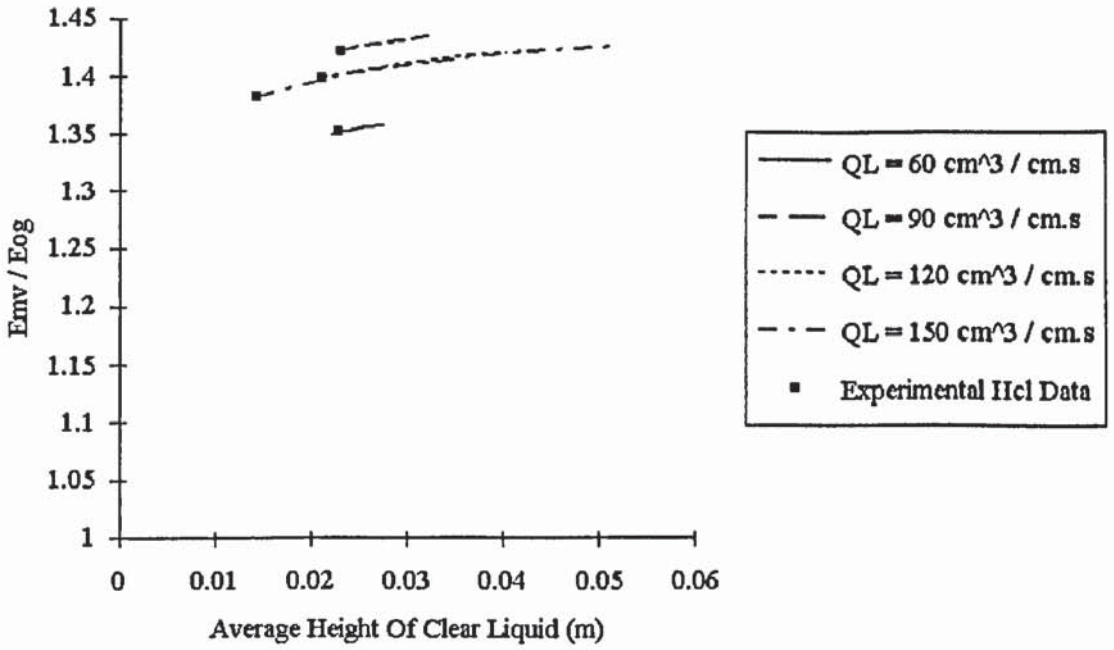

Figure 6.12: Variation in predicted tray enhancement factor with height of clear liquid for atmospheric pressure simulation

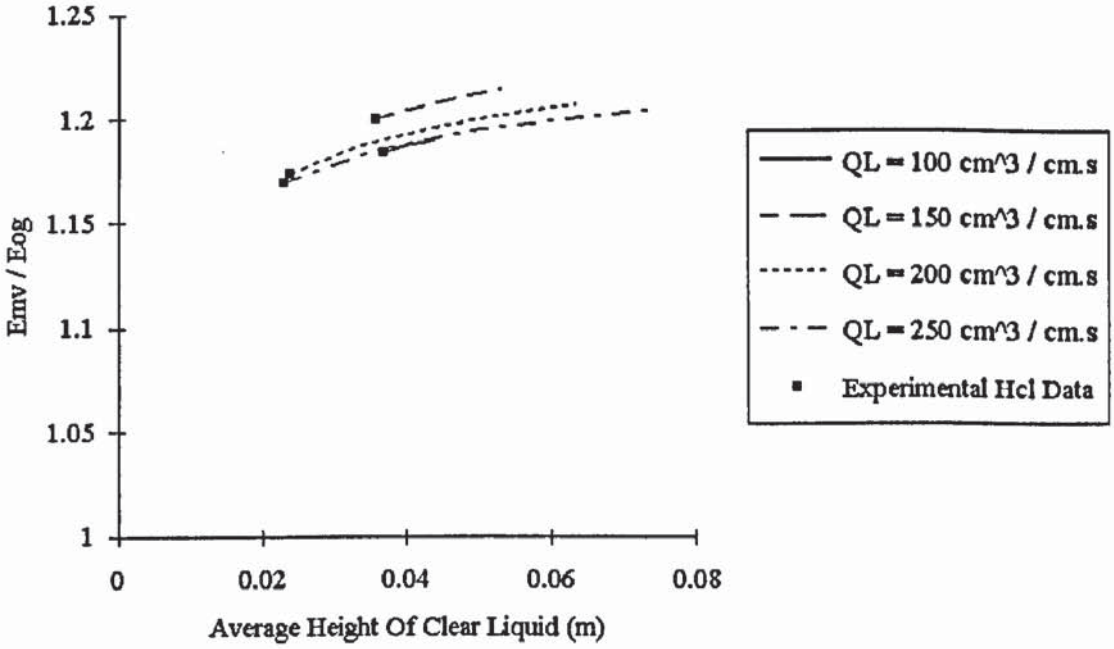

Figure 6.13: Variation in predicted tray enhancement factor with height of clear liquid for moderate pressure simulation

The additional data shown on these graphs correspond to the predicted tray enhancement factor when the experimental height of clear liquid is used for the calculations (ie the base case data originally used in the model).

6.5.4 Comments

There seems to be little variation in the predicted plate efficiency with height of clear liquid. This is due to the majority of the terms in the flow equations (Equations 6.1 to 6.3) not changing in relation to each other. The only differences are in the eddy Reynolds number, Re_{ED}, and the tray floor resistance term, Re_B. For an increase in the height of clear liquid there is a decrease in the eddy Reynolds number which promotes liquid movement in the side regions of the tray. This is accompanied by a decrease in the tray floor resistance term due to an increase in the predicted thickness of the boundary layer. This decreases the amount of liquid pushed into the side regions of the tray, partially off-setting the effects of the eddy Reynolds number. The net effect is a slight increase in tray efficiency.

6.6 Scale-Up

The expansion of the current data to the prediction of the liquid flow pattern on large trays is complex with the use of this model. The eddy Reynolds number would increase. This would indicate that the transfer of liquid momentum into the side regions of the tray by viscous mixing would be reduced. This would promote the formation of stagnant zones. This would be opposed by the resistance terms which would increase with increasing tray size (the boundary layer Reynolds number, Re_B, and the liquid - vapour flow parameter, F_{lv}, both decreasing). This reflects the tendency of the liquid to be pushed further into the side regions of the tray with flow path length by the combined resistances.

If we refer to the sensitivity analyses carried out above, we can see that an increase in the eddy Reynolds number has a more marked effect than a proportional increase in the size of the combined resistance terms. This would indicate that the overall effect of these two parameters opposing each other would be a decrease in the

predicted tray efficiency with size. In the extreme limit this may approach the flow pattern imposed by the *stagnant regions model* (Porter et al. 1972). This corresponds with experimental observations. This has not been verified by calculation because, while carrying out the sensitivity analysis, it was noted that the ease with which the numerical procedure obtained a converged solution to the flow equations was reduced with increasing eddy Reynolds number. Such a situation would be met while trying to simulate a large tray.

6.7 Conclusions

The sensitivity analysis carried out on this model has highlighted several aspects of the prediction of sieve tray efficiencies which concern, not only the model presented here, but a wide range of models.

It has been shown that current correlations for eddy diffusivity can produce a wide range of predicted values for the same set of conditions. A comprehensive survey of these correlations must be carried out in order to determine the *best* correlation for a give set of conditions.

Though the sensitivity of only the Yu fluid mechanical model to the prediction of eddy diffusivity was investigated, it is also possible to determine the effects of variations in this parameter on other models by simple comparison. It was found that if the Gerster et al. (1958) correlation was used to evaluate the tray efficiency, it could be over-predicted by up to approximately 10%. The sensitivity analysis has shown that the Gerster correlation generally predicts a higher value for the eddy diffusivity than other correlations tested here. If these other correlations are used then the efficiency could be decreased by up to 10%. This would still maintain the error margin for tray efficiencies predicted by this model to within 10% of the experimental efficiencies. For the majority of the cases studied, the error margin would actually be decreased if alternative eddy diffusivity correlations were used.

If we now consider the other tray efficiency models, we can easily see the trends in

the data. The *plug-flow plus back-mixing* model would predict a higher tray efficiency if a lower eddy diffusivity correlation were to be used. This can be predicted because, with the absence (or lessening) of the liquid back-mixing the predicted tray efficiency would more closely approximate the Lewis model (1936). It is well known that the tray efficiency predicted by the Lewis model is a theoretical maximum. This increase in the predicted tray efficiency would further increase an already large error margin for tray efficiencies predicted by this method.

The trend in data is less well defined for the *stagnant regions model.* For small trays the size of the stagnant regions at the sides would be small and so a reduction in the degree of mixing into these side regions may not decrease the predicted efficiency by a significant amount. On the other hand, the decrease in back-mixing in the central region would tend to increase the efficiency. The predicted efficiency for small trays could, therefore, increase with decreasing eddy diffusivity. For larger trays, the lack of mixing of the liquid into the stagnant zone would have a serious effect on the tray efficiency which could not be compensated for by a local increase in the central region. The net effect for trays of the size considered here would be to decrease the tray efficiency. It has already been shown that the efficiency predicted here is below the experimental, and so the accuracy of the model would suffer.

It has been shown that the accurate prediction of the average height of clear liquid is not necessary for the use of this model, the predicted tray efficiencies varying by only 1-2% with over a three-fold increase in the predicted clear liquid height.

The effect of the assumptions made in the determination of the resistance terms is smaller than the effect of the prediction of eddy diffusivity, but this too must be looked at in more detail if the model is to be used reliably for tray design. While simple experiments could be carried out in order to gain an insight into the magnitude of this term, it may be advantageous to approach this from a semi-theoretical point of view; experiments being backed up with a degree of theoretical modelling.

Prediction of the flow pattern for the limiting case of the tray diameter approaching

infinity has been studied in order to predict tray performances for large trays. This is complex due to the fact that an increase in tray diameter would increase both the eddy Reynolds number, indicating a reduction in the amount of liquid momentum transfered into the segmental regions of the tray by viscous mixing, and the dimensionless resistance terms, indicating a reduced liquid velocity in the centre region of the tray and liquid being pushed out towards the segmental regions. These phenomena have a contradictory effect on tray efficiency. Through a study of the sensitivity analysis it has been ascertained that the effect of an increase in the eddy Reynolds number is more significant than an increase in the resistance terms. This indicates that the tray efficiency predicted by the Yu fluid mechanical model would decrease with tray size. In the limit of the infinitely large tray, the predicted flow pattern may approach that of the *stagnant regions model* (Porter et al. 1972). This corresponds with experimental data.

CHAPTER 7

7. CONCLUSIONS

7.1 Introduction

Previous to this work no model existed which was easy to use, yet capable of reliably predicting a liquid flow pattern on a tray. Most models either were complex to use, or imposed a theoretical flow pattern approximately valid for a given geometry and set of flow conditions.

Through this work a new model has been presented and tested against experimental data. The results from models proposed by other authors have also been used for comparison. The findings from this work are summarised below. This summary has been divided into two sections; the first dealing with the modelling of a single tray and the second discussing the incorporation of such a model for tray efficiency into a column model.

Proposals for further work intended to improve our fundamental understanding and modelling of distillation trays are also presented.

7.2 The Yu Fluid Mechanical Model

The Yu fluid mechanical model presented here can predict liquid flow patterns from first principles based on factors which describe simply the tray geometry and liquid and vapour flow rates. Though the work carried out here is limited to a tray with chordal down-comers, the formulation of the equations which describe the model is such that they can be applied to any geometry of tray.

The flow patterns predicted by the Yu fluid mechanical model have been compared to flow pointer data gathered on a 2.44 meter diameter single tray air-water distillation simulation rig (see Section 3.5). Both sets of data show the liquid flows

predominantly down the centre of the tray, though the experimental data shows the liquid spreading out into the segmental areas for low liquid rates (vacuum simulation). This trend in the data is predicted by the fluid mechanical model. There is a small discrepancy in that the experimental data for the simulation of atmospheric and moderate pressure distillation can be interpreted to show that there were small regions of circulating liquid in the segmental regions of the trays. These were not predicted by the fluid mechanical model. Instead, the theoretical model predicted this region to be stagnant.

By comparison of the predicted tray efficiencies obtained from this model to experimental results obtained on a 2.44 metre diameter single tray air-water distillation simulation rig, it has been shown that the Yu fluid mechanical model is capable of predicting efficiencies to within 10% for atmospheric pressure simulation and to within 5% for moderate pressure simulation. Inspection of the experimental isotherms obtained from the water cooling experiments show them to be of similar shape to the theoretical U-shaped profiles predicted by the fluid mechanical model. These results are consistently higher than those predicted by the *stagnant regions model* (Porter et al. 1972).

From the observations based on comparison of the predicted flow patterns to the experimental flow pointer data, it would seem that the Yu fluid mechanical model can simulate the major flow features for the conditions tested. For the cases of atmospheric pressure and moderate pressure simulation the predicted concentration profiles and tray efficiencies also show a strong resemblance to the experimental data. The same is not true for the comparison of the predicted concentration profiles to experimental data for vacuum simulation, where large deviations are easily noted (see Figures 4.6 and 4.7).

Based on the comparison of the predicted concentration profiles and tray efficiencies to the experimental data, the conclusion must be reached that the Yu fluid mechanical model is not valid for the prediction of tray efficiencies for simulated vacuum distillation. This is thought to be due to the mechanism of liquid transport being

different for these conditions (Porter and Jenkins 1979). It is thought that the liquid is transported as a spray of droplets suspended in the vapour during vacuum simulation, whereas the Yu fluid mechanical model describes liquid transport in terms of a liquid continuous layer adjacent to the tray floor.

The resistance terms in the fluid mechanical model describe a mechanism whereby, in theory, the fast flowing liquid in the centre of the tray is slowed and diverted into the slower-moving side regions. This effect reduces the predicted size of the stagnant regions located in the segmental regions of the tray, increasing tray efficiency. Flow patterns predicted for the simulation of moderate pressure distillation are insensitive to variations in this term, while those predicted for atmospheric pressure distillation simulation are only slightly sensitive.

The eddy viscosity is the mechanism by which momentum transferred is simulated through the use of the fluid mechanical model. The effect of this is to simulate the transfer of momentum to the side regions of the tray preventing the formation of stagnant regions. Decreasing this value decreases the tray efficiency. Again, moderate pressure simulation is not sensitive to this parameter, but atmospheric pressure simulation is.

A sensitivity analysis carried out on the fluid mechanical model has shown that the model is insensitive to changes in the average height of clear liquid for the conditions tested. This is because there are two effects of lowering the height of clear liquid. The first is to decrease the effect of the viscous mixing, and the second is to increase the effect of the resistance terms. These effects counter-act each other and the resultant effect is little change in the tray efficiency.

Overall, the sensitivity analysis has shown that, although the model generally predicts higher tray efficiencies than those measured experimentally, the predicted data can be lowered by using alternative correlations for eddy diffusivity and lowering the predicted resistance term. The tray efficiency data originally calculated lies towards the upper end of the range of efficiencies calculated for a given set of conditions (see

Figure 6.3, 6.4, 6.7, 6.8). The accuracy of the model can therefore be improved by careful evaluation of these terms.

Prediction of the effects of scale-up are complex. The effect of the eddy viscosity in the transfer of momentum into the side regions of the tray diminishes. This would have the effect of increasing the size of the predicted stagnant regions. Conversely, the effect of the resistance term increases, an effect which would decrease the size of the predicted stagnant regions. From consideration of the sensitivity analysis (Chapter 6), it can be seen that the effect of reducing the eddy viscosity (increasing the eddy Reynolds number) has a much larger effect on the predicted tray efficiency than a change in the resistance term. It must, therefore, be assumed that this parameter is dominant. The overall effect will be for the size of the stagnant regions to increase with tray diameter. It is thought that the liquid flow pattern will approach that of the *stagnant regions model* (Porter et al. 1972).

7.3 DISTSIM - A Distillation Column Model

The Yu fluid mechanical model has been incorporated into a column model and has been used to interpret experimental data in order to find mass-transfer data. The results seem to follow the trends of the results calculated previously (Akebe 1983).

It has been shown that, for the geometry of tray used (1.2 metre diameter, 0.96 metre down-comer) the fluid mechanical model predicts a lower tray efficiency than the *stagnant regions model* (Porter et al. 1972). This is the reverse of the situation shown for the 2.44 metre diameter column studied earlier.

7.4 Further Work

The model presented here is limited in its handling of the structure of the froth on the tray. It is inherent in the model that the liquid is assumed to be transported as a liquid continuous layer of constant depth next to the tray floor.

Through appropriate adjustment of the two-dimensional fluid mechanical equations presented here it should be possible to expand the model in order to calculate a varying liquid surface and, hence, calculate a height of clear liquid on the tray from first principles.

A model which could predict variations in the height of clear liquid on a tray could be used to study vapour maldistribution on a tray and could help interpret and predict tray pressure drops.

In addition to the mechanism of liquid transport assumed to apply here, it should be possible to expand the series of equations presented to include a model which takes into account liquid transport in a vapour continuous layer above the froth. This could then create a mathematical model which would be valid for the spray regime in addition to the mixed-froth and emulsion flow regimes. One possible model for liquid transport could be a *diffusional-type* relationship such as the *spray diffusion model* proposed by Porter et al. (1977).

REFERENCES

Akebe, W.T., (1983) Statistical optimisation technique for the predicting of mass transfer coefficients on distillation trays from plant data, MSc Thesis, Aston University

Ashley, M.J., Haselden, G.G., (1970) The calculation of plate efficiency under conditions of finite mixing in both phases in multi-plate columns and the potential advantage of parallel flow, *Chem. Engng. Sci.*, **25**, 1665 - 1672

Bell, R.L., (1972) Residence time and fluid mixing on commercial scale sieve trays, *AIChE J.*, **18**, (3), 498 - 505

Bell, R.L., Solari, R.B., (1974a) Effect of non-uniform velocity fields and retrograde flow on distillation tray efficiency, *AIChE J.*, **20**, (4), 688 - 695

Bell, R.L., Solari, R.B., (1974b) G.V.C. / AIChE Joint meeting, Munich, Sept 1974

Bennett, C.O., Myers, E.J., (1982) Momentum, Heat and Mass Transfer, 3rd edition, pub. McGraw-Hill Inc

Bennett, D.L., Agrawal, R., Cook, P.J., (1983) New pressure drop correlation for sieve tray distillation columns, *AIChE. J.*, **29**, (3), 434 - 442

Biddulph, M.W., Bultitude, D.P., (1980) Flow characteristics of a small-hole sieve tray, *AIChE J.*, **36**, (12), 1913 - 1916

Brambilla, A., (1976) The effect of vapour mixing on efficiency of large diameter distillation plates, *Chem. Engng. Sci.*, **31**, 517 - 523

Browne, L.B.E., (1978), The marker and cell technique, in Noye, J., Numerical Simulation of Fluid Motion, pub. North-Holland Publishing Company, 223 - 247

Bruin, S., Freije, A.D., (1974) A simple liquid mixing model for distillation plates with stagnant zones, *Trans. Instn. Chem. Engrs.*, **52**, 75 - 79

Chambers, S., (1993) Flow patterns on sieve trays, PhD Thesis, Department of Chemical Engineering & Applied Chemistry, University of Aston in Birmingham, 1993

Chorin, A.J., (1968) Numerical solution of the Navier-Stokes equations, *Math. Comp.*, **22**, 745 - 762

Colwell, C.J., (1979) Clear liquid height and froth density on sieve trays, *Ind. & Engng. Chem. Proc. Des. & Dev.*, **20**, (2), 298 - 307

Daly, B.R., Quarini, G.L., Chambers, S., Porter, K.E., (1995) An investigation into the problems incurred in industrial sized distillation columns due to gas distribution, The 1995 IChemE Reseach Event, 191 - 194

Danckwerts, P.V., (1953) Continuous flow systems, *Chem. Engng. Sci.*, **2**, (1), 1 - 13

Davies, B.T., Porter, K.E., (1965) Some observations on sieve tray froths, Proc. Symposium on Two Phase Flow, 21 - 23 June, University of Exeter, UK, p. F301 - F324

Diener, D.A., (1967) Calculation of effect of vapour mixing on tray efficiency, *Ind. & Engng. Chem. Proc. Des & Dev.*, **6**, (4), 499 - 503

Fair, J.R., (1963) Tray hydraulics - perforated trays, in Smith, B.D., Design of Equilibrium Stage Processes, pub. McGraw-Hill, 539 - 569

Fenwick, K.S., Porter, K.E., (1995) Liquid distribution and mass transfer on a 2.4 m diameter distillation tray, The 1995 IChemE Reseach Event, 716 - 718

Fletcher, J.P., (1983) Private communications to W.T. Akebe, University of Aston in Birmingham

Fletcher, J.P., (1987) A method for the rigorous calculation of distillation columns using a generalised efficiency model, IChemE. Symp. Series No 104, A437-A448

Fluent (1990) User Manual Volume 1, Version 3.02, Tutorial 6

Fox, L., (1962) Finite difference formulae for elliptic equations in two dimensions, in Fox, L., Numerical Solution of Ordinary and Partial Differential Equations, pub. Pergamon Press

Francis, J.B., (1883) Lowell Hydraulic Experiments, 4th edition, pub. Van Nostrand Company, New York

Fredenslund, A., Gmehling, J., Rasmussen, P., (1977) Vapour-liquid equilibria using UNIFAC; a group contribution method, pub. Elsevier

Gatreaux, M.F., O'Connell, H.E., (1955) Effect of length of liquid path on plate efficiency, *Chem. Engng. Prog.*, **51**, (5), 232 - 237

Gerster, J.A., Hill, A.B., Hochgraf, N.N., Robinson, D.G., (1958) Tray efficiencies in distillation columns, Final Report, University of Delaware, AIChE, New York

Harada, M., Adachi, M., Eguchi, W., Nagata, S., (1964) Studies of fluid mixing on sieve plates, *Int. Chem. Engng.*, **4**, (1), 165 - 173

Harlow, F.H., Welch, J.E., (1965) Numerical calculation of time-dependent viscous incompressible flow of fluid with free surface, *The Phys. Fluids*, **8**, 2182 - 2189

Hausen, H., (1953) Zur Definition des Austauschgrades von Rektifizierböden bei Zwei- und Dreistoff- Gemischen, *Chemie-Ing. Techn.*, **25**, (10), 595 - 597

Hine, C.J., (1990) Effect of liquid flow patterns on distillation trays, PhD Thesis, Department of Chemical Engineering & Applied Chemistry, University of Aston in Birmingham, 1990

Hirose, Y., Kawase, Y., Sampei, K., Kawai, T., (1980) A new approach to distillation column at total reflux, *Computers Chem Engng*, **4**, (2), 133 - 138

Ho, G.E., Muller, R.L., Prince, R.G.H., (1969) Characterisation of two-phase flow patterns in plate columns, IChemE. Symp. Series, No 32, 2:10 - 2:21

Hofhuis, P.A.M., Zuiderweg, F.J., (1979) Sieve plates: dispersion density and flow regimes, IChemE. Symp. Series No 56, 2.2/1 - 2.2/26

Jeronimo, M.A.da S., Sawistowski, H., (1973) Phase inversion correlation for sieve trays, *Trans. Instn. Chem. Engrs.*, **51**, 265 - 266

Joseph, D.D., Renardy, Y.Y., Fundamentals of Two-Fluid Dynamics, Part 1: Mathematical Theory and Applications, pub. Springer-Verlag, 1992

Kafarov, V.V., Shestopalov, V.V., Bel'kov, V.P., (1972) Longitudinal mixing of liquid in a plate column with sieve trays for the absorption of nitric oxide, *Int. Chem. Engng.*, **12**, (2), 257 - 259

Kafarov, V.V., Sheptopalov, V.V., Komissarov, Y.A., (1979) Vapour - liquid flow structure on bubbler plates, IChemE. Symp. Series No 56, 2.3/79 - 2.3/98

Kirschbaum, E., (1934) Efficiency for rectification and appropriate path for liquid flow, *Forsch. Gebeite Ingenieur*, **5**, 245 - 252

Khan, R., (1995) Private communications, University of Aston in Birmingham.

Lewis, W.K., (1936) Rectification of binary mixtures, *Ind. & Engng. Chem.*, **28**, (4), 399 - 402

Lim, C.T., (1973) PhD Thesis, Department of Chemical Engineering, UMIST, 1973

Lim, C.T., Porter, K.E., Lockett, M.J., (1974) The effect of liquid channelling on two-pass distillation plate efficiency, *Trans. Instn. Chem. Engrs.*, **52**, 193 - 201

Lockett, M.J., (1981) The froth to spray transition on sieve trays, *Trans. Instn. Chem. Engrs.*, **59**, 26 - 34

Lockett, M.J., (1986) Distillation Tray Fundamentals, pub. Cambridge University Press

Lockett, M.J., Dhulesia, H.A., (1980) Murphree plate efficiency with non-uniform vapour distribution, *Chem. Engng. J.*, **19**, 183 - 188

Lockett, M.J., Lim, C.T., Porter, K.E., (1973) The effect of liquid channelling on distillation column efficiency in the absence of vapour mixing, *Trans. Instn. Chem. Engrs.*, **51**, 61 - 67

Lockett, M.J., Plaka, T., (1983) Effect of non-uniform bubbles in the froth on the correlation and prediction of point efficiencies, *Chem. Eng. Res. Dev.*, **61** (March), 119 - 124

Lockett, M.J., Porter, K.E., Bassoon, K.S., (1975) The effect of vapour mixing on distillation plate efficiency when liquid channelling occurs, *Trans. Instn. Chem. Engrs.*, **53**, 125 - 130

Lockett, M.J., Safekourdi, A., (1976) The effect of the liquid flow pattern on distillation plate efficiency, *Chem. Engng. J.*, **11**, 111 - 121

Loon, R.E., Pinczewski, W.V., Fell, C.J.D., (1973) Dependence of the froth to spray transition on sieve tray design parameters, *Trans. Instn. Chem. Engrs.*, **51**, 374 - 376

Mix, T.W., Dweck, J.S., Weinberg, M., Armstrong, R.C., (1980) Energy conservation in distillation, AIChE. Symp. Series No 192, **76**, 15 - 23

Muller, R.L., Prince, R.G.H., (1972) Regimes of bubbling and jetting from submerged orifices, *Chem. Engng. Sci.*, **27**, 1583 - 1592

Murphree, E.V., (1925) Rectifying column calculations with particular reference to N component mixtures, *Ind. Engng. Chem.*, **17**, (7), 747 - 750

Napthali, L.M., Sandholm, D.P., (1971) Multicomponent separation by linearization, *AIChE J.*, **17**, 148 - 153

Payne, G.J., Prince, R.G.H., (1975) The transition from jetting to bubbling at a submerged orifice, *Trans. Instn. Chem. Engrs.*, **53**, 209 - 223

Payne, G.J., Prince, R.G.H., (1977) The relationship between the froth and spray regimes and the orifice processes occurring on perforated plates, *Trans. Instn. Chem. Engrs.*, **55**, 266 - 273

Pinczewski, W.V., Fell, C.J.D., (1982) Froth to spray transition on sieve trays, *Ind. Engng. Chem. Proc. Des. & Dev.*, **21**, (4), 774 - 776

Pinczewski, W.V., Yeo, H.K., Fell, C.J.D., (1973) Transition behaviour at submerged orifices, *Chem. Engng. Sci.*, **28**, 2261 - 2263

Porter, K.E., Davies, B., Enjugu, B.A., Ani, C.C., (1987) Investigating the effect of the liquid flow pattern on sieve tray performance by means of the water cooling technique, IChemE. Symp. Series No 104, A569 - A588

Porter, K.E., Fletcher, J.P., Akebe, W.T., (1994) DISTSIM, a program for the evaluation and design of distillation columns, AIChE Research Event, San Francisco, Nov 1994

Porter, K.E., Jenkins, J.D., (1979) The interrelationship between industrial practice and academic research in distillation and absorption, IChemE. Symp. Series No 56, Vol. 3, 75 - 121

Porter, K.E., Jenkins, J.D., (1982) in Sharp, D., West, T.F., The Chemical Industry, Chapter 41, pub. Ellis Horwood Publishers

Porter, K.E., Lockett, M.J., Lim, C.T., (1972) The effect of liquid channelling on distillation plate efficiency, *Trans. Instn. Chem. Engrs.*, **50**, 91 - 101

Porter, K.E., Safekourdi, A., Lockett, M.J., (1977) Plate efficiency in the spray regime, *Trans Instn. Chem. Engrs.*, **55**, 190 - 195

Porter, K.E., Wong, P.F.Y., (1969) Transition from spray to bubbling on sieve plates, IChemE. Symp. Series, No 32, 2:22 - 2:33

Porter, K.E., Yu, K.T., Chambers, S., Zhang, M.Q., (1992) Flow patterns and temperature profiles on a 2.44m diameter sieve tray, IChemE. Symp. Series No 128, A257 - A276

Prince, R.G.H., Jones, A.P., Panic, R.J., (1979) The froth spray transition, IChemE. Symp. Series No. 56, 2.2/27 - 2.2/40

Raper, J.A., Hai, N.T., Pinczewski, W.V., Fell, C.J.D., (1979) Mass transfer efficiency on simulated industrial sieve trays operating in the spray regime, IChemE. Symp. Series No 56, 2.2/57 - 2.2/74

Rush, F.E., (1979) Energy saving alternatives to conventional distillation, IChemE. Symp. Series No 56, 4.1/1 - 4.1/13

Safekourdi, A., (1975) PhD Thesis, Department of Chemical Enginerring, UMIST, 1975

Sakata, M., Yanagi, T., (1979) Performance of a commercial sieve tray, IChemE. Symp. Series No 56, 3.2/21 - 3.2/34

Shore, D., Haselden, G.G., (1969) Liquid mixing on distillation plates and its effect on plate efficiency, IChemE. Symp. Series No 32, 2:54 - 2:62

Sohlo, J.J., Kouri, R.J., (1982) An analysis of enhanced transverse dispersion on distillation plates, *Chem. Engng. Sci.*, **37**, 193 - 197

Solari, R.B., Bell, R.L., (1978) The effect of transverse eddy dispersion on distillation tray efficiency, AIChE. Meeting, Feb. 1978, Atlanta

Solari, R.B., Saez, E., D'Apollo, I., Bellet, A., (1982) Velocity distribution and liquid flow patterns on industrial sieve trays, *Chem. Engng. Commun.*, **13**, 369 - 384

Standart, G., (1965) Studies on distillation - V, *Chem. Engng. Sci.*, **20**, 611 - 622

Stichlmair, J., (1978) Bodenkolonne, pub. Verlag Chemie

Strand, C.P., (1963) A new look at distillation - 3: bubble cap tray efficiencies, *Chem. Engng. Prog.*, **59**, (4), 58 - 64

Viecelli, J.A., (1971) A computing method for incompressible flows bounded by moving walls, *J.Comp. Phys.*, **8**, 119 - 143

Wehner, J.F., Wilhelm, R.H., (1956) Boundary conditions of flow reactors, *Chem. Engng. Sci.*, **6**, 89 - 93

Weiler, D.W., Delnicki, W.V., England, B.L., (1973) Distillation - flow hydraulics of large diameter trays, *Chem. Engng. Prog.*, **69**, (10), 67 - 76

Wilson, G.M., (1964) A new expression for excess energy of mixing, *J. Am. Chem. Soc.*, **86**, 127 - 130

Yu, K.T., Huang, J., Gu, F., (1983) Simulation and efficiency of a large tray, Selected papers of *J. Chem. Ind. & Eng. (China)*, **2**, June, 12 - 35

Yu, K.T., Huang, J., Li, J.L., Song, H.H., (1990) Two-dimensional flow and eddy diffusion on a sieve tray, *Chem. Engng. Sci.*, **45**, (9), 2901 - 2906

Yu, K.T., Li, J.L., Huang, J., (circa 1991) Theoretical computational of liquid flow distribution on a sieve tray, Private communications

Zuiderweg, F.J., (1982) Sieve trays - a view on the state of the art, *Chem. Engng. Sci.*, **37**, (10), 1441 - 1464

Zuiderweg, F.J., Hofhuis, P.A.M., Kuzniar, J., (1984) Flow regimes on sieve trays: the significance of the emulsion flow regime, *Chem. Engng. Res. Dev.*, **62**, 39 - 47

APPENDICES

Appendix 1 - The constants η and ξ used in the K.T. Yu model

In Chapter 3, the force balance equations (Equations 3.10 & 3.11) were derived and the numerical method for their solution was explained. The solution method contains the constants η and ξ (Equations 3.31 to 3.34) which were obtained when Equations 3.10 and 3.11 were put into finite difference form and re-arranged. This procedure is described in more detail below.

When the finite difference approximations (Equations 3.22 to 3.25) are substituted into the force balance relationships (Equations 3.10 and 3.11) we obtain:

$$\frac{u^{n+1}_{i+\frac{1}{2},j}-u^{n}_{i+\frac{1}{2},j}}{\delta t}+u^{n}_{i+\frac{1}{2},j}\left(\frac{u^{n}_{i,j}-u^{n}_{i-1,j}}{\Delta}\right)+v^{n}_{i+\frac{1}{2},j}\left(\frac{u^{n}_{i+\frac{1}{2},j+\frac{1}{2}}-u^{n}_{i+\frac{1}{2},j-\frac{1}{2}}}{\Delta}\right)=$$
$$-\frac{1}{\rho_L}\left(\frac{P^{n}_{i+1,j}-P^{n}_{i,j}}{\Delta}\right)+\nu_e\left(\frac{u^{n}_{i+\frac{3}{2},j}+u^{n}_{i-\frac{1}{2},j}+u^{n}_{i+\frac{1}{2},j-1}+u^{n}_{i+\frac{1}{2},j+1}-4u^{n}_{i+\frac{1}{2},j}}{\Delta^2}\right) \quad (A1.1)$$
$$-\frac{u^{n}_{i+\frac{1}{2},j}}{h_i\rho_L}(\tau_{\delta x}+\tau_{vx})$$

On re-arranging, this becomes:

$$u^{n+1}_{i+\frac{1}{2},j}=u^{n}_{i+\frac{1}{2},j}+\delta t\left(\nu_e\left\{\frac{u^{n}_{i+\frac{3}{2},j}+u^{n}_{i-\frac{1}{2},j}+u^{n}_{i+\frac{1}{2},j-1}+u^{n}_{i+\frac{1}{2},j+1}-4u^{n}_{i+\frac{1}{2},j}}{\Delta^2}\right\}-\right.$$
$$\left.u^{n}_{i+\frac{1}{2},j}\left\{\frac{u^{n}_{i+1,j}-u^{n}_{i,j}}{\Delta}\right\}-v_{i+\frac{1}{2},j}\left\{\frac{u^{n}_{i+\frac{1}{2},j+\frac{1}{2}}-u^{n}_{i+\frac{1}{2},j-\frac{1}{2}}}{\Delta}\right\}-\frac{u^{n}_{i+\frac{1}{2},j}}{h_i\rho_L}(\tau_{\delta x}+\tau_{vx})\right) \quad (A1.2)$$
$$+\frac{\delta t}{\rho_L\Delta}\left[P^{n+1}_{i,j}-P^{n+1}_{i+1,j}\right]$$

Since all terms evaluated at time-step n do not change during time-step n+1, this part of Equation A1.2 can be considered to be a constant for a given time-step. This can be written as:

$$u_{i+\frac{1}{2},j}^{n+1} = \eta_{i+\frac{1}{2},j}^{n} + \frac{\delta t}{\rho_L \Delta}\left[P_{i,j}^{n+1} - P_{i+1,j}^{n+1}\right] \tag{A1.3}$$

where:

$$\eta_{i+\frac{1}{2},j}^{n} = u_{i+\frac{1}{2},j}^{n} + \delta t\left(\nu_e\left\{\frac{u_{i+\frac{3}{2},j}^{n} + u_{i-\frac{1}{2},j}^{n} + u_{i+\frac{1}{2},j-1}^{n} + u_{i+\frac{1}{2},j+1}^{n} - 4u_{i+\frac{1}{2},j}^{n}}{\Delta^2}\right\} - u_{i+\frac{1}{2},j}^{n}\left\{\frac{u_{i+1,j}^{n} - u_{i,j}^{n}}{\Delta}\right\} - v_{i+\frac{1}{2},j}\left\{\frac{u_{i+\frac{1}{2},j+\frac{1}{2}}^{n} - u_{i+\frac{1}{2},j-\frac{1}{2}}^{n}}{\Delta}\right\} - \frac{u_{i+\frac{1}{2},j}^{n}}{h_1 \rho_L}\left(\tau_{\delta x} + \tau_{vx}\right)\right) \tag{A1.4}$$

Similarly, for the y-direction we can say:

$$v_{i,j+\frac{1}{2}}^{n+1} = \xi_{i,j+\frac{1}{2}}^{n} + \frac{\delta t}{\rho_L \Delta}\left[P_{i,j}^{n+1} - P_{i,j+1}^{n+1}\right] \tag{A1.5}$$

where:

$$\xi_{i,j+\frac{1}{2}}^{n} = v_{i,j+\frac{1}{2}}^{n} + \delta t\left(\nu_e\left\{\frac{v_{i,j+\frac{3}{2}}^{n} + v_{i,j-\frac{1}{2}}^{n} + v_{i-1,j+\frac{1}{2}}^{n} + v_{i+1,j+\frac{1}{2}}^{n} - 4v_{i,j+\frac{1}{2}}^{n}}{\Delta^2}\right\} - v_{i,j+\frac{1}{2}}^{n}\left\{\frac{v_{i,j+1}^{n} - v_{i,j}^{n}}{\Delta}\right\} - u_{i,j+\frac{1}{2}}\left\{\frac{v_{i+\frac{1}{2},j+\frac{1}{2}}^{n} - v_{i-\frac{1}{2},j+\frac{1}{2}}^{n}}{\Delta}\right\} - \frac{v_{i,j+\frac{1}{2}}^{n}}{h_1 \rho_L}\left(\tau_{\delta y} + \tau_{vy}\right)\right) \tag{A1.6}$$

Appendix 2 - The concentration wall boundary condition

In Chapter 4, a formula was derived which could be used to calculate the concentration profiles across a tray. It mentioned that the wall boundary condition was similar to that derived by Lim (1973) based on the a procedure described by Fox (1962).

For the purpose of simplicity in understanding, the position of boundary points will be referred to as compass bearings around a central point, O.

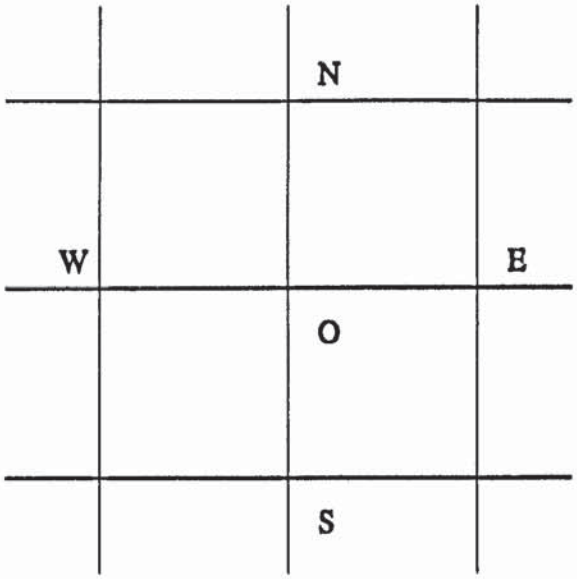

Figure A2.1: Nomenclature used for referencing grid point for the derivation of the wall boundary formulae

Using this new nomenclature, Equation 4.13 becomes:

$$C_O = k_N C_N + k_S C_S + k_E C_E + k_W C_W + k_V \qquad (A2.1)$$

where: k_V replaces k_5 / k_6 in Equation 4.14.

All the other constants (k_1, k_2, k_3 and k_4) have also been divided by k_6 before substitution for simplicity.

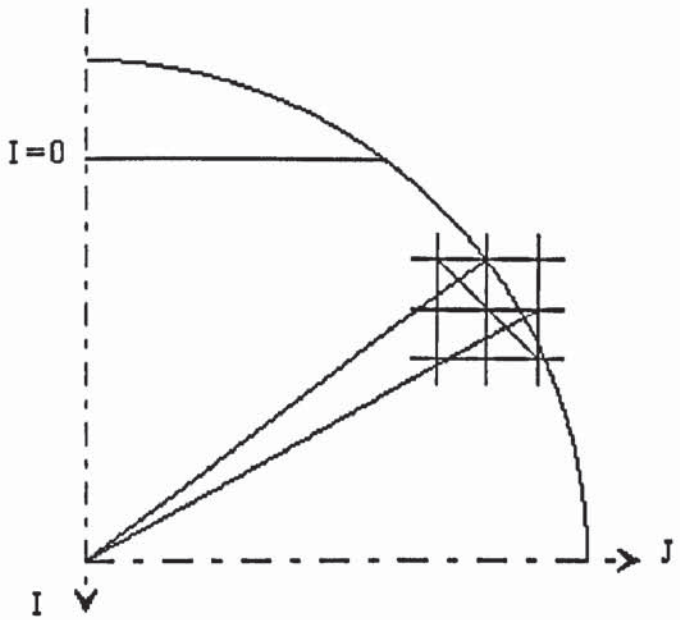

Figure A2.2: Intersection of the calculation mesh with the curved tray wall

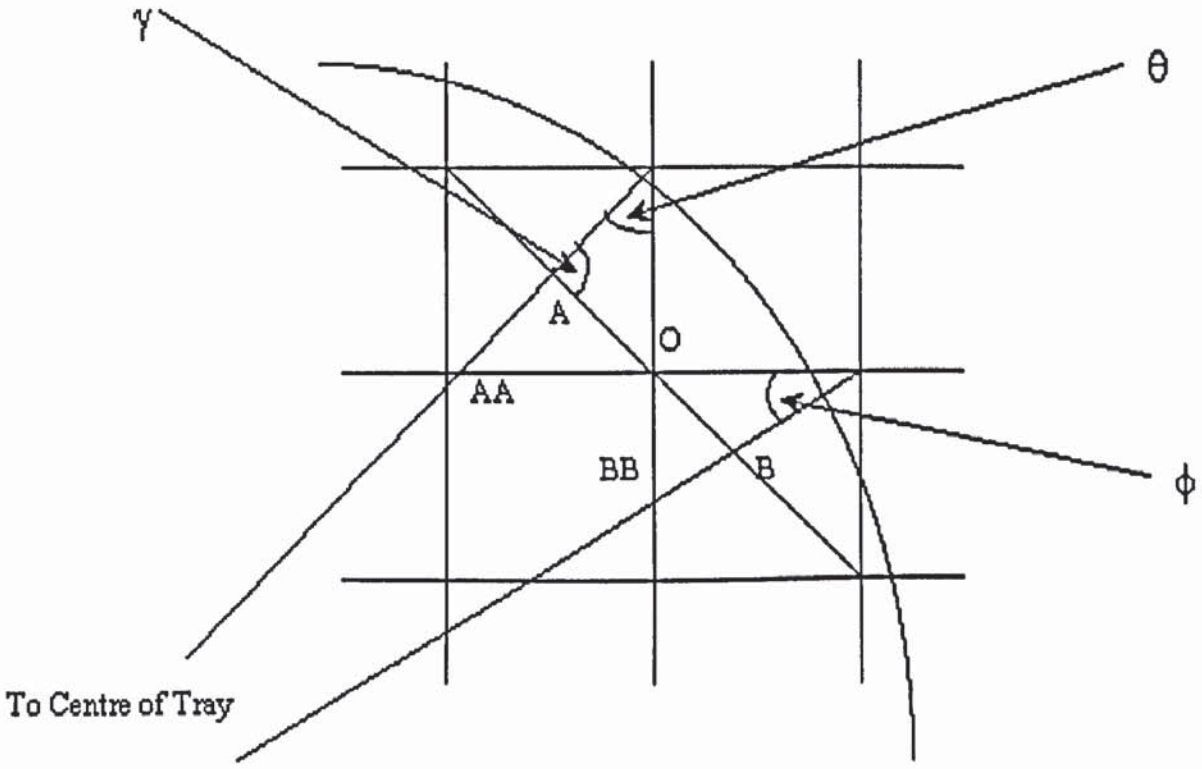

Figure A2.3: Enlarged section of the intersection of the calculation mesh with the curved tray wall

The angles indicated in Figure A2.3 are calculated as follows:

$$\tan\theta = \frac{(J-1)*H}{\text{abs}\left(\frac{Z}{2}-(I-2)*H\right)} \qquad \text{(A2.2)}$$

$$\gamma = \frac{3}{4}\pi - \theta \qquad \text{(A2.3)}$$

$$\tan\phi = \frac{J*H}{\text{abs}\left(\frac{Z}{2}-(I-1)*H\right)} \qquad \text{(A2.4)}$$

where H is the grid length used in the finite difference approximations (m)

Z is the flow path length (m)

Type 1:

The equation used to calculate the concentration is the same as Equation A2.1 since none of the points required for the calculation procedure lie outside the calculation domain.

Type 2:

We have to make the following approximations

$$C_E = C_O + \frac{OB}{OSE}(C_{SE} - C_O)$$

$$C_N = C_O + \frac{OAA}{H}(C_W - C_O)$$

Through substituting these terms into Equation A2.1 and re-arranging, we can get

$$C_O = \frac{k_S C_S + k_E \frac{OB}{OSE} C_{SE} + \left(k_W + \frac{OAA}{H} k_N\right) C_W + k_V}{1 + k_N\left(\frac{OAA}{H} - 1\right) + k_E\left(\frac{OB}{OSE} - 1\right)} \qquad \text{(A2.5)}$$

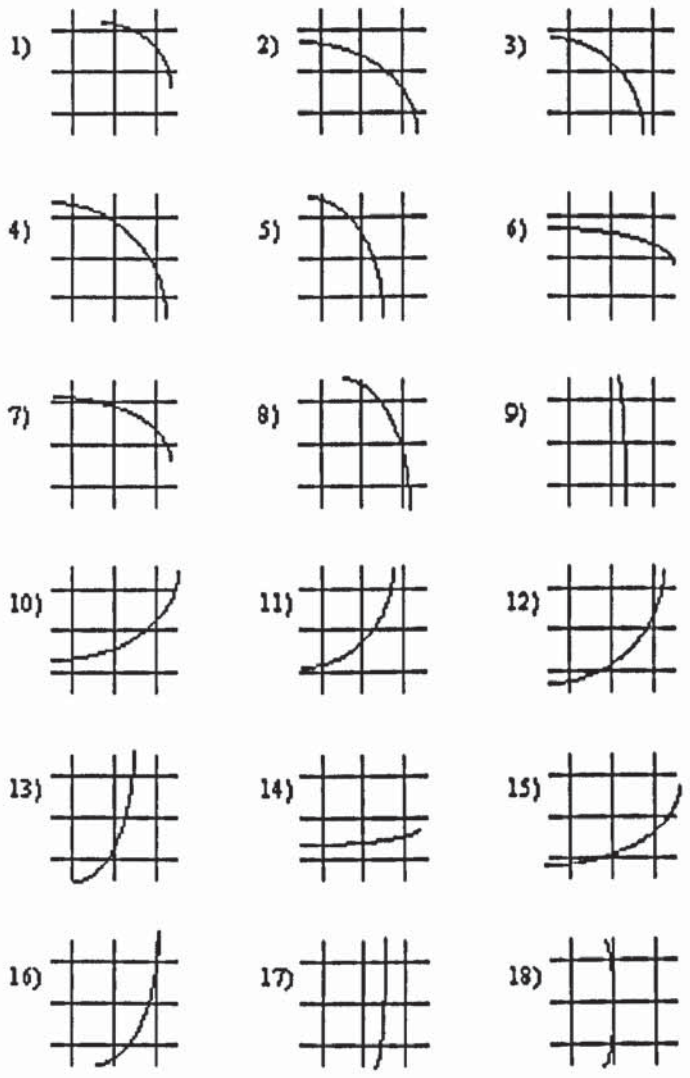

Figure A2.4: Various types of mesh points near the column walls

In a similar fashion, we can arrive at expressions for the remaining points.

Type 3:

$$C_O = \frac{\left(k_S + k_E \frac{OBB}{H}\right) C_S + \left(k_W + k_N \frac{OAA}{H}\right) C_W + k_V}{1 + k_N\left(\frac{OAA}{H} - 1\right) + k_E\left(\frac{OBB}{H} - 1\right)} \qquad (A2.6)$$

Type 4:

$$C_O = \frac{k_S C_S + k_N \frac{OA}{ONW} C_{NW} + k_E \frac{OB}{OSE} C_{SE} + k_W C_W + k_V}{1 + k_N\left(\frac{OA}{ONW} - 1\right) + k_E\left(\frac{OB}{OSE} - 1\right)} \qquad (A2.7)$$

Type 5:

$$C_O = \frac{\left(k_S + k_E \frac{OBB}{H}\right) C_S + k_N \frac{OA}{ONW} C_{NW} + k_W C_W + k_V}{1 + k_N\left(\frac{OA}{ONW} - 1\right) + k_E\left(\frac{OBB}{H} - 1\right)} \qquad (A2.8)$$

Type 6:

$$C_O = \frac{k_S C_S + k_E C_E + \left(k_W + k_N \frac{OAA}{H}\right) C_W + k_V}{1 + k_N\left(\frac{OAA}{H} - 1\right)} \qquad (A2.9)$$

Type 7:

$$C_O = \frac{k_S C_S + k_N \frac{OA}{ONW} C_{NW} + k_E C_E + k_W C_W + k_V}{1 + k_N\left(\frac{OA}{ONW} - 1\right)} \qquad \textbf{(A2.10)}$$

Type 8:

$$C_O = \frac{k_S C_S + k_N C_N + k_E \frac{OB}{OSE} C_{SE} + k_W C_W + k_V}{1 + k_E\left(\frac{OB}{OSE} - 1\right)} \qquad \textbf{(A2.11)}$$

Type 9:

$$C_O = \frac{\left(k_S + k_E \frac{OBB}{H}\right) C_S + k_N C_N + k_W C_W + k_V}{1 + k_E\left(\frac{OBB}{H} - 1\right)} \qquad \textbf{(A2.12)}$$

Type 10:

$$C_O = \frac{k_N C_N + k_E \frac{OB}{ONE} C_{NE} + \left(k_W + k_S \frac{OAA}{H}\right) C_W + k_V}{1 + k_S\left(\frac{OAA}{H} - 1\right) + k_E\left(\frac{OB}{ONE} - 1\right)} \qquad \textbf{(A2.13)}$$

Type 11:

$$C_O = \frac{\left(k_N + k_E \frac{OBB}{H}\right) C_N + \left(k_W + k_S \frac{OAA}{H}\right) C_W + k_V}{1 + k_S\left(\frac{OAA}{H} - 1\right) + k_E\left(\frac{OBB}{H} - 1\right)} \qquad \textbf{(A2.14)}$$

Type 12:

$$C_O = \frac{k_N C_N + k_S \frac{OA}{OSW} C_{SW} + k_E \frac{OB}{ONE} C_{NE} + k_W C_W + k_V}{1 + k_S\left(\frac{OA}{OSW} - 1\right) + k_E\left(\frac{OB}{ONE} - 1\right)} \qquad \textbf{(A2.15)}$$

Type 13:

$$C_O = \frac{\left(k_N + k_E \frac{OBB}{H}\right) C_N + k_S \frac{OA}{OSW} C_{SW} + k_W C_W + k_V}{1 + k_S\left(\frac{OA}{OSW} - 1\right) + k_E\left(\frac{OBB}{H} - 1\right)} \qquad \textbf{(A2.16)}$$

Type 14:

$$C_O = \frac{k_N C_N + k_E C_E + \left(k_W + k_S \frac{OAA}{H}\right) C_W + k_V}{1 + k_S\left(\frac{OAA}{H} - 1\right)} \qquad \textbf{(A2.17)}$$

Type 15:

$$C_O = \frac{k_N C_N + k_S \frac{OA}{OSW} C_{SW} + k_E C_E + k_W C_W + k_V}{1 + k_S\left(\frac{OA}{OSW} - 1\right)} \qquad \textbf{(A2.18)}$$

Type 16:

$$C_O = \frac{k_N C_N + k_S C_S + k_E \frac{OB}{ONE} C_{NE} + k_W C_W + k_V}{1 + k_E\left(\frac{OB}{ONE} - 1\right)} \qquad \textbf{(A2.19)}$$

Type 17:

$$C_O = \frac{\left(k_N + k_E \frac{OBB}{H}\right) C_N + k_S C_S + k_W C_W + k_V}{1 + k_E\left(\frac{OBB}{H} - 1\right)} \qquad \textbf{(A2.20)}$$

Type 18:

$$C_O = \frac{k_S \frac{OB}{OSW} C_{SW} + k_N \frac{OA}{ONW} C_{NW} + (k_E + k_W) C_W + k_V}{1 + k_S\left(\frac{OB}{OSW} - 1\right) + k_N\left(\frac{OA}{ONW} - 1\right)} \qquad \textbf{(A2.21)}$$

Appendix 3 - Precision and convergence of the numerical algorithms

A3.1 Introduction

From the descriptions of the numerical algorithms for the solutions of the velocity and concentration profiles, found in Chapters 3 and 4 respectively, it can be seen that several numerical constants must be chosen in order to carry out the calculations. These constants define the *rate* at which the calculations converge and the point at which it is assumed that convergence has been achieved. Careful choice of these parameters can lead to a rapid solution of the equations, whereas inappropriate choices may lead to numerical instability which could delay or prevent a solution being reached.

A brief discussion of the values chosen for these parameters is presented here together with the effects of choosing alternative values. The values chosen are justified by the fact that they have been found to work in the majority of calculations. No attempt has been made to carry out a theoretical analysis.

A3.2 Velocity calculations

The time step, δt

The time interval used in the calculation of all cases presented in this report, including those evaluated for the sensitivity analysis, was 0.01 s. Alternative values were initially tried in order to assess the solutions gained. Time intervals greater than 0.01 s frequently failed to produce a converged solution, whereas time intervals less than 0.01 s increased the solution time. A value of 0.001 s was found not to effect the final solution to the velocity calculations.

Convergence of the time iteration

The value used to determine whether a time interval is converged is the maximum allowable divergence from continuity at a position in the calculation domain (see

Section 3.3.2). For the calculations carried out in this thesis, a value of D_{max} equal to $1*10^{-4}$ s^{-1} was used, as suggested by Browne (1978). Lower values ($5*10^{-5}$ s^{-1}) were found to increase the calculation times. In cases where problems are found in obtaining a converged solution to time iterations, reducing this value may increase the numerical stability of the calculations.

Convergence of the velocity profiles

The velocity calculation are judged to have reached steady-state when the change in the velocity profiles from one time iteration to the next becomes small.

$$\frac{\frac{1}{N}\sum^{N}(u^{n}-u^{n-1})}{\delta t} < dv_{min} \qquad \text{(A3.1)}$$

For the purposes of this work dv_{min} was taken to be $1*10^{-4}$ ms^{-2}. Smaller values of dv_{min} prevented convergence of the calculations.

A3.3 Concentration calculations

The relaxation parameter, β

The relaxation parameter used in the calculation of the concentration profiles must be a value between 0 and 1. The lower this value, the more likely a converged solution is reached, but the longer the calculation procedure lasts. The calculation of the concentration profiles has been found to take a short time compared to the calculation of the velocity profiles; hence, finding a value of this parameter which yields the fastest solution time has not been a priority in this work. A value of 0.2 has been found to consistently produce a solution to the equations. Alternative values for this parameter were found not to effect the calculated concentration profiles.

Convergence of the concentration profiles is deemed to have been achieved when the average change in the liquid concentration from one iteration to the next becomes small. An average change of $1*10^{-7}$ has been used without any problems. Trouble may be found in trying to achieve a higher degree of convergence (a smaller average

change) as minor errors in the calculation of the concentrations may become significant. The use of a higher value of the average change in concentration has little effect on the overall run-time of the program.

A3.4 Precision of calculations

It has been calculated in this thesis that the Yu fluid mechanical model presented here is capable of predicting tray efficiencies to within approximately 10% of experimental data (see Chapter 4). The sensitivity analysis (Chapter 6) has shown that the predicted value of the tray efficiency may vary by up to 10 - 15% depending upon the value chosen for some of the model parameters. Therefore, it can be seen that a high degree of precision in carrying out the velocity and concentration calculations will not have any real impact on the effectiveness of this model. It is for this reason that all variables calculated in this work have been designated as *single-precision* variables in the FORTRAN code, i.e. they are only accurate to about 8 significant figures. The use of higher precision variables in the calculations would prove to be more costly in terms of time and the memory requirements of the computer used. It would also have little effect on the results obtained.

Appendix 4 - Tray efficiency data predicted using various theoretical models

	Experimental Point Efficiency	Experimental Tray Efficiency	Plug Flow Plus Back-Mixing Model	Stagnant Regions Model	Fluid Mechanical Model
	E_{OG}	E_{MV}/E_{OG}	E_{MV}/E_{OG}	E_{MV}/E_{OG}	E_{MV}/E_{OG}
Vacuum Case 1	0.36	1.90	2.71	1.64	2.31
Vacuum Case 2	0.41	1.83	3.12	1.82	2.60
Vacuum Case 3	0.45	1.78	3.52	1.98	2.87
Vacuum Case 4	0.48	1.95	3.71	2.07	3.03

Table A4.1: A comparison of tray efficiency models for simulated vacuum distillation

	Experimental Point Efficiency	Experimental Tray Efficiency	Plug Flow Plus Back-Mixing Model	Stagnant Regions Model	Fluid Mechanical Model
	E_{OG}	E_{MV}/E_{OG}	E_{MV}/E_{OG}	E_{MV}/E_{OG}	E_{MV}/E_{OG}
Atmospheric Pressure Case 1	0.77	1.29	1.63	1.15	1.35
Atmospheric Pressure Case 2	0.86	1.34	1.73	1.22	1.42
Atmospheric Pressure Case 3	0.82	1.28	1.68	1.20	1.40
Atmospheric Pressure Case 4	0.81	1.24	1.67	1.19	1.38

Table A4.2: A comparison of tray efficiency models for simulated atmospheric pressure distillation

	Experimental Point Efficiency	Experimental Tray Efficiency	Plug Flow Plus Back-Mixing Model	Stagnant Regions Model	Fluid Mechanical Model
	E_{OG}	E_{MV}/E_{OG}	E_{MV}/E_{OG}	E_{MV}/E_{OG}	E_{MV}/E_{OG}
Moderate Pressure Case 1	0.88	1.17	1.32	1.08	1.19
Moderate Pressure Case 2	0.94	1.13	1.34	1.10	1.20
Moderate Pressure Case 3	0.87	1.09	1.32	1.07	1.17
Moderate Pressure Case 4	0.83	1.11	1.30	1.08	1.17

Table A4.3: A comparison of tray efficiency models for simulated moderate pressure distillation

Appendix 5 - Predicted tray enhancement factors and mass transfer data calculated using the DISTSIM program

Tray Enhancement Factors	Lewis Model	Stagnant Regions Model	Yu Fluid Mechanical Model
2	1.236	1.191	1.165
3	1.239	1.198	1.169
4	1.245	1.203	1.172
5	1.254	1.203	1.177
6	1.265	1.217	1.184
7	1.280	1.230	1.196
8	1.299	1.247	1.211
9	1.327	1.267	1.228
10	1.358	1.290	1.251
11	1.392	1.318	1.272
N_G	1.388	1.534	1.704
N_L	2.690	2.750	2.617

Table A5.1: Predicted tray enhancement factors and mass transfer data calculated using the DISTSIM distillation column simulation program assuming total vapour mixing between trays

Tray Enhancement Factors	Lewis Model	Stagnant Regions Model	Yu Fluid Mechanical Model
2	1.225	1.152	1.083
3	1.229	1.161	1.086
4	1.232	1.167	1.090
5	1.241	1.172	1.097
6	1.252	1.179	1.105
7	1.267	1.195	1.119
8	1.286	1.208	1.133
9	1.311	1.234	1.162
10	1.339	1.248	1.184
11	1.370	1.323	1.287
N_G	1.406	1.647	1.914
N_L	2.826	2.614	2.709

Table A5.2: Predicted tray enhancement factors and mass transfer data calculated using the DISTSIM distillation column simulation program assuming no vapour mixing between trays

Appendix 6 - Predicted eddy diffusivity data used in the sensitivity analysis

Case	Gerster et al. (1958) / $m^2 s^{-1}$	Harada et al. (1964) / $m^2 s^{-1}$	Shore & Haselden (1969) / $m^2 s^{-1}$	Kafarov et al. (1972) / $m^2 s^{-1}$	Zuiderweg (1982) / $m^2 s^{-1}$
Vacuum Case 1 (ε = 0.763)	$7.44*10^{-4}$	$8.51*10^{-4}$	$2.39*10^{-3}$	$1.86*10^{-3}$	$1.83*10^{-3}$
Vacuum Case 2 (ε = 0.817)	$1.45*10^{-3}$	$1.33*10^{-3}$	$4.03*10^{-3}$	$4.16*10^{-3}$	$2.83*10^{-3}$
Vacuum Case 3 (ε = 0.855)	$2.40*10^{-3}$	$1.69*10^{-3}$	$5.34*10^{-3}$	$7.59*10^{-3}$	$2.85*10^{-3}$
Vacuum Case 4 (ε = 0.885)	$3.57*10^{-3}$	$1.93*10^{-3}$	$6.31*10^{-3}$	$1.28*10^{-3}$	$2.39*10^{-3}$
Atmospheric Pressure Case 1 (ε = 0.733)	$2.17*10^{-3}$	$1.17*10^{-3}$	$3.16*10^{-3}$	$2.42*10^{-3}$	$8.48*10^{-4}$
Atmospheric Pressure Case 2 (ε = 0.791)	$4.38*10^{-3}$	$1.81*10^{-3}$	$5.29*10^{-3}$	$5.24*10^{-3}$	$1.13*10^{-3}$
Atmospheric Pressure Case 3 (ε = 0.832)	$7.35*10^{-3}$	$2.34*10^{-3}$	$7.20*10^{-3}$	$9.46*10^{-3}$	$1.45*10^{-3}$
Atmospheric Pressure Case 4 (ε = 0.874)	$1.11*10^{-2}$	$2.30*10^{-3}$	$7.44*10^{-3}$	$1.60*10^{-2}$	$8.22*10^{-4}$
Moderate Pressure Case 1 (ε = 0.731)	$5.03*10^{-3}$	$1.75*10^{-3}$	$5.80*10^{-3}$	$3.82*10^{-3}$	$2.05*10^{-3}$
Moderate Pressure Case 2 (ε = 0.761)	$8.77*10^{-3}$	$2.19*10^{-3}$	$7.17*10^{-3}$	$5.62*10^{-3}$	$1.88*10^{-3}$
Moderate Pressure Case 3 (ε = 0.825)	$1.45*10^{-2}$	$1.75*10^{-3}$	$7.77*10^{-3}$	$1.01*10^{-2}$	$1.10*10^{-3}$
Moderate Pressure Case 4 (ε = 0.851)	$2.18*10^{-2}$	$1.94*10^{-3}$	$1.01*10^{-2}$	$1.61*10^{-2}$	$1.27*10^{-3}$

Table A6.1 A comparison of eddy diffusivity data predicted using various literature correlations.

Note: the vapour hold-up fraction, ε, used in the calculation of some of these data is given. This term was calculated using the Colwell (1979) correlation.

Appendix 7 - Average height of clear liquid data predicted for use in the sensitivity analysis

	Exp	1	2	3	4	5
Atmospheric Case 1	22.8	25.3 (ε=0.44)	24.2 (ε=0.69)	27.6 (ε=0.69)	22.1 (ε=0.74)	25.1 (ε=0.73)
Atmospheric Case 2	23.1	25.6 (ε=0.57)	24.1 (ε=0.77)	32.0 (ε=0.77)	23.1 (ε=0.79)	32.9 (ε=0.77)
Atmospheric Case 3	21.1	25.7 (ε=0.67)	22.7 (ε=0.84)	33.8 (ε=0.84)	23.7 (ε=0.83)	41.9 (ε=0.79)
Atmospheric Case 4	14.2	25.5 (ε=0.74)	20.1 (ε=0.89)	32.5 (ε=0.89)	24.2 (ε=0.85)	52.0 (ε=0.80)

Table A7.1: Predicted height of clear liquid and vapour hold-up fraction data for atmospheric pressure distillation simulation calculated for use in the sensitivity analysis (height of clear liquid data is given in mm)

	Exp	1	2	3	4	5
Moderate Case 1	36.6	42.5 (ε=0.51)	38.9 (ε=0.74)	41.6 (ε=0.74)	40.0 (ε=0.72)	44.1 (ε=0.72)
Moderate Case 2	35.5	44.2 (ε=0.57)	41.8 (ε=0.77)	46.1 (ε=0.77)	45.0 (ε=0.74)	53.0 (ε=0.73)
Moderate Case 3	23.7	42.0 (ε=0.67)	38.9 (ε=0.84)	46.5 (ε=0.84)	46.0 (ε=0.88)	63.2 (ε=0.76)
Moderate Case 4	22.8	40.2 (ε=0.74)	34.1 (ε=0.89)	43.6 (ε=0.89)	46.9 (ε=0.81)	74.8 (ε=0.78)

Table A7.2: Predicted height of clear liquid and vapour hold-up fraction data for moderate pressure distillation simulation calculated for use in the sensitivity analysis (height of clear liquid data is given in mm)

Details of the correlations used in the calculation of these data can be found in Section 6.5.2.

Appendix 8 - The TRAYSIM tray efficiency program

A8.1 Introduction

The TRAYSIM suite of FORTRAN subroutines written for this project contain two tray efficiency models; the K.T. Yu fluid mechanical model as described in Chapter 3, and the *stagnant regions model* (Porter et al. 1972). These are solved for a single tray and mass-transfer calculations are performed in order to calculate tray efficiencies.

The following sections contain the program listing, a brief description of the function of each of the program subroutines and details of the data file required to run the program.

A8.2 TRAYSIM - compilation, linking and execution

TRAYSIM was compiled using the Salford FTN77 / 486 FORTRAN compiler version 2.60. The program is contained in four source files: TRAYMAIN.FOR, TRAYSUBS.FOR, TRAYMODL.FOR and TRAYCONC.FOR. They are compiled in the usual manner and are linked using the MSDOS batch file TRAYLINK.BAT included on the accompanying 3.5 inch floppy disk. The resultant executable file is called TRAYSIM.EXE.

In order to execute the program a data file is required (the information can be input via the keyboard, but this is tedious and time consuming). The file can have any valid MSDOS file name. Details of the contents of this file are contained in Section A6.4.

On execution of this program, the user is prompted to input some initial data via the keyboard. This data includes options about whether the user requires to input data via the keyboard or from a data file (the latter is strongly recommended), the name of the data file and verification that the data file name is correct. This last piece of information requires a "YES" or "NO" answer. Note that this must be in upper case as lower case is not recognised by the program.

If the user requires to input all data via the keyboard then after this option has been selected, data can be input after the appropriate prompts appear on the screen. The order in which the data are input and the units are the same as those for the data file.

During execution two data files are written (the name of this file corresponds to the case name input by the user with either the extension ".OUT" or ".UNI". The former contains details of the process variables and the results for reference by the user, while the latter is a data file for the MULTIPLOT program which utilises the UNIRAS graphics subroutines.

A8.3 Subroutines

TRAYMAIN (TRAYMAIN.FOR)

Reads data from either keyboard or data file and calculates constants; e.g. eddy diffusivity, height of clear liquid (if not specified) and thickness of tray floor boundary layer. These data are written to the output data file. The flow pattern model is then called.

TBOUND (TRAYSUBS.FOR)

Calculates the position of the tray boundaries for a tray with chordal downcomers. The wall boundaries are categorised as preparation for use of the fluid mechanical model.

VELWRITE (TRAYSUBS.FOR)

Writes the velocity profiles to a data file.

MESH (TRAYSUBS.FOR)

Categorises tray wall boundary points into the 18 type defined by in Appendix 1.

VELCONV (TRAYSUBS.FOR)

Interpolates the velocity profiles calculated by the fluid mechanical model from the M.A.C. finite difference grid to one with velocities defined on the grid nodes.

PCOLWALL (TRAYSUBS.FOR)

Allows for the pressure to be calculated on *corner* boundary points.

UNIFILE (TRAYSUBS.FOR)

Prints out a data file to be read by the MULTIPLOT program which utilises the UNIRAS graphics subroutines. This is discussed in more detail in Appendix 9.

PORTERSRM (TRAYMODL.FOR)

Calculates velocity profiles associated with liquid channelling, i.e. the *stagnant regions model* (Porter et al. 1972)

V1YUMECH (TRAYMODL.FOR)

Calculates the velocity profiles using the Yu fluid mechanical model.

ETAF (TRAYMODL.FOR)

A function which calculates the η constant described in Appendix 1.

XIF (TRAYMODL.FOR)

A function which calculates the ξ constant described in Appendix 1.

ANYVEL (TRAYMODL.FOR)

A function which calculates the velocity at a point given the pressure gradient and the appropriate constant (η or ξ).

CONCPROF (TRAYCONC.FOR)

Calculates the concentration profiles and tray efficiency for a given velocity profile.

CCOLWALL (TRAYCONC.FOR)

Calculates the concentration for tray wall boundary points using the formulae derived in Appendix 2.

A8.4 Data Input File

This is the data file which is used in conjunction with the TRAYSIM program described above. The format of the file is common to both the fluid mechanical model and the *stagnant regions model.*

Test Run Based on Moderate Pressure Case 4	*(1)*
YES	*(2)*
MOD4TEST	*(3)*
YUMECH1	*(4)*
YES	*(5)*
2.4	*(6)*
1.44	*(7)*
.050	*(8)*
.0168	*(9)*
.00625	*(10)*
.1	*(11)*
998	*(12)*
3.600E-2	*(13)*
.8937E-3	*(14)*
0.0228	*(15)*
1.177	*(16)*
10.1325	*(17)*
YES	*(18)*
.2	*(19)*
.15	*(20)*
0.62	*(21)*
0.83	*(22)*
30	*(23)*
20000	*(24)*
5E-05	*(25)*
.01	*(26)*
.1	*(27)*
5000	*(28)*
1E-7	*(29)*

1) Title (maximum 80 characters)

2) Do you want data to be output to a file ? (upper case YES / NO reply)

3) Case name used for creating data files (maximum 8 characters). Files created in the form:

<*case name*>.OUT - output data file

<*case name*>.UNI - data file for MULTIPLOT program

4) Model (*YUMECH1* or *STAGREG*)

5) DO you want to use the *Dankwerts' style* inlet boundary condition for the concentration calculations ?

6) Tray diameter (in metres)

7) Weir length (in metres)

8) Inlet gap / outlet weir height (in metres)

9) Hole pitch (in metres)

10) Hole diameter (in metres)

11) Fractional free area

12) Liquid density (kg m^{-3})

13) Liquid flow rate (m^3 s^{-1})

14) Liquid dynamic viscosity (kg m^{-1} s^{-1})

15) Average height of clear liquid (in metres)

16) Vapour density (kg m^{-3})

17) Vapour flow rate (m^3 s^{-1})

18) Do you want to carry out concentration calculations ?

19) Inlet liquid concentration

20) Vapour concentration

21) Lambda value

22) Murphree point efficiency

23) Number of grid points in x-direction to be used for calculations (maximum of 40)

24) Maximum number of iterations for the velocity calculations

25) Convergence parameter for the velocity calculations

26) Time interval used for solving the velocity calculations (seconds)

27) Relaxation parameter used for solution of the concentration profiles

28) Maximum number of iterations for the concentration calculations

29) Convergence parameter for the concentration calculations

Appendix 9 - Incorporation of a fluid mechanical model into the DISTSIM suite of programs

A9.1 Introduction

Due to previous modifications to the DISTSIM suite of programs, few modifications had to be carried out in order to include further tray efficiency models. The areas which required modification can be split into three sections:

1) data input
2) selection of the correct tray efficiency model
3) calculation of the tray efficiency

The program listings can be found in Appendix 11 (the enclosed computer disk).

A9.2 Data input

To cope with the additional data required by the fluid mechanical model a new data file was created. This file has the extension CF1. All data is read in through the LBREAD subroutine contained in DISTMAIN.FOR. Details of the contents of this data file are given below:

```
1.20   0.61   0.051  0.94   0.016  0.06   0.14   9.00
650.0  650.0         .0008937      95.0   95.0   -1.0   1.0
25.0   10000.        .00005        0.01
0.25   10000.        .000001       0.0    0.0
```

The contents of the data file are described below:

Line 1:

1) column diameter (m)
2) tray spacing (m)
3) weir height (m)
4) weir length (m)
5) hole pitch (m)
6) hole diameter (m)

7) fractional hole area of tray

8) number of separation stages

Line 2:

1) mass density of component 1 (kg m^{-3})

2) mass density of component 2 (kg m^{-3})

3) liquid kinematic viscosity (kg m^{-1} s^{-1})

4) molecular mass of component 1

5) molecular mass of component 2

6) average height of clear liquid - calculated by correlation if ≤ 0 (m)

7) average column pressure ($*10^5$ Pa)

Line 3:

1) no of grid meshes in x-direction

2) max. no. of iterations for velocity calculations

3) velocity convergence criterion

4) time step used in velocity calculations (s)

Line 4:

1) convergence parameter for concentration profiles

2) max. no. of iterations for concentration profiles

3) tray flow parameter (0: counter-current / 1: co-current)

4) vapour mixing (0: no mixing / 1: partial mixing / 2: total mixing)

A9.3 Selection of the tray efficiency model

The nature of the column program was such that an area already existed which was capable of accepting tray efficiency data from an individual tray model and transferring it to the main column model. This section was simply modified in order to allow for an additional model to be called. This is done through the MODELS subroutine contained in DISTEMOD.FOR.

A9.4 Calculation of the tray efficiency

Incorporation of a new tray efficiency model required that the majority of the TRAYSIM code had to be modified and included into the DISTSIM code. It was decided that since the DISTSIM code allowed for the liquid and vapour flow rates to differ on the trays and at different stages through the calculation procedure, then it would be necessary to recalculate both the velocity profiles and the concentration profiles on each tray for each of the column iterations. This can be a time consuming operation if the velocity profiles are calculated from scratch every time, so a system was developed where, if velocity profiles had been calculated for previous trays, the velocity profile with a liquid rate which most closely approximates to the one required is used as an initial estimate for a tray.

With the exception of this stage for the estimation of the initial velocity profile for a tray, the calculation procedure is the same as that for a single tray. The velocity and the concentration profiles are stored for all trays.

Appendix 10 - The use of the UNIRAS graphics subroutines

A10.1 Introduction

Previous workers (Hine 1990, Chambers 1993) used the UNIRAS graphics subroutines to plot experimental reduced temperature and height of clear liquid data. Since the theoretical data obtained from these simulations were to be compared to the previously collected experimental data, it was decided that it would be best if it was presented in a similar form. With this goal *in mind, the* 2D3DTEMP program written by Chambers (1993) was modified in order to utilise the theoretical data. The program listings are included in Appendix 11 (the enclosed computer disk).

A10.2 MULTIPLOT - compiling, linking and execution

The MULTIPLO.F program was written for use with the UNIRAS suite of graphics subroutines on a SUN computer. The file must be compiled and linked with the UNIRAS. Exact details on how to accomplish this depend upon the set up of the local system.

To execute this program, an input data file is required. The name of the data file will be requested on initiating the execution of the program. Depending on the options as to the method of display a data file may be produced (only for the postscript option and not for displaying of results on the screen). The name of this file is set in the UNIRAS subroutines and depends on the computer system which is being used. For the version of UNIRAS used by this operator on a SUN computer system the file was named "POST".